Report MDC E1734

FLUTTER OF CONTROL SURFACES WITH STRUCTURAL NONLINEARITIES

Robert M. Laurenson and Robert M. Trn
McDonnell Douglas Astronautics Company - East
St. Louis, Missouri 63166

31 August 1977
Final Report for Period 1 June 1976 - 31 August 1977

Prepared for
DEPARTMENT OF THE NAVY
NAVAL AIR SYSTEMS COMMAND
Washington, DC 20361

(14) **REPORT DOCUMENTATION PAGE**

READ INSTRUCTIONS BEFORE COMPLETING FORM

1. REPORT NUMBER	2. GOVT ACCESSION NO.	3. RECIPIENT'S CATALOG NUMBER
Report MDC-E1734		

(6) 4. TITLE (and Subtitle)

FLUTTER OF CONTROL SURFACES WITH STRUCTURAL NONLINEARITIES.

(9) 5. TYPE OF REPORT & PERIOD COVERED

Final Report.
1 June 1976 - 31 August 1977

6. PERFORMING ORG. REPORT NUMBER

(10) 7. AUTHOR(s)

Robert M. Laurenson
Robert M. Trn

(15) 8. CONTRACT OR GRANT NUMBER(s)

N0019-76-C-0524

9. PERFORMING ORGANIZATION NAME AND ADDRESS

McDonnell Douglas Astronautics Company - East
P.O. Box 516
St. Louis, MO 63166

10. PROGRAM ELEMENT, PROJECT, TASK AREA & WORK UNIT NUMBERS

(11) 11. CONTROLLING OFFICE NAME AND ADDRESS

Department of the Navy
Naval Air System Command
Washington, DC 20361

12. REPORT DATE

31 August 1977

13. NUMBER OF PAGES

110

14. MONITORING AGENCY NAME & ADDRESS (if different from Controlling Office)

(12) 111p.

15. SECURITY CLASS. (of this report)

Unclassified

15a. DECLASSIFICATION DOWNGRADING SCHEDULE

16. DISTRIBUTION STATEMENT (of this Report)

Approved for Public Release - Distribution Unlimited

17. DISTRIBUTION STATEMENT (of the abstract entered in Block 20, if different from Report)

18. SUPPLEMENTARY NOTES

19. KEY WORDS (Continue on reverse side if necessary and identify by block number)

Missile Control Surface Flutter
Nonlinear Flutter Analysis
Structural Dynamic Analysis

20. ABSTRACT (Continue on reverse side if necessary and identify by block number)

Missile control surface systems often contain structural nonlinearities which affect their performance characteristics and flutter boundaries. Presented in this report are flutter analysis procedures which have been developed to evaluate the potential influence of these nonlinearities on control surface flutter. Three type nonlinearities, freeplay, preload, and friction, have been investigated. The describing function technique, which has found application

DD FORM 1 JAN 73 1473 EDITION OF 1 NOV 65 IS OBSOLETE

UNCLASSIFIED

SECURITY CLASSIFICATION OF THIS PAGE (When Data Entered)

AD A 03 930

20. ABSTRACT

in dealing with nonlinearities in automatic control systems, has been used to mathematically represent these nonlinearities during the investigation. A simplified representation of the aerodynamic loadings acting on the control surface has been assumed and the techniques have application for either a rigid or flexible control surface. Numerous examples of the application of the developed flutter analysis techniques are presented.

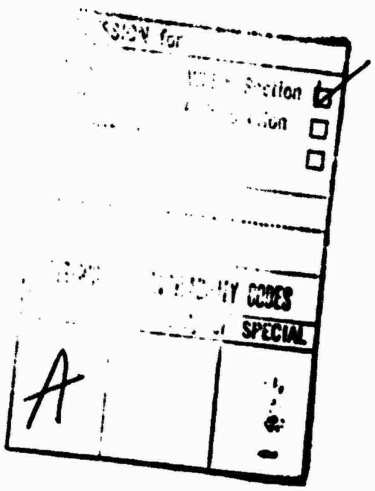

DISCLAIMER NOTICE

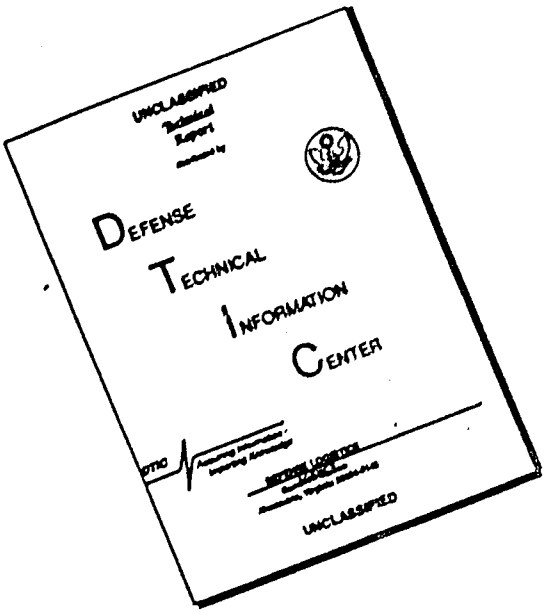

THIS DOCUMENT IS BEST QUALITY AVAILABLE. THE COPY FURNISHED TO DTIC CONTAINED A SIGNIFICANT NUMBER OF PAGES WHICH DO NOT REPRODUCE LEGIBLY.

FOREWORD

This report was prepared by the McDonnell Douglas Corporation, McDonnell Astronautics Company - East, St. Louis, Missouri 63166, under Contract N00019-76-C-0524, "Flutter of Control Surfaces With Structural Nonlinearities." It covers the period 1 June 1976 through 1 June 1977. This program was administered under the direction of Naval Air Systems Command with Dr. Allan Somoroff as program monitor and Mr. George Maggos as technical monitor.

Dr. Robert M. Laurenson was Program Manager of this study. Mr. Robert M. Trn assisted in performing the technical work of this investigation and in the preparation of the final report. The effort was performed in the Structural Dynamics Department of McDonnell Douglas Astronautics Company - East.

THIS PAGE INTENTIONALLY LEFT BLANK

TABLE OF CONTENTS

TABLE OF CONTENTS (Concluded)

LIST OF PAGES

COVER

i thru x

1 thru 110

LIST OF ILLUSTRATIONS

LIST OF ILLUSTRATIONS (Continued)

LIST OF ILLUSTRATIONS (Continued)

LIST OF ILLUSTRATIONS (Concluded)

Section I
INTRODUCTION

Although flutter is an exceedingly dangerous phenomenon which can cause structural failure, it is possible to approach instability without destructive results. If the system is unstable, the amplitude of oscillation begins to build up, but the extent to which this increase continues depends on the nature of stiffness characteristics of the system. If the system is nonlinear, the oscillations might increase to some amplitude and become stable again with a limit cycle oscillation. For missile control surfaces having large starting friction or a deadspace ("slop") in the control system, the natural frequency is a function of the amplitude of oscillation.

At a speed slightly in excess of the critical flutter speed, the amplitudes of oscillation (caused by external excitation) would start to build up. Since the critical flutter speed is a function of the natural frequency of the system, it would be possible that the change in natural frequency attendant on the increased amplitude of oscillation would raise the critical flutter speed. The oscillations would then decrease until stability would be achieved. Thus, although the critical flutter speed of the original configuration might be exceeded, destructive oscillations would not necessarily result from the instability. The possibility of fatigue failure from low-amplitude oscillations is of course not ruled out.

A control surface flutter analysis technique accounting for these nonlinearities and an understanding of their potential influence on the flutter mechanism greatly increases the efficiency of the control surface design process. Benefits in the form of reduced system weight and program cost could potentially be realized with the inclusion of nonlinearities in the design process. This study was undertaken to provide a better understanding of the effect of various nonlinearities on the dynamics of a missile control surface and to establish procedures to include the influence of these nonlinearities in the flutter analysis process.

In the past, limited analyses have been conducted to evaluate the influence of structural nonlinearities on control surface flutter. For example, the

analyses of References 1 and 2 were for a rigid control surface with a single nonlinearity. In these references the nonlinear flutter problem was studied using basic linearization techniques and an analog computer. The present study extended these results in order to: (a) develop techniques to handle flexible control surfaces having structural nonlinearities, (b) remove the limitation of allowing only a single nonlinearity in the system, and (c) improve the techniques for including the influence of the nonlinearities in the dynamic analysis of control surfaces.

Specifically, the problem that was addressed during this study consisted of dealing with a missile control surface, Figure 1, exposed to subsonic flow. Structural nonlinearities were associated with the root rotational support springs K_θ and K_ϕ. Definition of the load acting on the control surface used the "simplified" representation defined in References 3 and 4. The basic assumption of the simplified approach is that the lift force is proportional to and in phase with the torsional motion. The primary concern of this investigation was the evaluation of the influence of structural nonlinearities on control surface flutter. The attractiveness of the simplified approach to this initial understanding of nonlinearities is that it permits a more direct physical feeling of the flutter mechanism while under certain conditions yielding approximately the same results as more complicated analysis methods with much less computation.

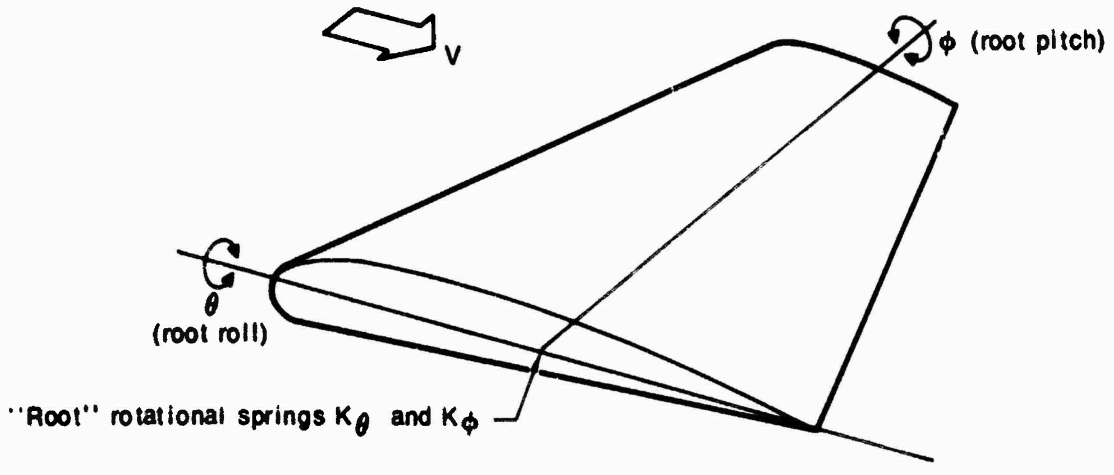

Figure 1 Missile control surface configuration

Three types of structural nonlinearities, as shown in Figure 2 were dealt with during the study. The freeplay nonlinearity, Figure 2(a), might represent a loose hinge or linkage of a control system or possible joint slippage. The preload nonlinearity, Figure 2(b), corresponds to a control surface with a basic freeplay nonlinearity and subjected to a preload which shifts the equilibrium position. The friction nonlinearity, Figure 2(c), is characteristic of control surfaces with freeplay if friction exists in the control system linkage or joints.

During this study the control surface flutter problem was represented by the following system of nonlinear equations.

$$M\ddot{X} + K(X)X = q\,A\,X \tag{1}$$

Referring to Figure 1, the detailed elements of Equation (1) are given as:

$$\left[\begin{array}{cc|c|c} I_\phi & I_{\theta\phi} & & \\ I_{\phi\theta} & I_\phi & PF & \\ \hline & PF^T & m_n & \end{array}\right]\left\{\begin{array}{c}\ddot{\theta}\\ \ddot{\phi}\\ \hline \ddot{q}_n\end{array}\right\} + \left[\begin{array}{cc|c|c} K(\theta) & 0 & & \\ 0 & K(\phi) & 0 & \\ \hline & 0 & m_n\omega_n^2 & \end{array}\right]\left\{\begin{array}{c}\theta\\ \phi\\ \hline q_n\end{array}\right\} = q\left[\begin{array}{cc|c} A_r & A_{re} & \\ \hline A_{er} & A_e & \end{array}\right]\left\{\begin{array}{c}\theta\\ \phi\\ \hline q_n\end{array}\right\} \tag{2}$$

A baseline control surface was assumed for evaluating the various coefficients of Equation (2). This baseline configuration was based on the Harpoon Anti-Ship missile quick-attach control surface. Details of this Harpoon control surface are presented in Appendix A.

With no nonlinearities in the system, that is when $K(\theta)$ and $K(\phi)$ are constants and not a function of system response, standard solution techniques may be used to obtain flutter solutions to Equation (1). A common approach is to assume harmonic motion and conduct eigenvalue analyses on the resulting free vibration problem. For varying magnitudes of dynamic pressure, the form of the resulting complex eigenvalues is used to determine system stability,

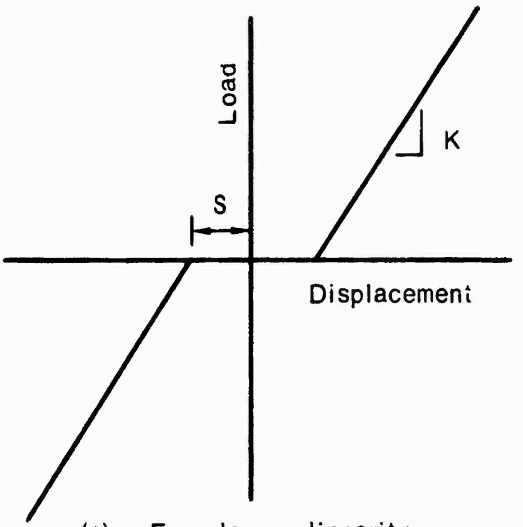

(a) – Freeplay nonlinearity

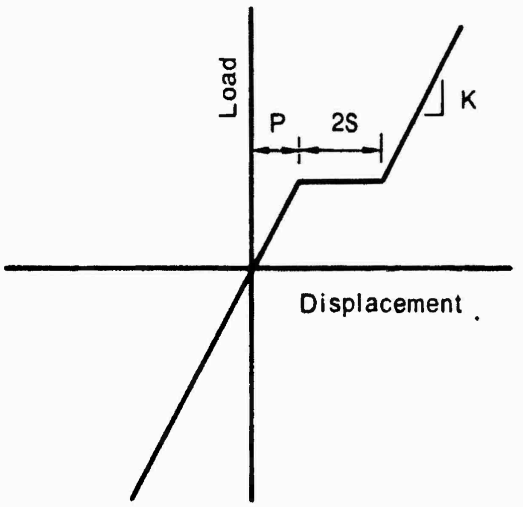

(b) Preload nonlinearity

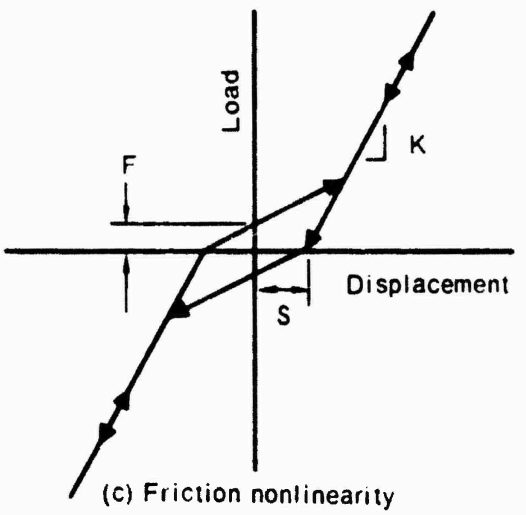

(c) Friction nonlinearity

Figure 2 Characteristics of structural nonlinearities

i.e., flutter. In addition, the "flutter mode shape" is obtained when the eigenvalue analysis is conducted for the flutter critical value of dynamic pressure. As will be discussed in following sections, during analysis of the nonlinear system, flutter results for an "effective" linear system are required. For these analyses, the eigenvalue approach was employed for obtaining flutter solutions.

During these investigations, the nonlinear flutter problem was anlayzed through application of the "describing function" approach. As discussed in References 5 and 6 this technique is used in dealing with nonlinearities in control systems. This technique is based on a time averaging approach for defining the input-output characteristics of a nonlinear system. It is assumed that for a sinusoidal input the output is also sinusoidal with the same frequency as the input and all other harmonics can be neglected. Based on these assumptions, the linearized quantities relating system output to input are expressed in terms of the fundamental component of the output's Fourier series representation. In the literature of mechanical vibrations, this technique is also often referred to as the method of "harmonic balance," for instance Reference 7. Further details on applying these methods may be found in the Reference 8 text on solution techniques for nonlinear differential equations.

The developed flutter analysis procedures, including the effects of structural nonlinearities, and illustrative results when applying these techniques are presented in the following three sections of this report. In Section II, a summary is presented of the describing function representation for each of the nonlinearities shown in Figure 2. The developed flutter analysis procedures are then discussed in Section III. Numerical time history solutions were obtained for the governing system of nonlinear equations. Results from these numerical simulation studies are compared with describing function predictions in Section IV. This process verified the developed flutter analysis procedures employing the describing function technique and led to a better understanding of the flutter mechanism as influenced by structural nonlinearities. These sections are followed by study conclusions, Section V, and recommendations, Section, VI. Included in this latter section is an illustration of how the presence of structural nonlinearities can influence the definition of the allowable flight conditions for a missile control surface.

Supporting information is presented in the report appendices. Appendix A describes the baseline control surface used in this study. Appendix B is a detailed analysis of the describing function for each nonlinearity studied in this program and Appendix C explains the load versus amplitude characteristics of the friction type nonlinearity. Solutions to example problems illustrating application of the developed analysis procedures are given in Appendix D.

Section II
DESCRIBING FUNCTION ANALYSIS

Application of the describing function technique forms the basis of the developed flutter analysis procedures for missile control surfaces with structural nonlinearities. With this approach, the nonlinear equations of motion, Equation (1), are linearized for subsequent flutter analysis.

The basic approach in the describing function method is to assume that the system displacement is sinusoidal and of the form:

$$x(t) = A \sin t \text{ or } x(t) = A \cos t \tag{3}$$

For this displacement expression, the form of the load developed in the nonlinear spring is defined and this load relationship is then expanded in a Fourier series. The higher harmonics in the series expansion of the load time history are neglected. That is, for a sinusoidal input displacement, it is assumed that the output load is also sinusoidal with the same frequency. The ratio of the single term Fourier series expansion of the developed load and the assumed displacement are then used to define an "effective" linear spring rate for the nonlinear element.

A summary of the describing function approach for each of the three nonlinearities shown in Figure 2 is presented in the following sections. Detailed development of the describing functions for these nonlinearities is presented in Appendix B.

A. FREEPLAY NONLINEARITY

For a nonlinear spring with freeplay characteristics, as illustrated in Figure 2(a), the waveform of the developed load may take one of the two shapes shown in Figure 3. These waveforms are dependent on the relationship between the magnitudes of the freeplay and the amplitude of displacement, Equation (3). For a displacement amplitude A less than the magnitude of the dead space S no load is developed, Figure 3(b). When A is greater than S the developed load is as shown in Figure 3(c).

The "effective" stiffness $\bar{K}$ of the nonlinear spring including the

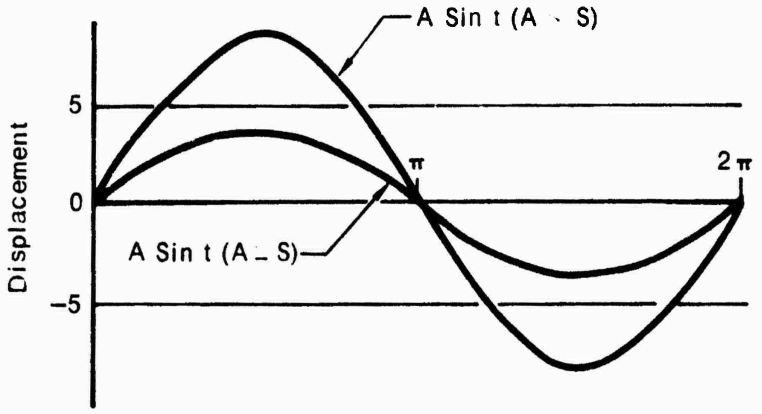

(a) Displacement

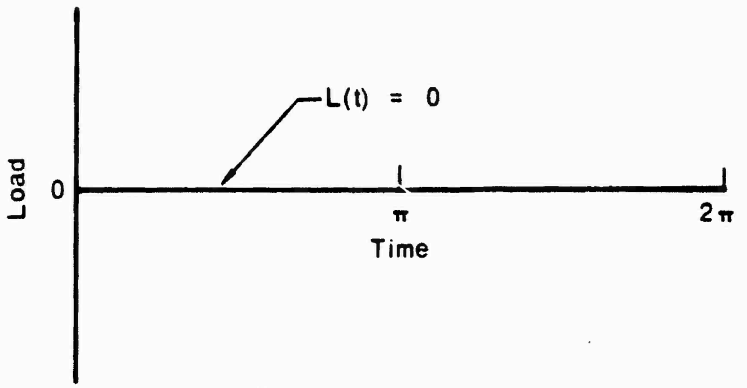

(b) Load (A S)

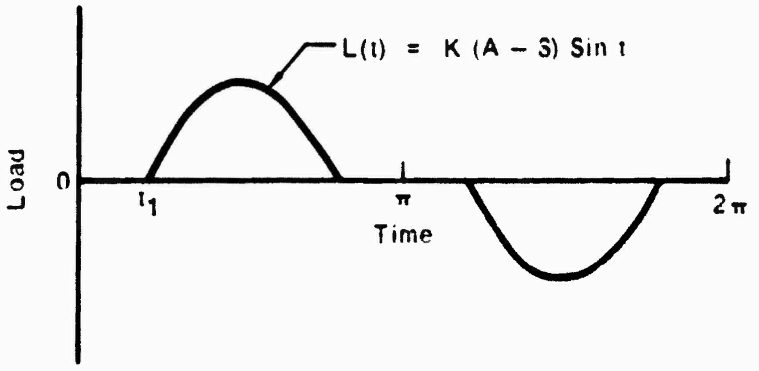

(c) Load (A S)

Figure 3. Developed load for freeplay nonlinearity

influence of freeplay is now defined as

$$\overline{K} = \delta K \tag{4}$$

In this expression δ is the describing function which accounts for the presence of the freeplay nonlinearity. Using the describing function technique we acquire a representation for the freeplay nonlinearity of the form (from Appendix B-1)

$$\delta = 0 \quad \text{for} \quad A \leq S \tag{5}$$

and

$$\delta = \frac{1}{\pi} (\pi - 2t_1 - \text{Sin } 2t_1) \text{ for } A > S \tag{6}$$

where t_1 is given by

$$t_1 = \text{Sin}^{-1} (S/A) \tag{7}$$

Employing Equations (5) and (6), the relationship between the effective stiffness and the linear spring rate for a freeplay nonlinearity may be obtained. This relationship is shown in Figure 4 as a function of the amplitude of motion to freeplay ratio. For amplitude ratios A/S less than one, the effective stiffness is zero. As the amplitude increases, the linear spring predominates and the magnitude of $\overline{K}$ approaches that of K.

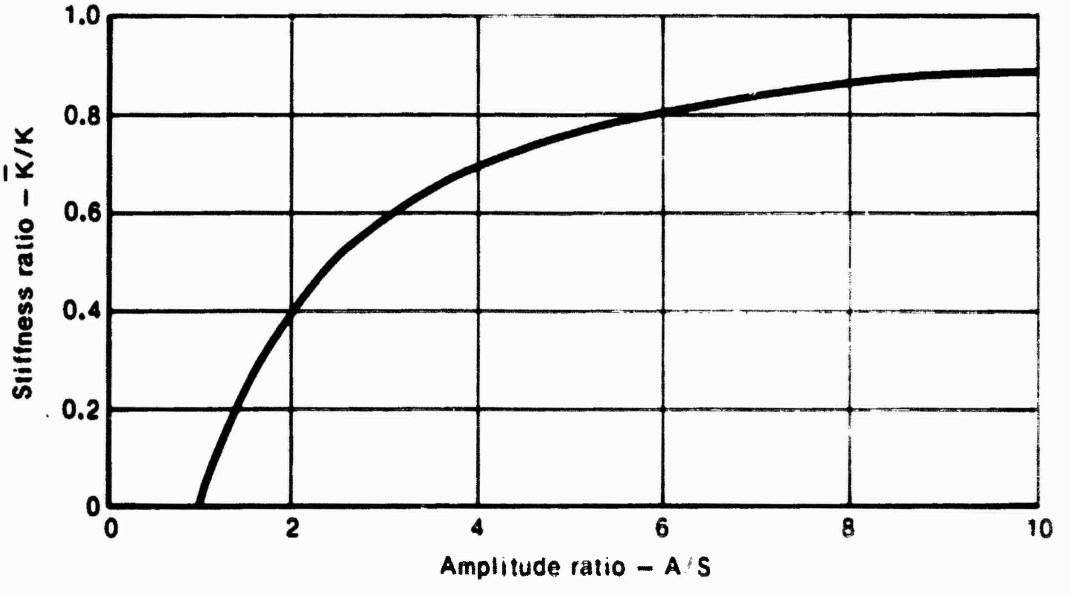

Figure 4 Effective stiffness for freeplay nonlinearity

Numerical solutions have been obtained for a single degree of freedom system containing a freeplay type nonlinearity. From these numerical time histories, the effective natural frequencies of the nonlinear system were determined. Comparison of these with frequencies predicted by the describing function technique allowed evaluation of the describing function approach.

A comparison such as this is presented in Figure 5. Here the ratio of the effective frequency ω_e to the linear frequency ω_0 ratio, as a function of deadspace S to amplitude of motion A ratio, is given. The parameter ω_0 is defined as

$$\omega_0 = \sqrt{K/m} \tag{8}$$

where K is the linear spring rate of the freeplay nonlinearity. Also shown in Figure 5 is the frequency ratio obtained from the "exact" piecewise linear solution to the nonlinear problem, Reference 9. As indicated in this figure the describing function technique predicts frequency ratios very close to those given by the exact or the numerical solution.

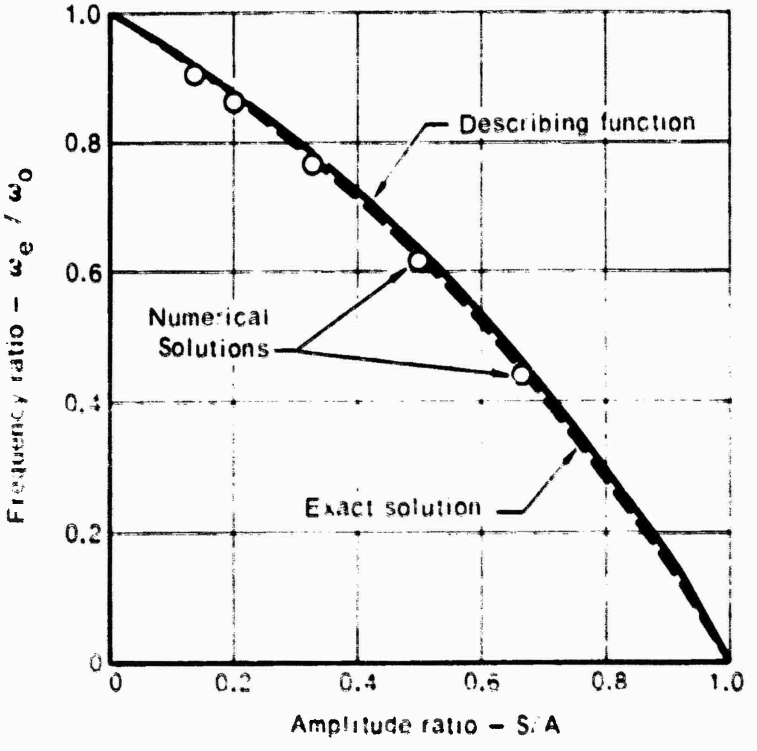

Figure 5 Frequency ratio for freeplay nonlinearity

B. PRELOAD NONLINEARITY

A modified displacement function was assumed during the describing function development for a preload nonlinearity. This displacement function was of the form

$$x(t) = A_0 + A_1 \text{ Cos } t \tag{9}$$

where the coefficients A_0 and A_1 were defined such that the energy stored in the nonlinear spring is the same for both positive and negative displacements. This displacement function is required to represent the nonsymmetric form, about the origin, of the motion which results with a preload nonlinearity. In addition it was required that Equation (9) result in a positive amplitude equal to the initial displacement. Thus these coefficients are obtained from

$$A_1 = \frac{A}{2} + \frac{1}{2}\sqrt{2PA-P^2} \text{ for } P < A \leq (P + 2S) \tag{10}$$

or

$$A_1 = \frac{A}{2} + \frac{1}{2}\sqrt{(A-2S)^2 + 4PS} \text{ for } A > (P + 2S) \tag{11}$$

In both cases, the coefficient A_0 is obtained from the relationship

$$A = A_0 + A_1 \tag{12}$$

Note that it has been assumed that the influence of a preload nonlinearity is related to positive displacements A of the system. It should also be pointed out that when A is less than the preload P, A_1 equals A and A_0 is zero. For this situation, the nonlinear problem reduces to a simple linear problem.

With the definition of Equation (9) in mind, the waveforms of the developed load will take the shapes shown in Figure 6. As before, these waveforms are dependent on the relationship between the magnitudes of freeplay, preload, and amplitude of motion.

Proceeding as before, the fundamental components of the Fourier series representation of these developed load waveforms were obtained. This leads to the following definition for the describing function for a preload

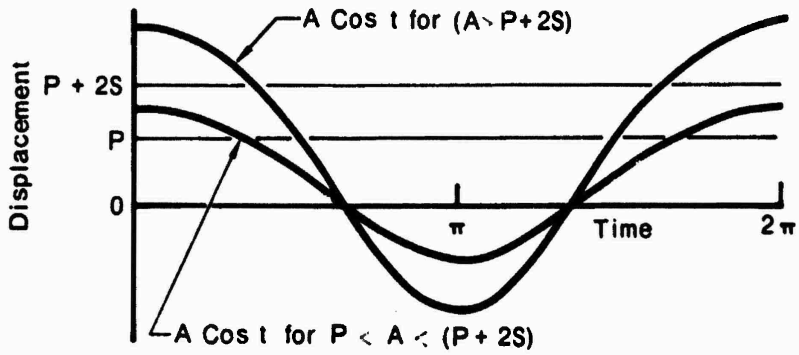

(a) Displacement

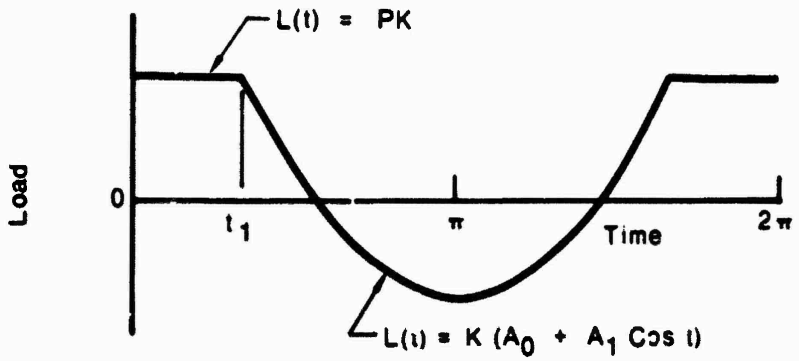

(b) Load (P < A < P + 2S)

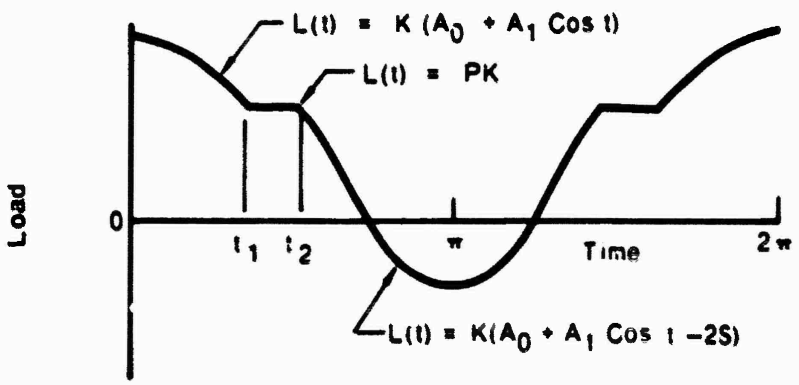

(c) Load (A > P +2S)

Figure 5 Developed load for preload nonlinearity

nonlinearity

$$\delta = 1.0 \text{ for } A \leq P \tag{13}$$

and

$$\delta = \frac{1}{\pi}\left[\pi - t_1 + \frac{2}{A_1}(P-A_0)\text{Sin } t_1 - \frac{1}{2}\text{Sin } 2t_1\right] \text{ for } P < A \leq (P+2S) \tag{14}$$

where t_1 is given by

$$t_1 = \text{Cos}^{-1}\left(\frac{P-A_0}{A_1}\right) \tag{15}$$

Finally

$$\delta = \frac{1}{\pi}\left[\pi + t_1 - t_2 - \frac{2}{A_1}(P+2S-A_0)\text{Sin } t_1 + \frac{2}{A_1}(P-A_0)\text{Sin } t_2 + \frac{1}{2}(\text{Sin } 2t_1 - \text{Sin } 2t_2)\right] \tag{16}$$

$$\text{for } A > (P + 2S)$$

where t_1 is given as

$$t_1 = \text{Cos}^{-1}\left(\frac{P-A_0}{A_1}\right) \tag{17}$$

and t_2 is expressed as

$$t_2 = \text{Cos}^{-1}\left(\frac{P+2S-A_0}{A_1}\right) \tag{18}$$

Shown in Figure 7 is the stiffness ratio as a function of the amplitude of motion to freeplay ratio for several freeplay to preload ratios. As can be seen from this figure, for amplitudes of motion less than the preload P, the stiffness ratio is one and the system is linear. With increasing amplitudes of motion the stiffness decreases. This is due to the deadspace in the spring causing the effective stiffness to be less than the linear value. As the amplitude increases further, the influence of the nonlinearity becomes small and the magnitude of $\bar{K}$ approaches that of K.

To aid in evaluating the results of the describing function representation of a preload nonlinearity, the influence of this nonlinearity on the dynamics of a single degree of freedom have been studied. Numerical solutions of the nonlinear equation of motion were obtained for various magnitudes of the nonlinearity. By examining the resulting time history information, effective stiffnesses were obtained which could be compared with predicted describing function values.

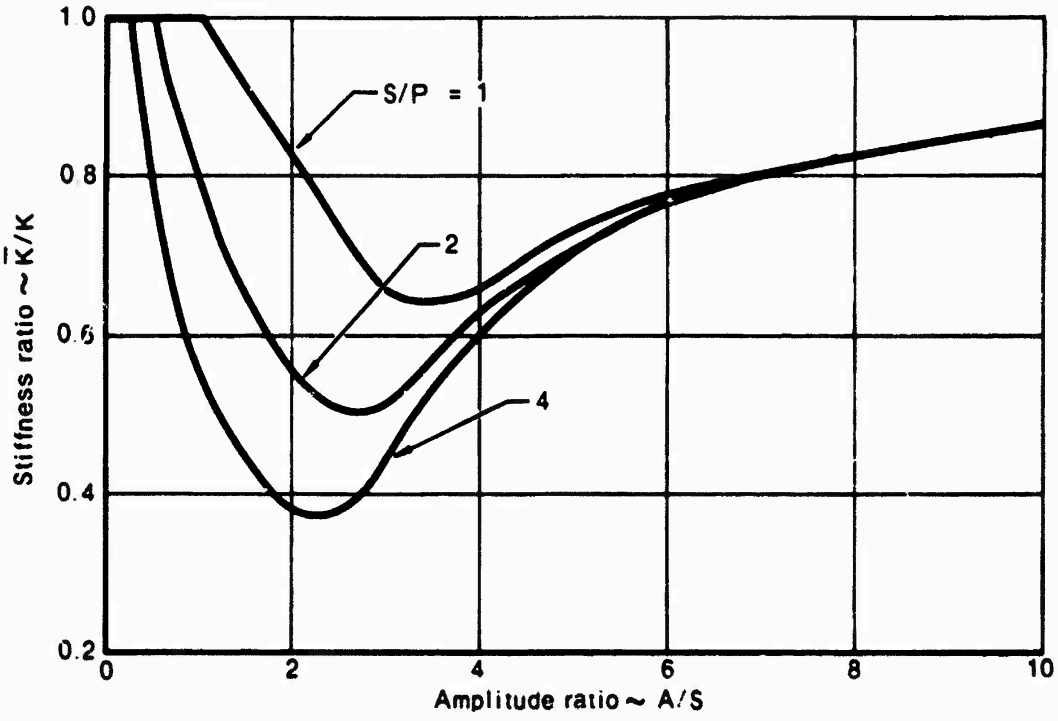

Figure 7 Effective stiffness for preload nonlinearity

A numerical solution for the single degree of freedom with an initial amplitude of six inches was obtained as shown in Figure 8. Also included in this figure is the displacement time history given by Equation (9) having an amplitude A also equal to six inches. This corresponds to the assumed displacement function employed during the describing function development. As can be seen from this figure the results obtained with the describing functions compare well with the numerical data. Also, the numerical solution illustrates the nonsymmetric nature of the motion for a system with a preload nonlinearity.

A comparison between these numerical solutions and the describing function results are illustrated in Figure 9. The results presented in this figure correspond to the information given in Figure 7 for a deadspace to preload ratio of one. As can be seen in Figure 9 the comparison between the two solution techniques is very good.

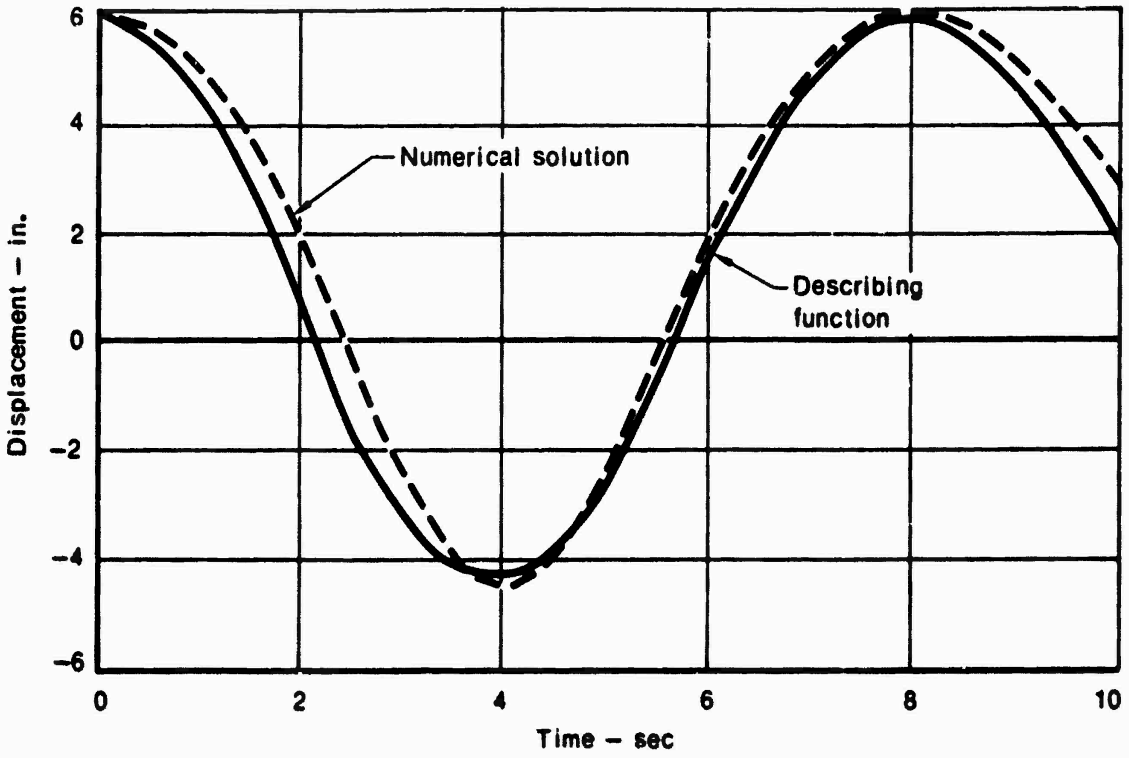

Figure 8 Comparison of displacement response for single degree of freedom system with a preload nonlinearity

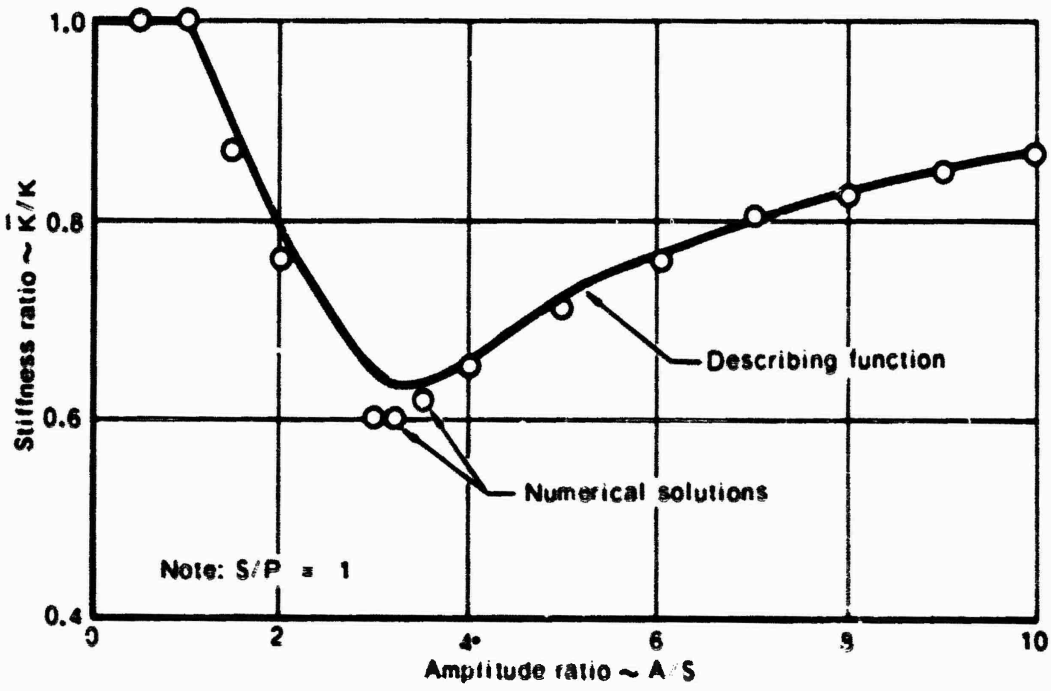

Figure 9 Comparison of solution techniques for a single degree of freedom system with a preload nonlinearity

C. FRICTION NONLINEARITY

For a nonlinear spring with friction nonlinearities, the waveform of the developed load will take the form shown in Figure 10. This waveform is produced when the amplitude of displacement A is greater than the limits of the hysteresis envelope. By geometry, this limiting value of motion is given as:

$$H = \pm \frac{S\,(KS + F)}{KS - F} \tag{19}$$

Proceeding as before, the fundamental components of the Fourier series representation of the developed load waveforms were obtained. Thus, in the case of the friction nonlinearity, the expansion leads to a load relationship of the form.

$$L(t) = a_1 \text{ Cos } t + b_1 \text{ Sin } t \tag{20}$$

where coefficients a_1 and b_1 are defined in Appendix B.

For this nonlinearity there is both an amplitude and phase relationship between the load output and the input displacement. The load relationship may be expressed as

$$L(t) = \phi \text{ Cos } (t + \alpha) \tag{21}$$

where

$$\phi = \sqrt{a_1^2 + b_1^2} \tag{22}$$

and

$$\alpha = \text{Tan}^{-1}\ (a_1/b_1) \tag{23}$$

Thus, this representation is analogous to a spring and structural damping combination.

From the above results the effective stiffness of a friction nonlinearity is of the form.

$$\bar{K} = \frac{\sqrt{a_1^2 + b_1^2}}{A} \tag{24}$$

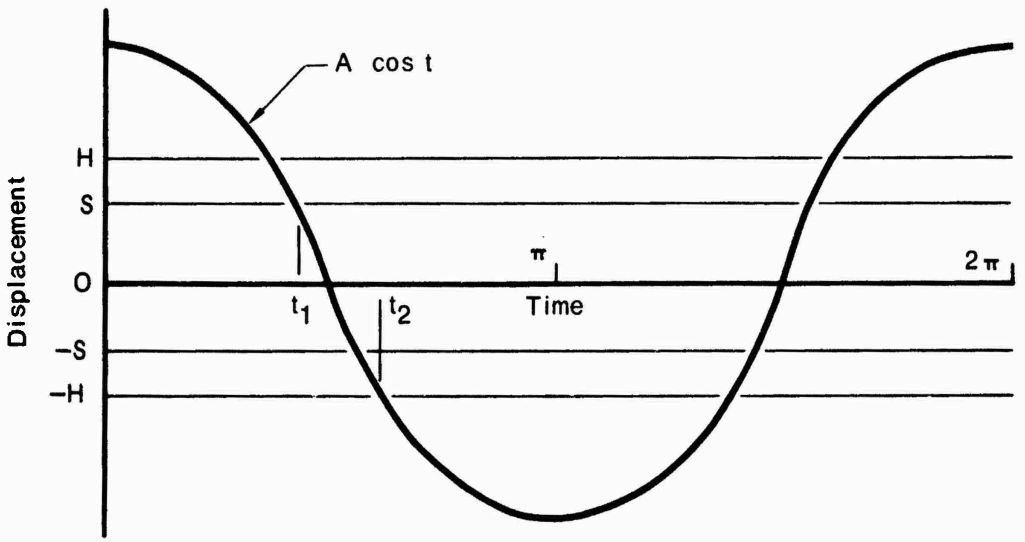

(a) Displacement

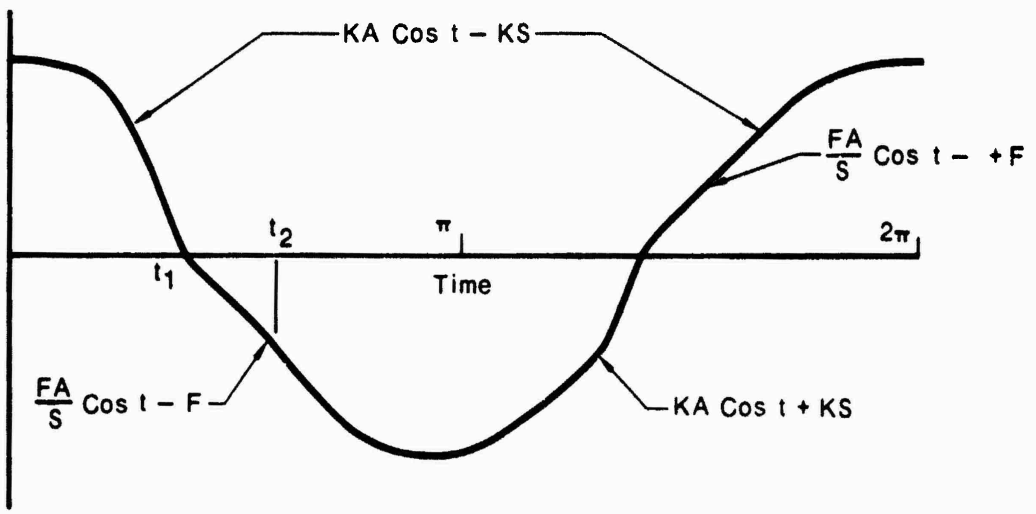

(b) Load

Figure 10 Developed load for friction nonlinearity

Thus the describing function is given as:

$$\delta = \frac{\sqrt{a_1^2 + b_1^2}}{KA} \tag{25}$$

Note that this definition only applies for amplitudes of motion which are greater than the parameter H given by Equation (19).

The equivalent viscous damping, or effective damping, associated with the friction nonlinearity was obtained using the procedure discussed in Reference 10. Here the work done during a cycle of motion by the load from the nonlinear spring, Equation (20), is equated to the work done by a viscous damper during a cycle of motion. In this manner, the effective structural damping coefficient $\bar{g}$ may be defined as a function of the amplitude of motion. This approach leads to the following definition of the effective $\bar{g}$ for a given friction nonlinearity.

$$\bar{g} = \frac{b_1}{2A\sqrt{\bar{K}m}} \tag{26}$$

Trends in the effective stiffness and damping are presented in Figure 11. These data are presented for various deadspace S to friction F ratios. As can be seen, the effective stiffness approaches that of the linear system for large motions. In addition, the effective damping goes to zero as the amplitude of motion increases.

To gain insight into the influence of a friction nonlinearity on the dynamics of a system, the vibration of a nonlinear single degree of freedom system was investigated. The system was given an initial displacement and numerical solutions obtained for the nonlinear equation of motion. Frequency and decay times were then compared with describing function predictions to evaluate the accuracy of the predictions.

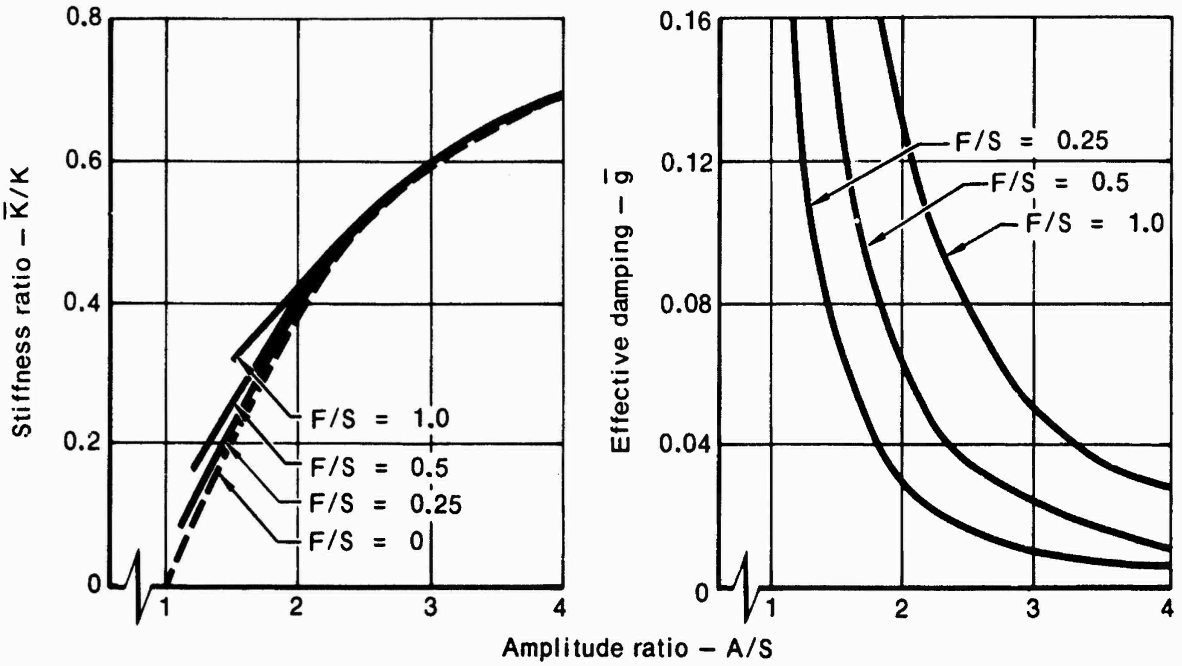

Figure 11 Effective stiffness and damping for friction nonlinearity

A typical numerically obtained displacement time history is presented in Figure 12. The influence of the nonlinear spring can be noted by the form of these results. The decaying nature of the response is a result of the system damping due to the nonlinearity. The difference in times between successive peaks indicates the dependence of the effective stiffness on the amplitude of motion.

Effective stiffness and damping, as a function of amplitude of motion, were estimated from the numerical results. The time between successive peaks was used to estimate the system's effective natural frequency. The effective system stiffness was then defined in terms of this frequency. A comparison between these numerically obtained effective stiffnesses and describing function predictions is shown in Figure 13. The average amplitude of motion between successive peaks was used as the amplitude in defining the plotted A over S ratios. The difference in magnitudes of successive peaks was used to estimate the effective damping over a particular cycle. These results are compared with describing function predictions in Figure 14. From the results presented in Figures 13 and 14, it can be seen that there is good correlation between the numerical and describing function results.

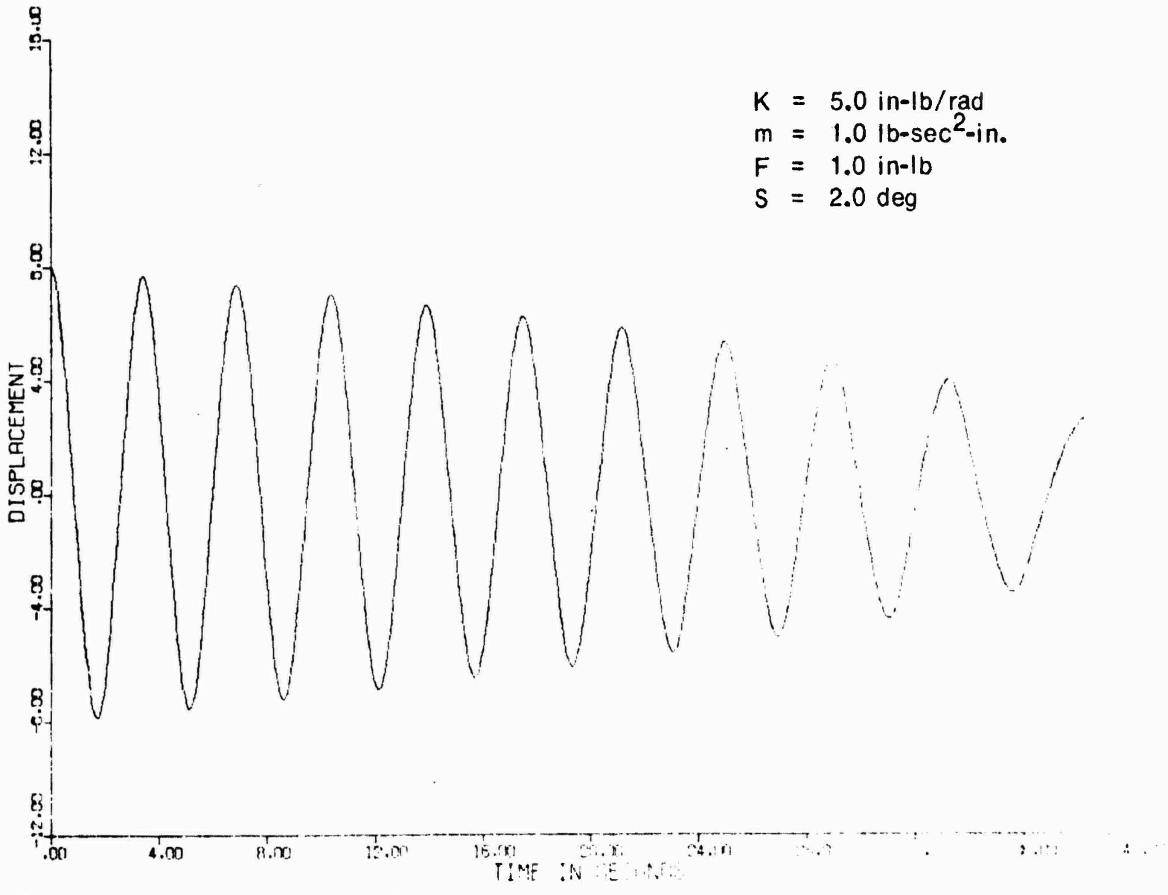

Figure 12 Simulation results for single degree of freedom system with a friction nonlinearity

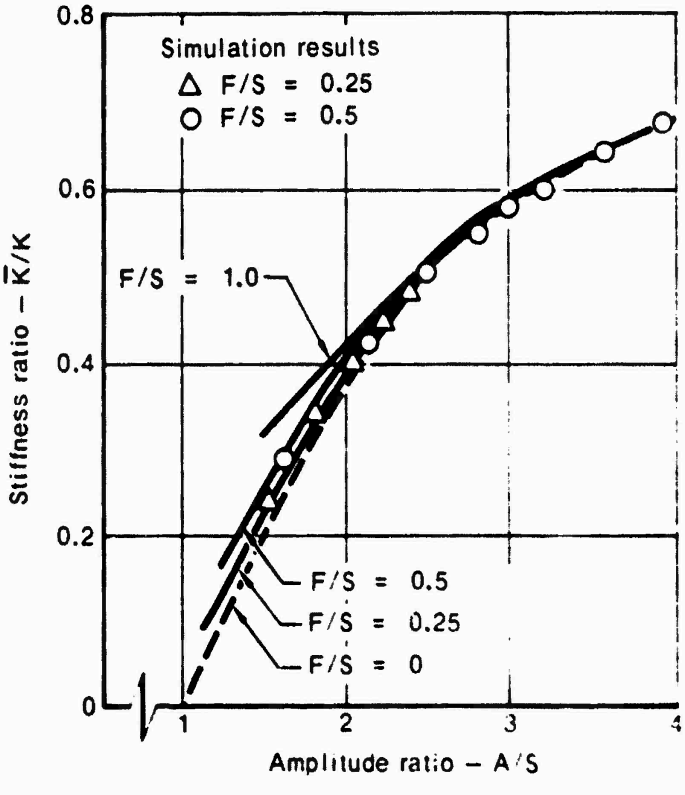

Figure 13 Comparison of effective stiffness for friction nonlinearity

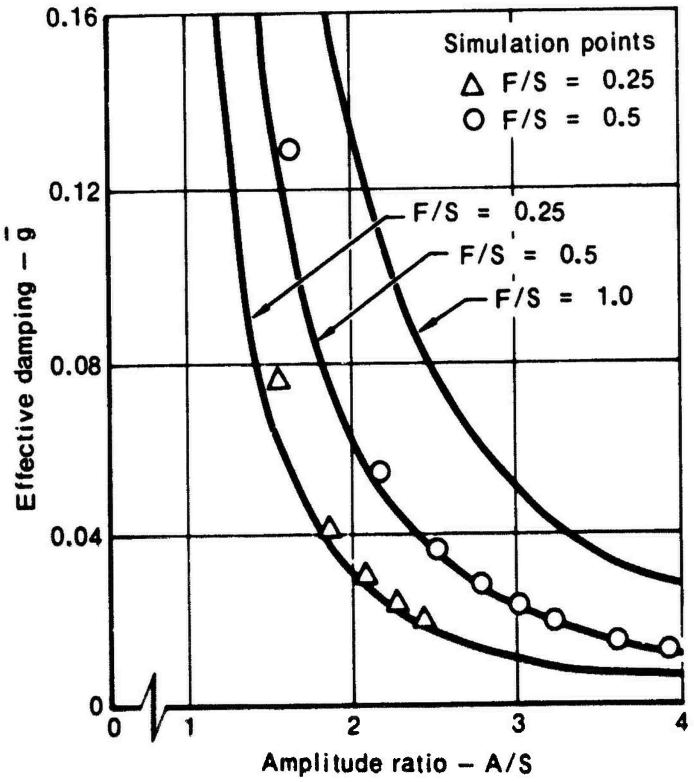

Figure 14 Comparison of effective damping for friction nonlinearity

THIS PAGE INTENTIONALLY LEFT BLANK

Section III
FLUTTER ANALYSIS

Application of the describing function technique for the flutter analysis of control surfaces with structural nonlinearities employs the previously discussed concept of effective stiffness. As with a linear system, flutter analyses are conducted for variations in these effective stiffness parameters. These flutter results are then modified to account for the presence of the system nonlinearities.

Throughout this study the control surface flutter problem is represented by the system of nonlinear equations of motions given in Equation (1). In the relationship of Equation (1), K(X) is the nonlinear system stiffness matrix. With no nonlinearities in the system, that is when $K(\theta)$ and $K(\phi)$ are constants and not a function of system response, standard solution techniques may be used to obtain flutter solutions to Equation (1). At this point the definition of the effective stiffness parameters given by Equation (4) is employed. The nonlinear stiffness terms $K(\theta)$ and $K(\phi)$ in Equation (1) are replaced with the corresponding effective parameters $\bar{K}_\theta$ and $\bar{K}_\phi$. In this manner the system equations of motion are "linearized" and for specific values of $\bar{K}_\theta$ and $\bar{K}_\phi$, standard analysis techniques may be used to obtain flutter solutions. The approach that has been used throughout this study is to assume harmonic motion and conduct eigenvalue analyses on the resulting free vibration problem. For varying magnitudes of dynamic pressure, the form of the resulting complex eigenvalues is used to determine system stability, i.e., flutter. In addition to defining the flutter critical dynamic pressure, the "flutter mode shape" is obtained during this eigenanalysis. From this mode shape, the relative root motions at flutter are defined.

Representative flutter results for the effective, or linearized system take the form as illustrated in Figures 15 and 16. These results are for the baseline control surface which is defined in Appendix A. The results given in Figure 15 are for a rigid fin while those for a flexible fin are given in Figure 16.

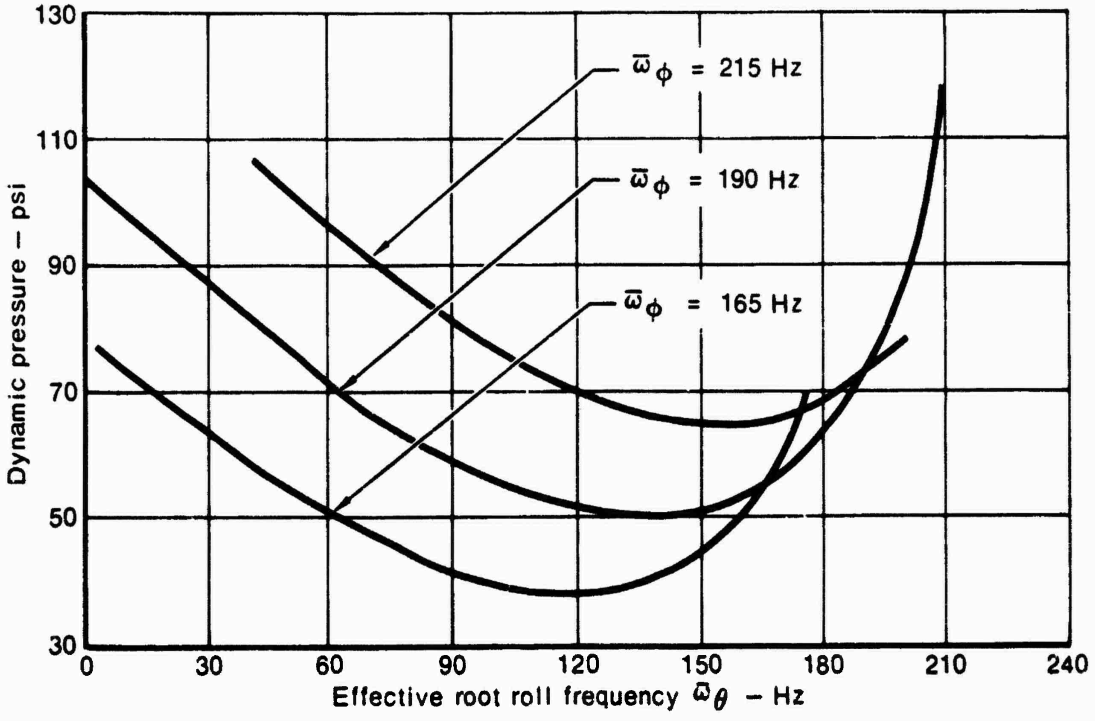

(a) Dynamic pressure

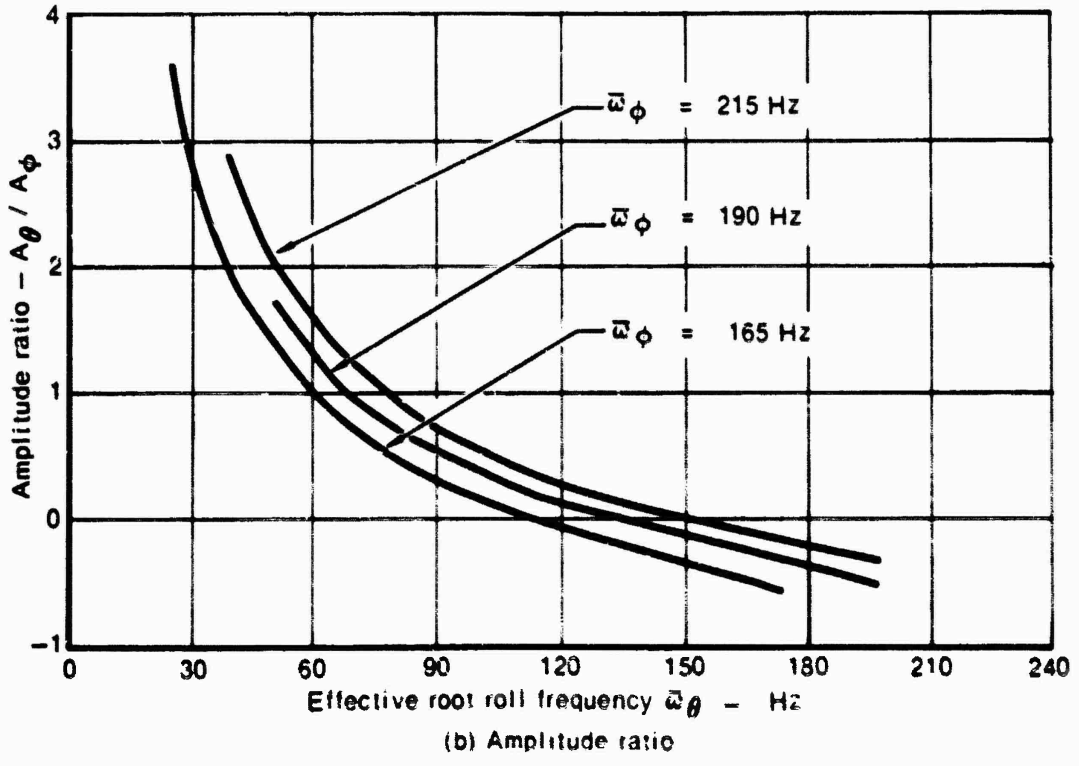

(b) Amplitude ratio

Figure 15 Effective system rigid control surface flutter results

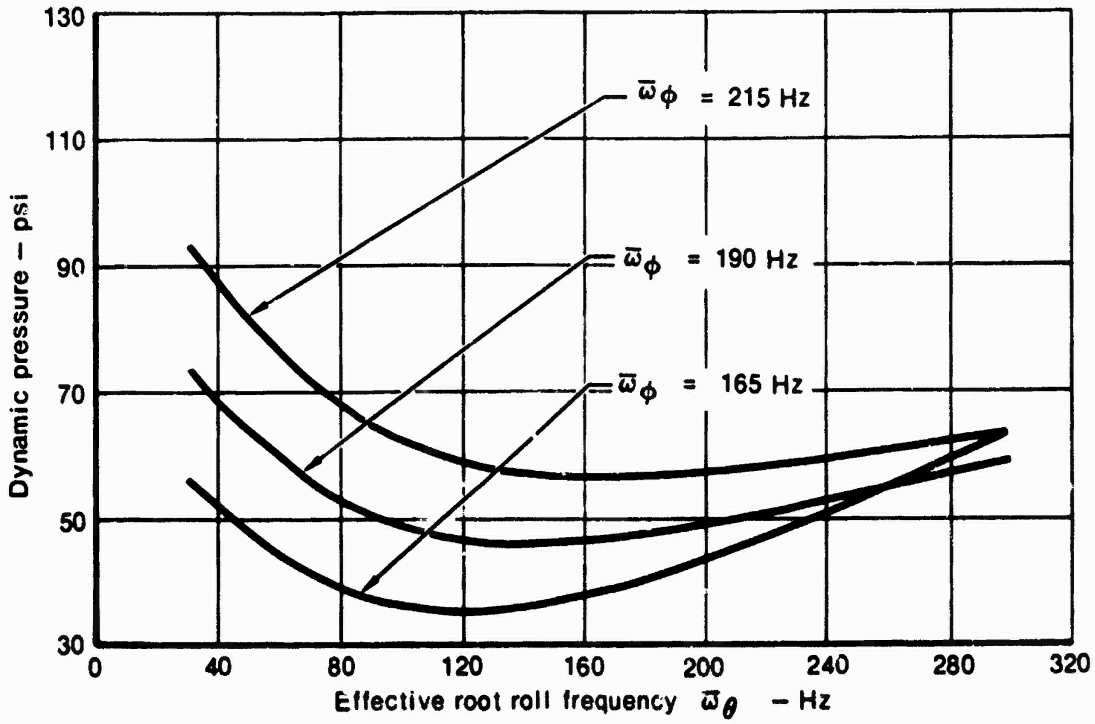

(a) Dynamic pressure

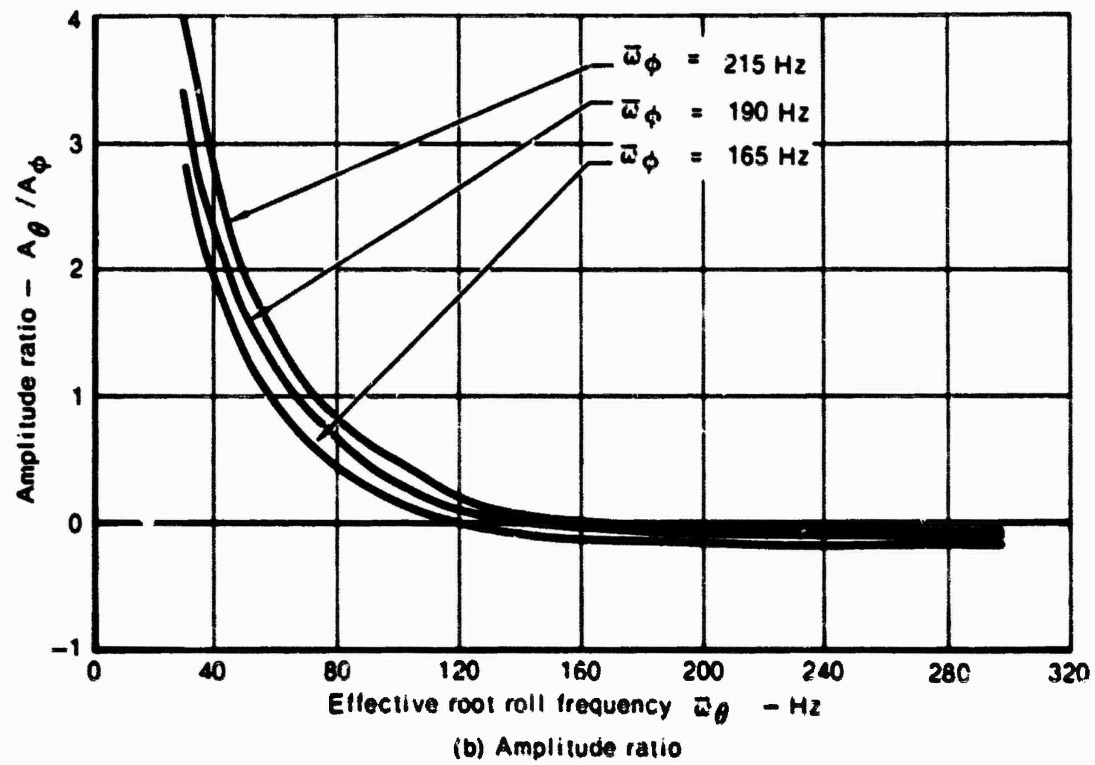

(b) Amplitude ratio

Figure 16 Effective system flexible control surface flutter results

Shown in Figures 15 and 16 are variations in flutter critical dynamic pressure as a function of effective root pitch uncoupled frequencies $\bar{\omega}_\phi$. The relationship between the effective uncoupled frequency ω_ϕ is of the form

$$\bar{\omega}_\phi = \sqrt{\delta_\theta}\, \omega_\theta \tag{27}$$

In this expression, δ_θ is the describing function for the nonlinearity in question. The magnitude of δ_θ depends on the amplitude of motion in the root roll degree of freedom. Expressions for evaluating δ_θ for the various nonlinearities considered during the study are given in Section II. A similar relationship holds for the root pitch parameter $\bar{\omega}_\phi$. Also shown in these figures are the relative magnitude of motion in the nonlinear root springs.

Presented in the following paragraphs is a discussion of the computational steps required when employing the describing function approach during control surface flutter analyses. Details of the required steps are given for each of the three nonlinearities investigated. The case of both rigid and flexible control surfaces are discussed. Effective system flutter results shown in Figures 15 and 16 form the starting point for all these discussions.

A. FREEPLAY NONLINEARITY

The procedure to be followed in obtaining the flutter boundaries of a control surface including the influence of root freeplay structural nonlinearities is summarized in Figure 17. This approach modifies the flutter results obtained for the effective system (either Figure 15 or 16) to account for the presence of the nonlinearities. For the control surface of interest, a magnitude of root pitch freeplay is selected. For a freeplay nonlinearity in a single root degree of freedom, such as root roll ($\delta_\phi = 0$), the initial step is to select magnitudes of root roll motion A_θ and effective root roll frequency $\bar{\omega}_\theta$. For the magnitude of A_θ, the describing function δ_θ is obtained from either Equation (5) or (6). Using Equation (27) the corresponding magnitude of root roll frequency ω_θ is determined. This is followed by obtaining the flutter critical dynamic pressure q for the selected value of $\bar{\omega}_\theta$ from the effective system flutter results (Figure 15 or 16). This procedure is then repeated for other values of ω_θ and A_θ and a relationship between dynamic pressure and root roll frequency ω_θ is obtained.

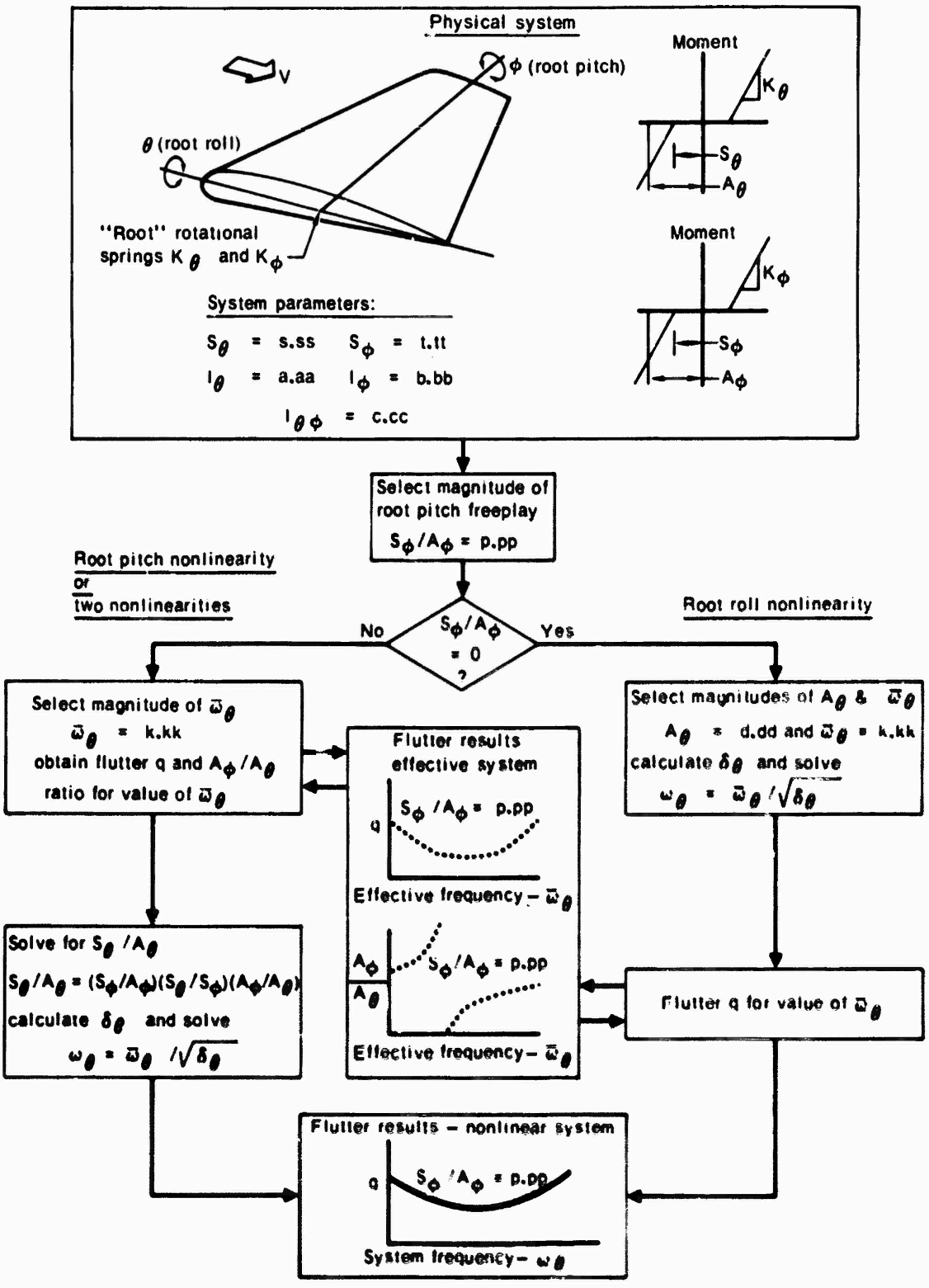

Figure 17. Computational procedure for freeplay nonlinearities

For the case of a system with two nonlinearities, ($S\phi \neq 0$), a value for the effective root roll frequency $\bar{\omega}_\theta$ is selected following the definition of the pitch freeplay. The flutter critical dynamic pressure q and amplitude ratio A_ϕ/A_θ corresponding to this value of $\bar{\omega}_\theta$ are obtained from the effective system flutter results (Figure 15 or 16). Following evaluation of the relationship

$$S_\theta/A_\theta = (S_\phi/A_\phi)(S_\theta/S_\phi)(A_\phi/A_\theta) \qquad (28)$$

the magnitude of the describing function δ_θ is obtained from Equation (5) or (6). Through application of Equation (27), the corresponding system frequency ω_θ is then defined. This procedure is repeated for additional values of the parameter $\bar{\omega}_\theta$.

For either of these cases, one or two nonlinearities, the preceding steps lead to a definition of the flutter critical dynamic pressure as a function of root roll frequency ω_θ. Such a relationship might take the form as indicated by the last step of Figure 17. A family of these curves can be obtained which will account for variations in the magnitude of root pitch freeplay.

Results for a rigid control surface with a freeplay nonlinearity in the root pitch degree of freedom are shown in Figure 18. These results are for a deadspace S_θ of 0.2 degrees and various uncoupled root roll frequencies ω_θ. For small motion in the pitch degree of freedom the effective frequency $\bar{\omega}_\theta$ approaches ω_ϕ and the critical dynamic pressure approaches that of the linear system.

Extending these procedures to a control surface with two freeplay nonlinearities yields results such as shown in Figure 19. The cause of the branch in the flutter critical dynamic pressure is apparent when considering the relationships of Figure 20 and the computational steps of Figure 17. Shown in Figure 20 are typical variations in the dynamic pressure and the root motion flutter mode shape A_ϕ/A_θ as a function of effective root roll frequency $\bar{\omega}_\theta$.

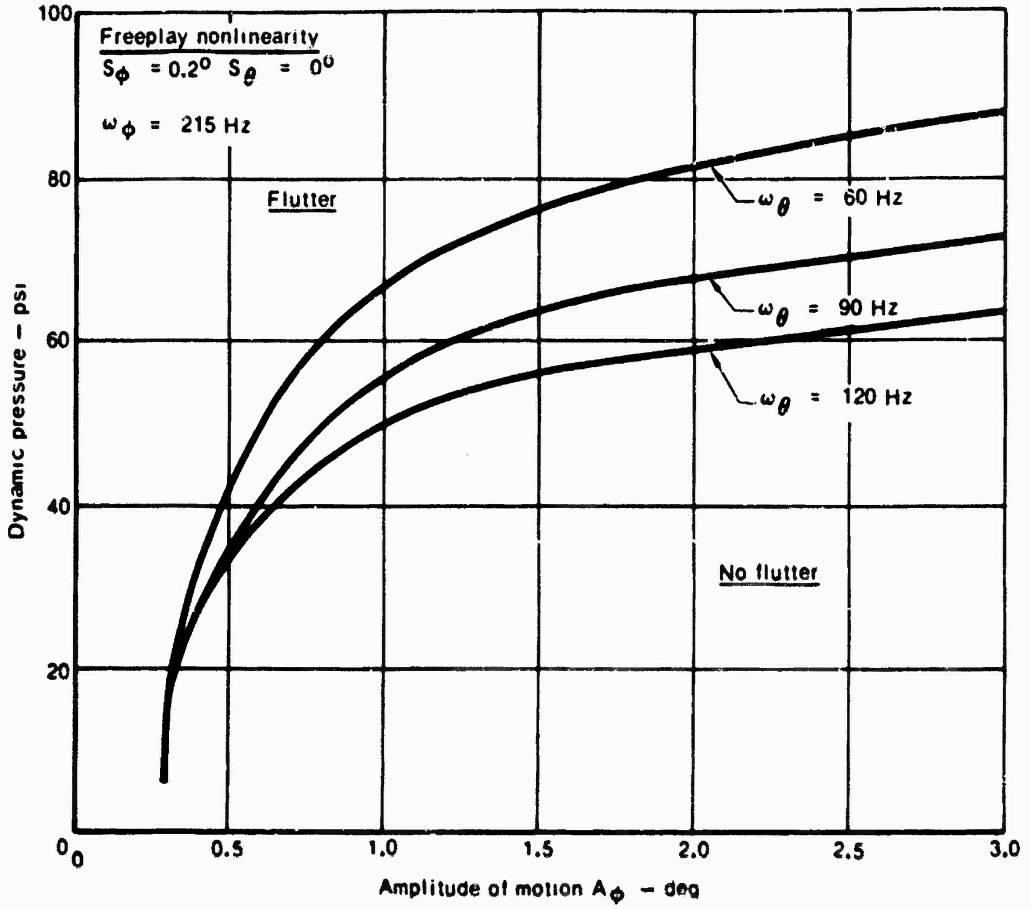

Figure 18 Flutter results for a rigid control surface with a root pitch freeplay nonlinearity

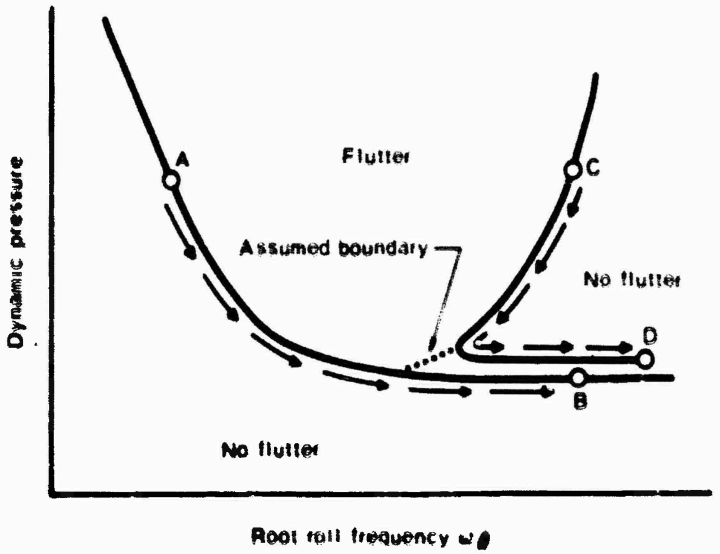

Figure 19 Typical flutter results with two nonlinearities

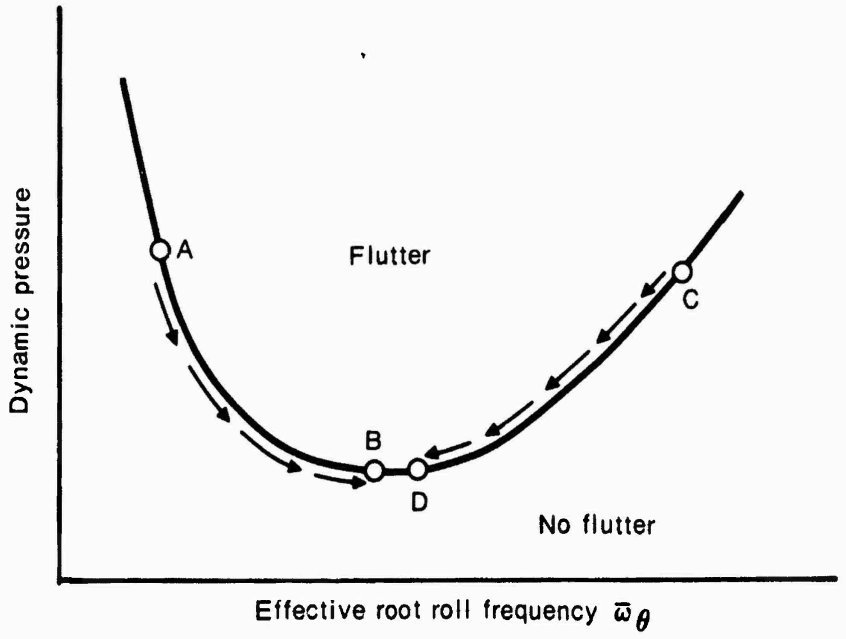

(a) Dynamic pressure

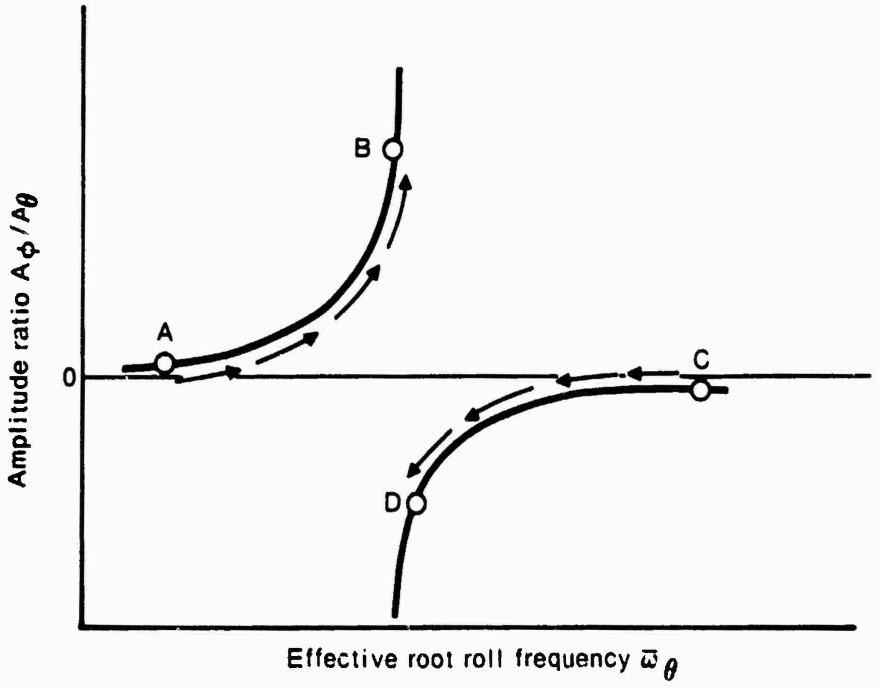

(b) Amplitude ratio

Figure 20 Typical effective system flutter results

As the magnitudes of the assumed values of $\bar{\omega}_\theta$'s approach the point of minimum dynamic pressure from the left, points A to B in Figure 20 (a), the amplitude ratio A_ϕ/A_θ approaches infinity, points A to B in Figure 20 (b). Referring to Equation (28), it is seen that this causes the amplitude of motion parameter S_θ/A_θ to approach, and possibly exceed, one. This results in the describing function δ_θ approaching zero. Since the effective and actual root roll frequencies are related by

$$\omega_\theta = \bar{\omega}_\theta/\sqrt{\delta_\theta} \tag{29}$$

this trend in δ_θ requires that ω_θ approach infinity to yield the assumed magnitude of $\bar{\omega}_\theta$. This accounts for the lower branch, points A to B, shown in Figure 19.

A similar result is obtained when the magnitude of the assumed $\bar{\omega}_\theta$'s approach the point of minimum dynamic pressure from the right, points C to D in Figure 20 (a), the amplitude ratio also approaches infinity, points C to D in Figure 20 (b). Following the same reasoning as before, the required ω_θ's also approach infinity. This accounts for the upper branch, points C to D in Figure 19.

Throughout the following discussions, the narrow flutter region to the right of the dip in the dynamic pressure has been neglected. Numerical solutions, Section IV, of the nonlinear flutter problem did not uncover this indicated strip of flutter critical dynamic pressure. This is reasonable since the configuration of the nonlinear system in this flutter region would change as its response grows. This configuration change is due to changes in the effective stiffnesses of the nonlinear elements as the motion becomes large. This would result in the system moving to a stable state and away from a flutter condition. Thus, the flutter boundary is assumed to be continuous from points A to C as indicated in Figure 19.

Following the steps outlined in the preceding paragraphs, the effective system flutter boundaries shown in Figures 15 and 16 are converted to a definition of the flutter critical dynamic pressure accounting for the presence of two root freeplay nonlinearities. Typical results for two control surface configurations, rigid or flexible, are shown in Figures 21 and 22.

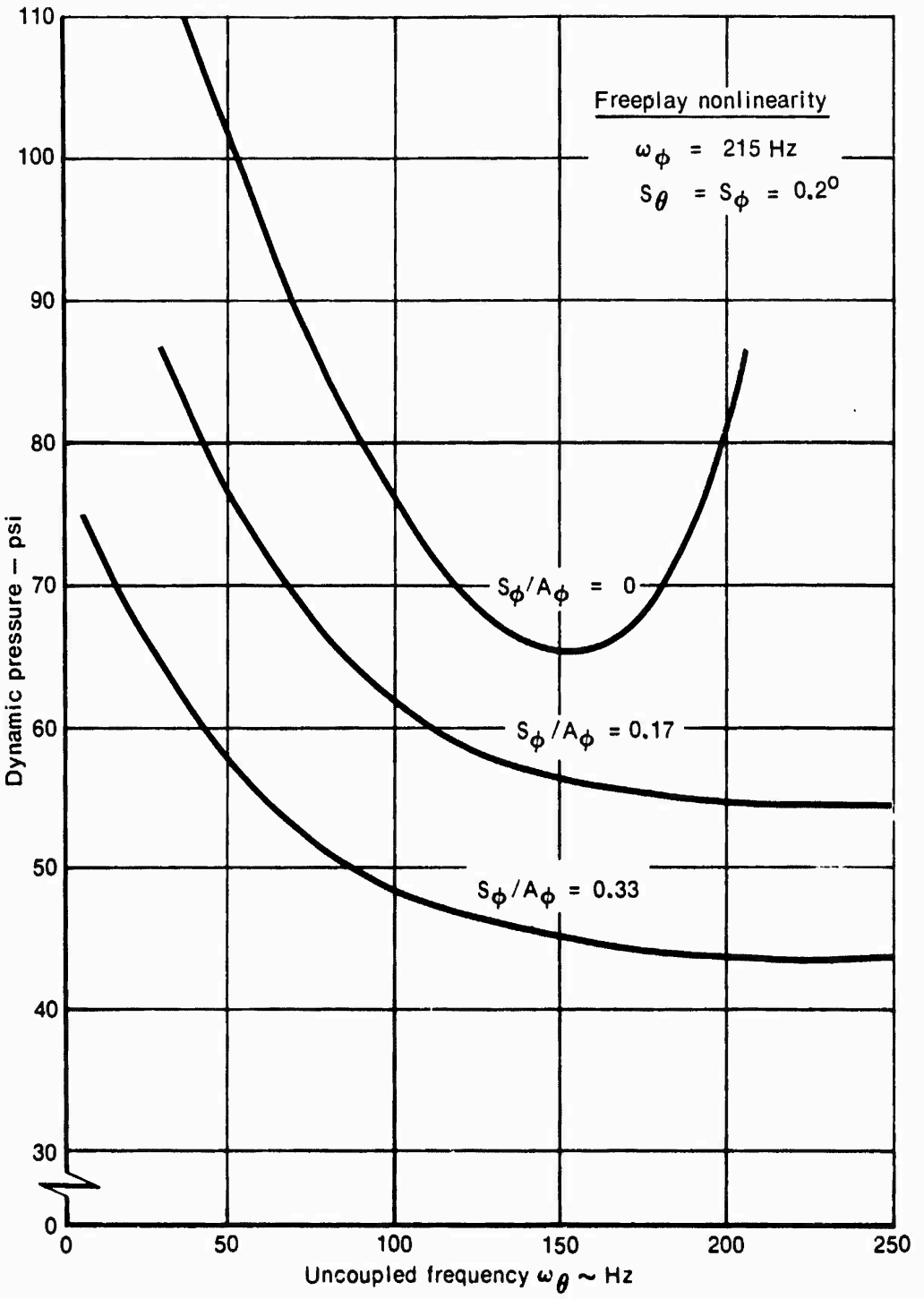

Figure 21 Flutter results for a rigid control surface with two freeplay nonlinearities

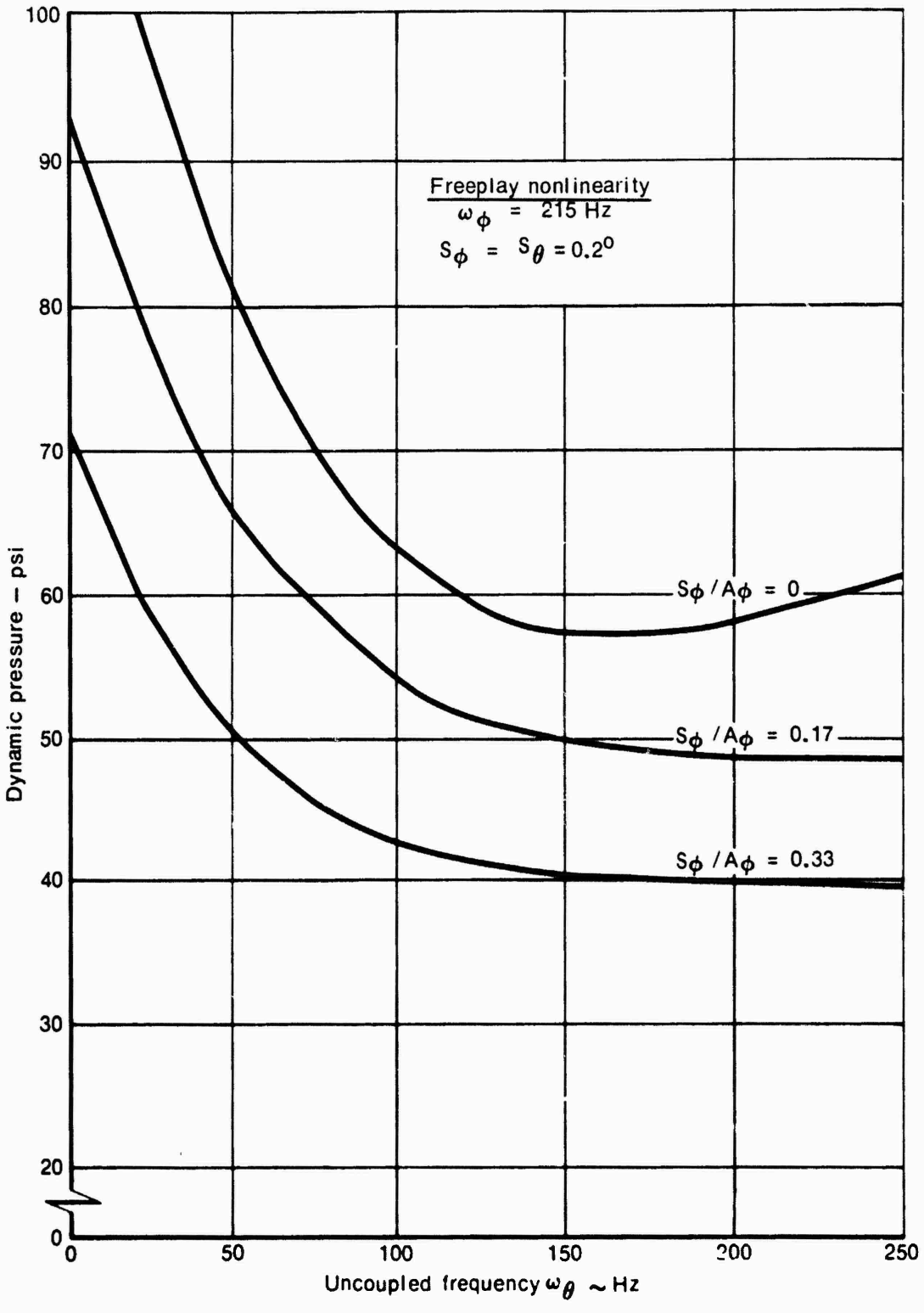

Figure 22 Flutter results for a flexible control surface with two freeplay nonlinearities

These results are presented as a function of the uncoupled root roll frequency ω_θ. The family of curves shown in these figures account for variations in the magnitude of the amplitude of motion ratio S_ϕ/A_ϕ. The physical properties of the rigid and flexible control surfaces are presented in Appendix A.

In the case of two system nonlinearities, it should be noted that only the dynamic pressure versus effective root roll frequency curve corresponding to the system's uncoupled root pitch frequency ($\bar{\omega}_\phi = \omega_\phi$) in Figure 15 (a) represents a flutter boundary. The remaining curves are indicative of the stable limit cycle amplitudes of oscillation of the system for dynamic pressures below the critical flutter value. The effective root pitch frequency curves of Figure 15 (a) can also be interpreted as individual S_ϕ/A_ϕ, δ_ϕ or A_ϕ curves.

B. PRELOAD NONLINEARITY

The procedure to be followed when conducting the flutter analysis of a control surface with preload nonlinearities are very similar to that presented in the preceding section for the case of freeplay nonlinearities. As with freeplay nonlinearities, flutter studies for a control surface system having preload nonlinearities employ the concept of effective stiffnesses. In a manner similar to that for a linear system, flutter analyses are conducted for variations in the effective stiffness parameter. These flutter results are then modified to account for the presence of the structural nonlinearities.

The computational steps to be followed during the flutter analysis of a control surface including the influence of preload nonlinearities are presented in Figure 23. For the control surface of interest, a magnitude of root roll preload is selected. With a nonlinearity in just the root roll degree of freedom, (S_ϕ = 0) the initial step is to select magnitudes of root roll motion A_θ and effective root roll frequency $\bar{\omega}_\theta$. For the selected magnitude of A_θ, the describing function N_θ is obtained from the Equation (14) or (16).

The actual uncoupled roll frequency ω_θ is related to the effective frequency $\bar{\omega}_\theta$ by the expression given as Equation (27). The actual roll frequency can then be calculated from this relationship for the particular value of the describing function. This is followed by obtaining the flutter critical dynamic pressure q for the selected value of ω_θ from the effective system flutter results, Figure 15 or 16. This procedure is then repeated for

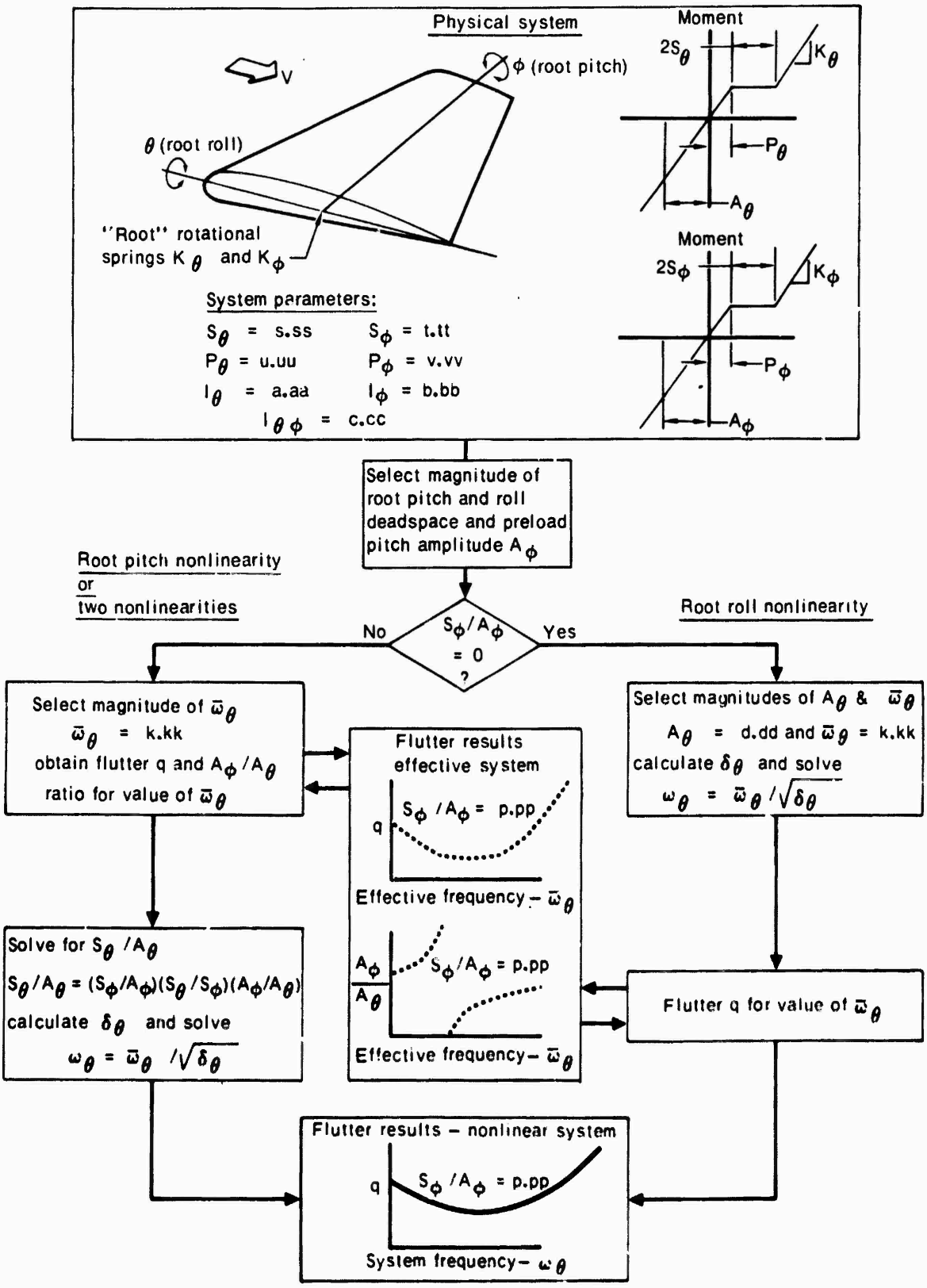

Figure 23 Computational procedure for preload nonlinearities

other values of $\bar{\omega}_\theta$ and A_θ and a relationship between the dynamic pressure and root roll frequency is obtained.

For the case of a system with two nonlinearities ($S_\phi \neq 0$), a value for the effective root roll frequency $\bar{\omega}_\theta$ is selected following definition of the pitch degree of freedom dead space and preload. The flutter critical dynamic pressure q and amplitude ratio A_ϕ/A_θ corresponding to this value of $\bar{\omega}_\theta$ are obtained from the effective system flutter results, Figure 15 or 16. Following evaluation of Equation (28) to obtain the corresponding S_θ/A_θ ratio, the magnitude of the describing function δ_θ is obtained from Equation (14) or (16).

It is possible for the amplitude ratio A_ϕ/A_θ to be negative. Calculation of the describing function from this case involves determining the positive amplitude corresponding to the negative A_θ. The positive A^+ and negative A^- amplitudes of motion for a preload nonlinearity are related by the expression

$$A^- = \sqrt{(A^+ - 2S)^2 + 4\,PS} \qquad (30)$$

With the positive A_θ from Equation (30), the describing function δ_θ is obtained from Equation (14) or (16) and the corresponding system frequency, ω_θ, is found. This procedure is then repeated for additional values of the parameter $\bar{\omega}_\theta$.

For either of these cases, one or two nonlinearities, the preceding steps lead to the definition of the flutter critical dynamic pressure as a function of root roll frequency ω_θ. Such a relationship might take the form as indicated by the last step of Figure 23. A family of these curves can be obtained which will account for variations in the magnitude of root pitch preload nonlinearity.

Flutter results have been obtained, Figure 24, for a rigid control surface having a single root roll preload nonlinearity. Presented in this figure is the flutter critical dynamic pressure as a function of root roll amplitude of motion for varying freeplay to preload, S_θ/P_θ, ratios. For amplitudes of motion less than the preload, the critical dynamic pressure equals the linear system value. As the amplitude of motion increases the influence of the deadspace is reflected in the raising of the critical

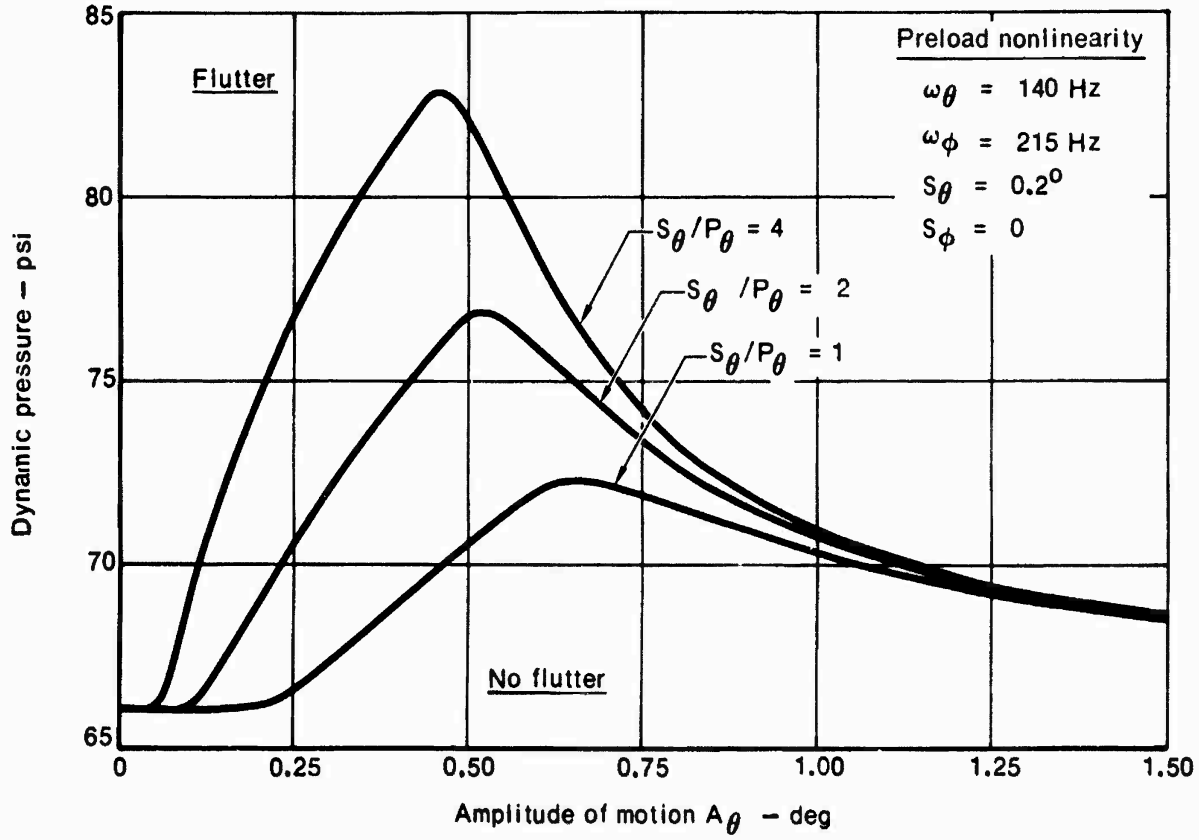

Figure 24 Flutter results for a rigid control surface with a single root roll preload nonlinearity

dynamic pressure. This is due to the softening effect on the effective root roll stiffness which results in a higher flutter critical dynamic pressure. As the amplitude of motion continues to increase, the influence of the nonlinearity decreases and the results again approach those of the linear system.

A rigid control surface having preload nonlinearities in both root degrees of freedom was also studied. Flutter results are presented in Figure 25 for a 0.2 degree deadspace in both root degrees of freedom and a deadspace to preload (S/P) ratio of two. The family of curves shown in this figure account for variations in the magnitude of the amplitude of motion ratio, S_ϕ/A_ϕ. It should be noted that the effective stiffness of a preload nonlinearity is a double valued function as illustrated in Figure 7. Thus the results indicated in Figure 25 are for double valued magnitudes of motion ratios. The larger S_ϕ/A_ϕ values correspond to amplitudes less than the quantity P + 2S whereas the lower ratios correspond to amplitudes in excess of this value.

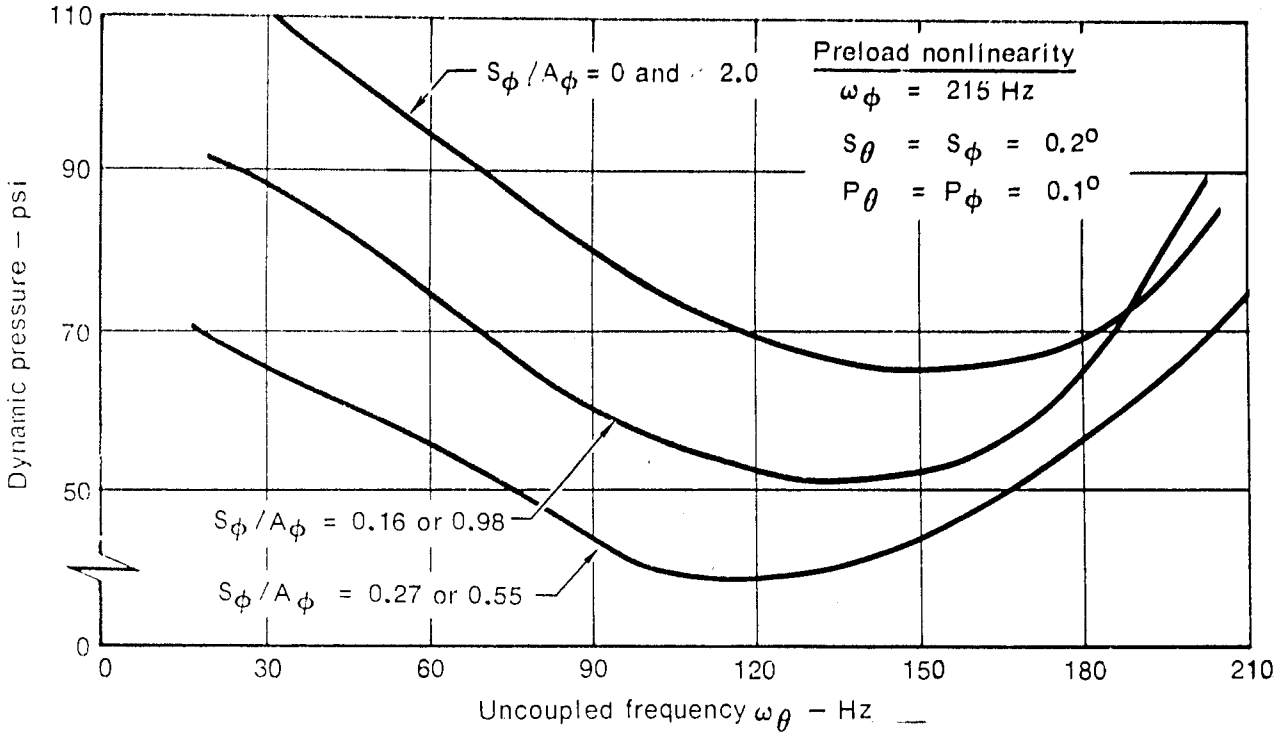

Figure 25 Flutter results for a rigid control surface with two preload nonlinearities

Finally a flexible control surface having preload nonlinearities in both root degrees of freedom was studied. Presented in Figure 26 are flutter results for a 0.2 degree deadspace in both root degrees of freedom and deadspace to preload ratios (S/P) of two. The curves depict the dynamic pressure as a function of uncoupled root roll frequency ω_θ for various amplitude of motion ratios S_ϕ/A_ϕ. As with the rigid control surface case, the amplitude ratios are double valued. The larger S_ϕ/A_ϕ values correspond to amplitudes less than the quantity P + 2S whereas the lower ratios are for amplitude values in excess of this quantity. The change in slope on the curve for an S_ϕ/A_ϕ of 0.27 or 0.55 is caused by the root roll amplitude of motion moving in and out of the linear range on the preload root roll spring.

C. FRICTION NONLINEARITY

The procedures to be followed when conducting the flutter analysis of a control surface with friction nonlinearities are very similar to that presented in the preceding sections for the freeplay and preload cases. As with a linear system, flutter analyses are conducted for variations in the effective stiffness parameter. The flutter results are then modified to account for the presence of the friction nonlinearities.

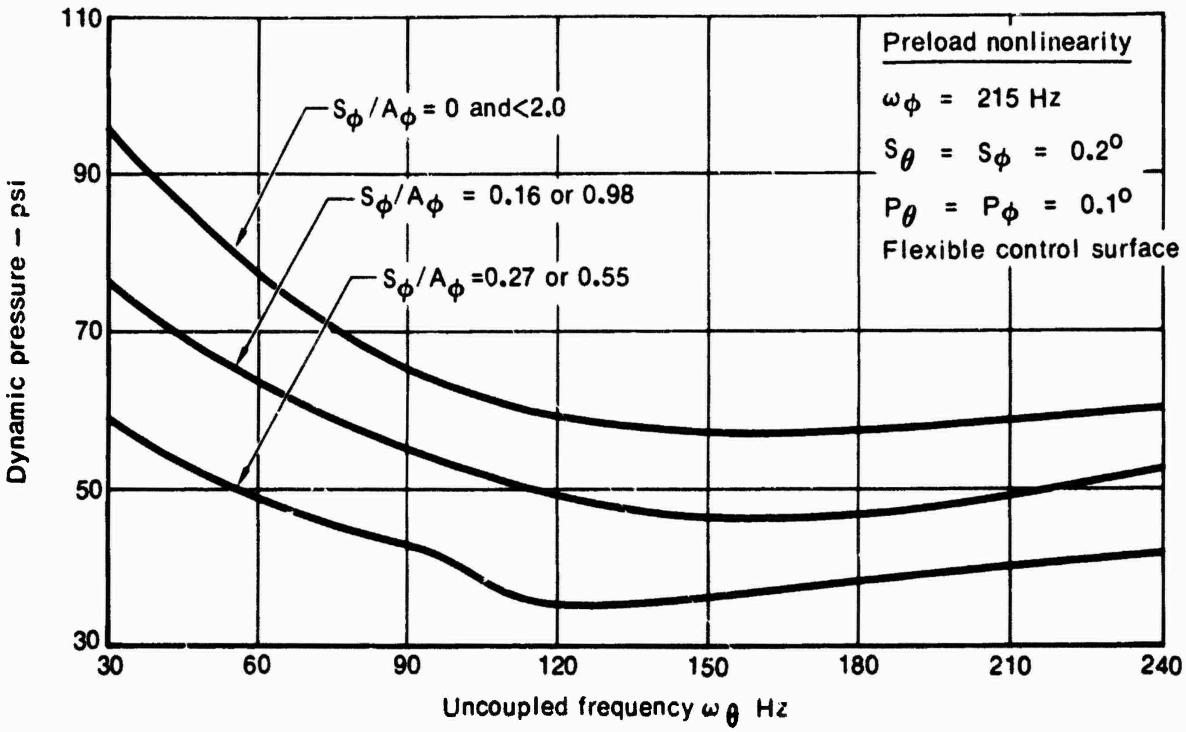

Figure 26 Flutter results for a flexible control surface with two preload nonlinearities

The presence of damping in the friction nonlinearity will potentially cause the flutter analysis procedure to differ from that of the other two nonlinearities. The concept of effective stiffnesses is still employed but an additional parameter, the effective damping g, will play a role in the analysis procedure. As with a linear system, flutter analyses are conducted for variations in the effective stiffness. The approach of the flutter analysis is to assume harmonic motion and conduct eigenvalue analyses on the resulting free vibration problem. For varying magnitudes of dynamic pressure, the form of the resulting complex eigenvalues is used to determine system stability i.e., flutter.

Typical flutter analyses results take the form of Figure 27 (a). For given system parameters and dynamic pressures less than the critical flutter value for the assumed simplified aerodynamics, the eigenvalue analysis predicts unequal real roots. At the flutter point and points beyond flutter we obtain complex roots having equal real parts or frequency coalescence, and nonzero imaginary parts. The amount of damping required to maintain stable system oscillations above the flutter critical dynamic pressure can be

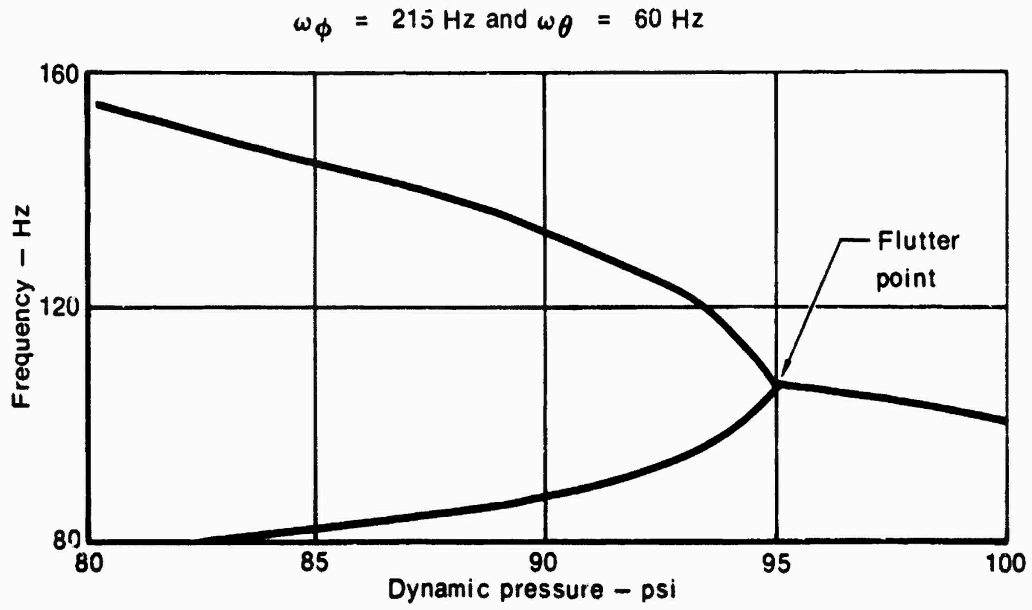

(a) Frequency coalescence

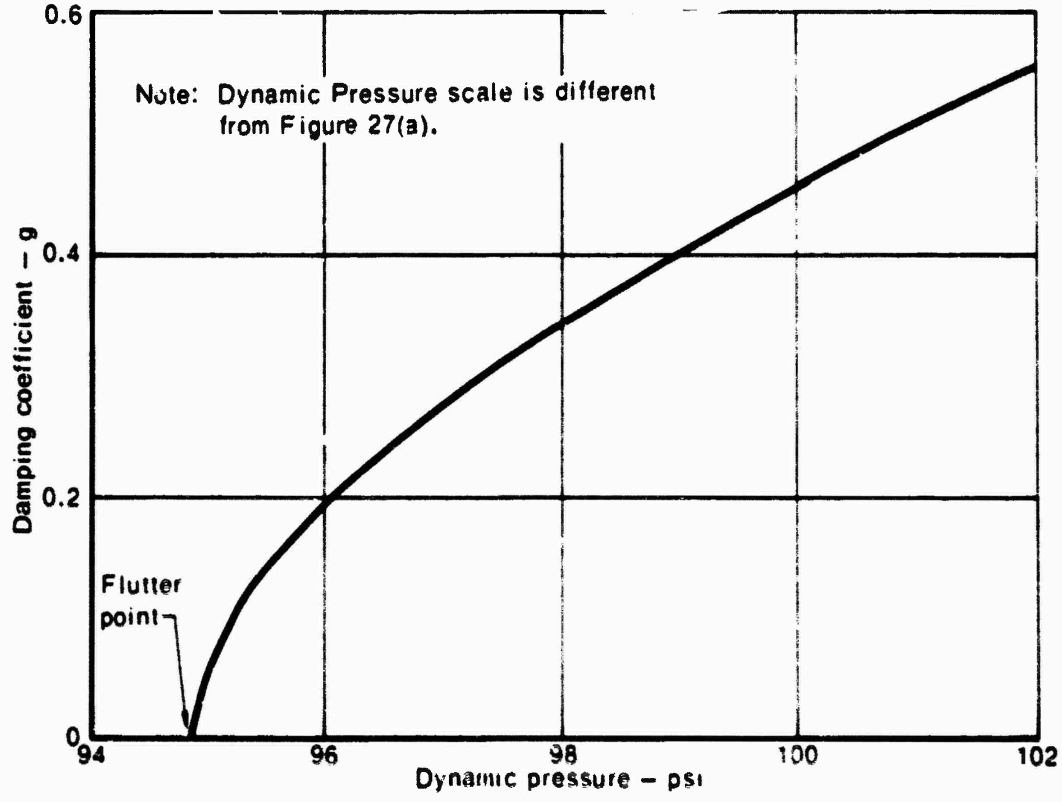

(b) Damping

Figure 27 Results from simplified flutter analysis

related to increasing dynamic pressure as illustrated in Figure 27 (b). Attributing system damping to the friction nonlinearity in a system, we can obtain the family of flutter curves such as shown in Figure 28 for a single root nonlinearity. In Figure 28, the variation of dynamic pressure as a function of the effective root roll frequency $\bar{\omega}_\theta$ is illustrated for various effective root pitch frequencies $\bar{\omega}_\phi$ and effective damping coefficients $\bar{g}$ corresponding to each $\bar{\omega}_\phi$.

The computational procedure to be followed for a single friction nonlinearity is summarized in Figure 29. If we assume a single nonlinearity in the root pitch degree of freedom, the effective root roll frequency and the uncoupled root roll frequency will be one and the same. Choosing a root pitch amplitude, A_ϕ, we can calculate the describing function "delta" δ_ϕ, the effective damping $\bar{g}$, and the effective root pitch frequency $\bar{\omega}_\phi$ corresponding to the particular S_ϕ/A_ϕ value. The flutter critical dynamic pressure corresponding to these parameters is then obtained from the effective system flutter results such as Figure 28. These steps lead to the definition of the flutter critical dynamic pressure as a function of root roll frequency ω_θ. Such a

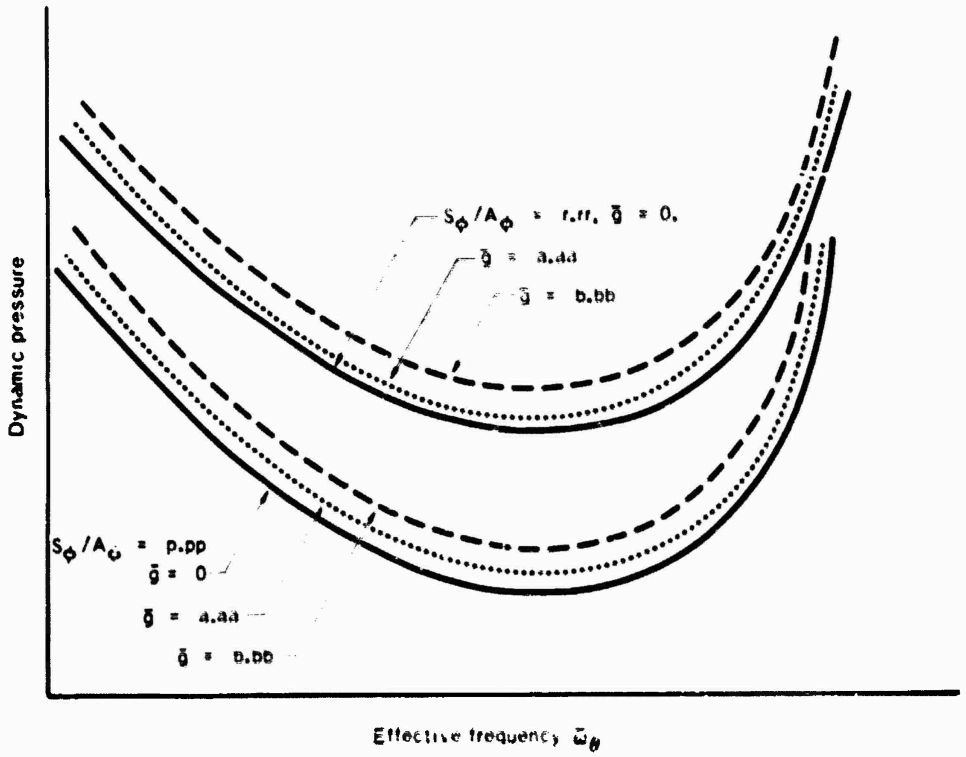

Figure 28 Effective system flutter results for friction nonlinearity with damping

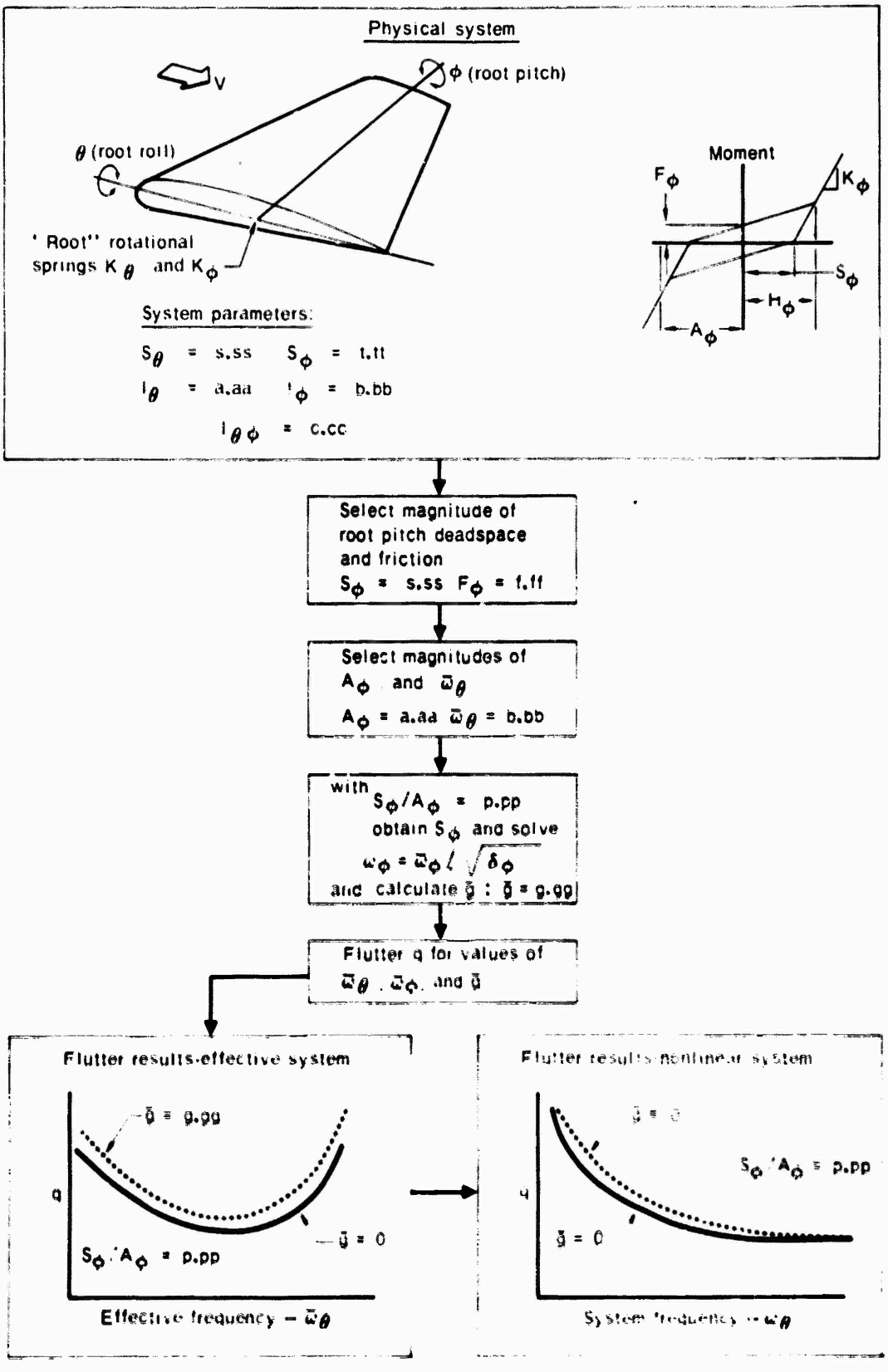

Figure 29 Computational procedure for a single friction nonlinearity

relationship might take the form as indicated by the last step of Figure 29. A family of these curves can be obtained which will account for variations in the magnitude of root pitch nonlinearity.

Flutter results have been obtained, Figure 30, for a rigid control surface having a single root pitch nonlinearity. Presented in this figure is the amplitude ratio S_ϕ/A_ϕ as a function of the flutter critical dynamic pressure. The describing function prediction curves are shown both with and without damping included. The influence of the damping on the flutter dynamic pressure is very small. It is of interest to note that effective damping of a friction nonlinearity is greater at small amplitudes of motion, Figure 14. Thus as the amplitude A_ϕ increases toward divergent flutter, Figure 30, it would be expected that the effective damping will become less important.

This negligible influence of the effective damping associated with a friction nonlinearity is apparent from the results of Figure 30. It is also significant that this influence is even smaller close to the point of divergent flutter. For these reasons, and because of the major complication it

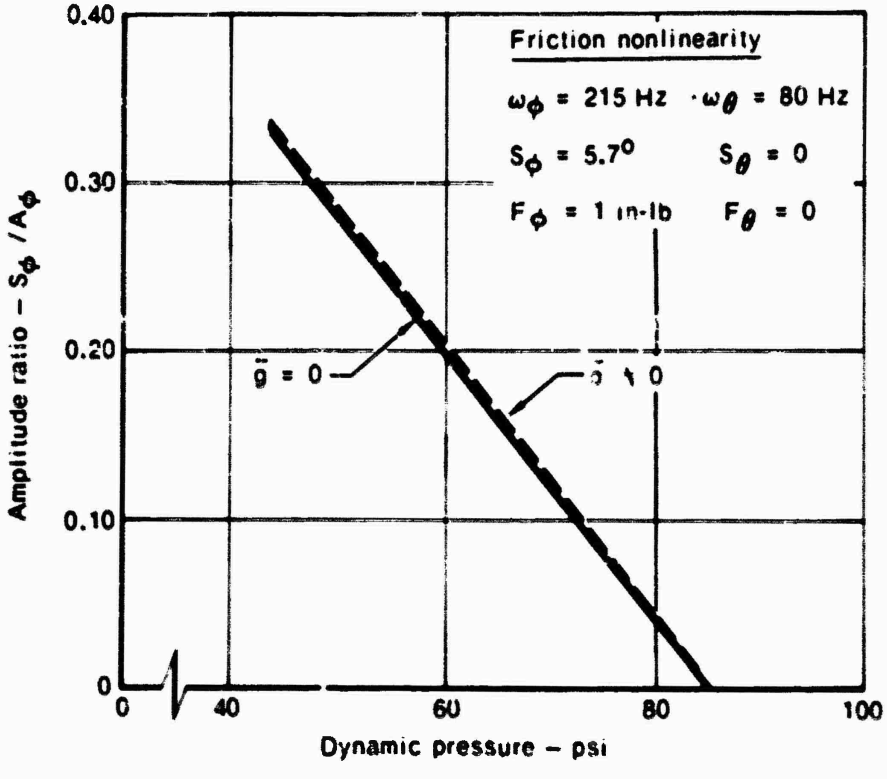

Figure 30 Flutter results for a rigid control surface with a root pitch friction nonlinearity

would cause in the flutter analysis procedure, it has been assumed that this damping term may be neglected in the final analysis procedure for friction nonlinearities.

Thus the computational steps to be followed during the flutter analysis, including the influence of friction nonlinearities, are presented in Figure 31. For the control surface of interest a magnitude of root roll deadspace and friction is selected. With a nonlinearity in just the root roll degree of freedom (S_ϕ and $F_\phi = 0$) the initial step is to select magnitudes of root roll motion A_θ and effective root roll frequency $\bar{\omega}_\theta$. For the selected magnitude of A_θ, the describing function δ_θ is obtained from Equation (25).

The actual uncoupled frequency ω_θ is a function of the effective frequency $\bar{\omega}_\theta$ and the describing function as defined by Equation (27). The actual roll frequency can then be calculated from this relationship. This is followed by obtaining the flutter critical dynamic pressure q for the selected value of ω_θ from the effective system flutter results, Figure 15 or 16. This procedure is then repeated for other values of $\bar{\omega}_\theta$ and A_θ.

For the case of a system with two nonlinearities (S_ϕ and $F_\phi \neq 0$), a value for the effective root roll frequency $\bar{\omega}_\theta$ is selected following the definition of the pitch deadspace and friction. The flutter critical dynamic pressure and amplitude ratio A_ϕ/A_θ corresponding to this value of $\bar{\omega}_\theta$ are obtained from the effective system flutter results, Figure 15 or 16. Following evaluation of equation (28) to obtain S_ϕ/A_θ the describing function is determined by Equation (25). Thus the corresponding system frequency ω_θ can be found from Equation (29). This procedure is repeated for additional values of the parameter $\bar{\omega}_\theta$.

For either of these cases, one or two nonlinearities, the preceding steps lead to the definition of the flutter critical dynamic pressure as a function of root roll frequency ω_θ. Such a relationship might take the form as indicated by the last step of Figure 31. A family of these curves can be obtained which will account for variations in the magnitude of root pitch freeplay and friction.

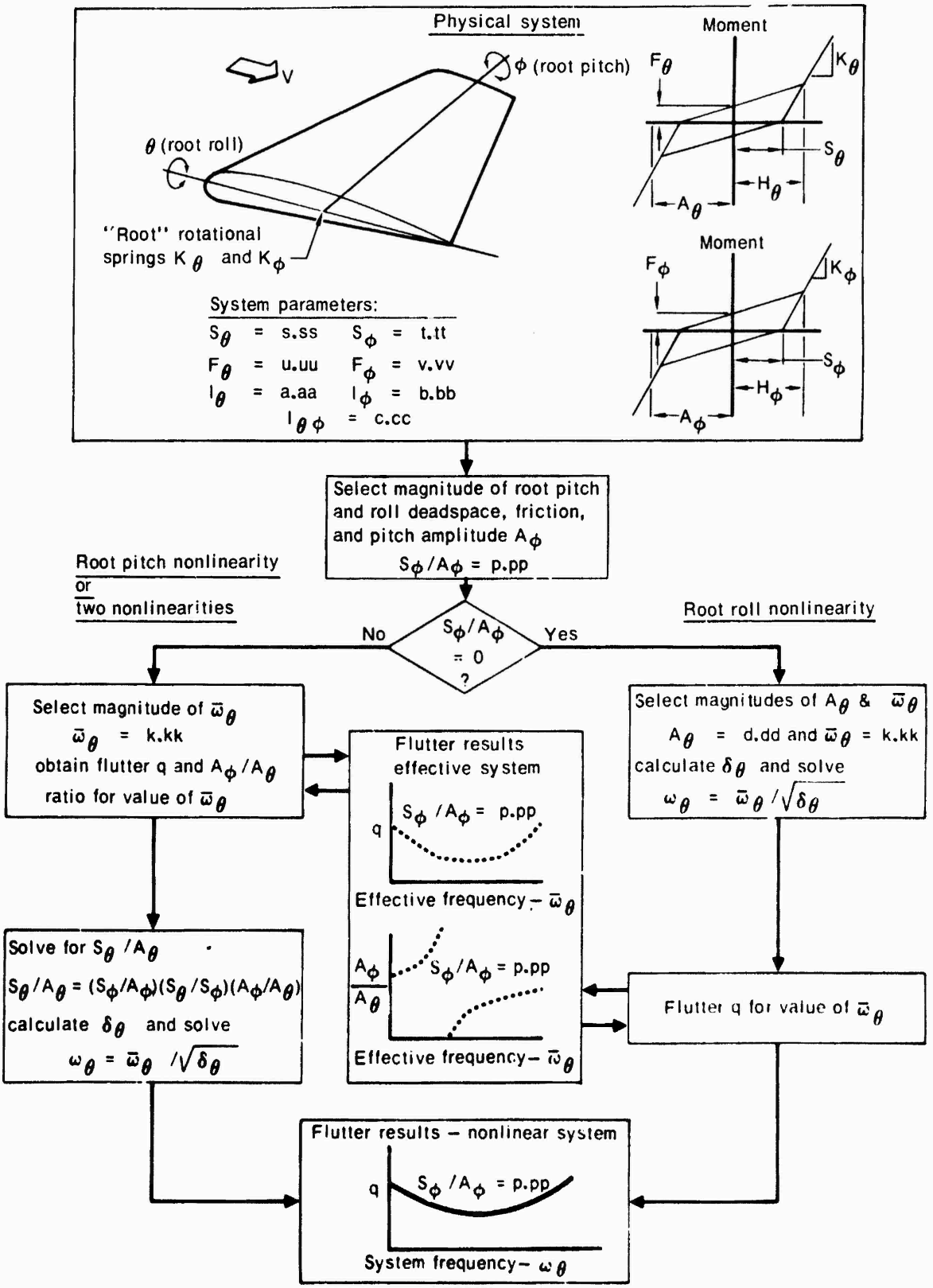

Figure 31. Computational procedure for friction nonlinearities

Flutter results for a control surface with a single friction nonlinearity will continue to take the form as illustrated in Figure 30. However, in this case, the recommended procedures of Figure 31 will correspond to the results of Figure 30 where the effective damping is zero.

Flutter results for a rigid control surface having friction nonlinearities in both root degrees of freedom are presented in Figure 32. These results are presented for 0.2 degree deadspaces in both root springs and friction terms of 25 in.-lb. An uncoupled root pitch stiffness corresponding to an uncoupled frequency ω_ϕ of 215 Hz was used in this analysis. Flutter results are presented in the form of a dynamic pressure versus uncoupled root roll frequency ω_θ for varying values of effective root pitch frequency $\bar{\omega}_\phi$ or S_ϕ/A_ϕ ratios. Notice that some of the curves predicted by the describing function analysis do not extend as far as others along the ω_θ axis. This is because the root amplitudes as predicted by the describing function technique for roll frequencies ω_ϕ in excess of the end points are less than H. Since no describing function has been written for cases where the amplitude is less than H, the describing function predictions end at their corresponding ω_θ values.

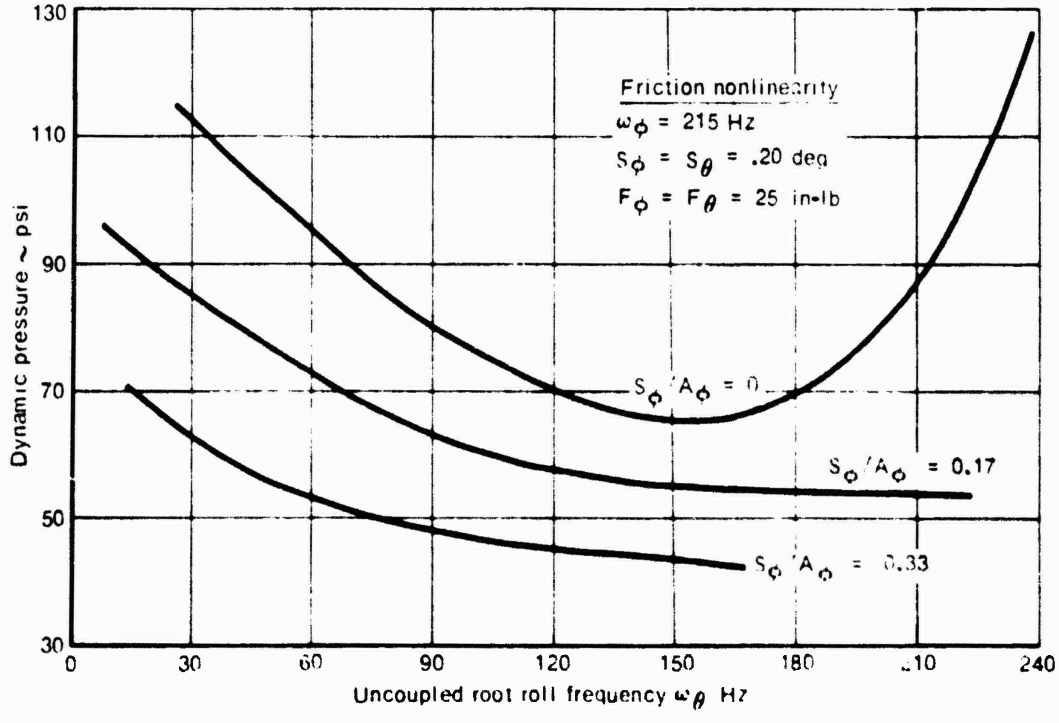

Figure 32 Flutter results for a rigid control surface with two friction nonlinearities

Finally, flutter results were obtained for the case of a flexible control surface with friction nonlinearities in both root degrees of freedom, Figure 33. As for the rigid fin, results are presented in the form of dynamic pressure as a function of the uncoupled root roll frequency for an uncoupled root pitch frequency ω_ϕ, and various effective root pitch frequencies, $\bar{\omega}_\phi$. The friction nonlinearities consisted of root roll and pitch deadspaces of 0.2 degrees and friction terms, F_θ and F_ϕ and F_ϕ, of 25 in.-lb. As mentioned for the rigid control surface studies, the describing function definition does not apply when the amplitude of motion is less than the critical H value of the system.

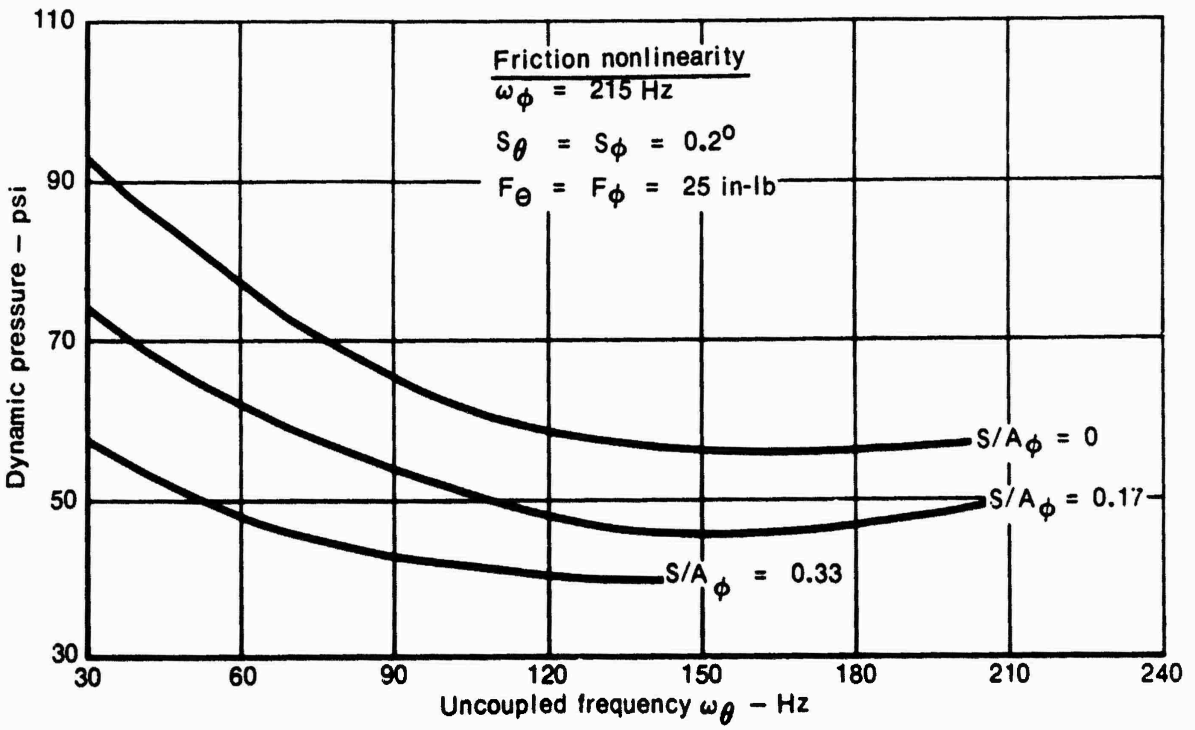

Figure 33. Flutter results for a flexible control surface with two friction nonlinearities

Section IV
ANALYSIS VERIFICATION

Ideally, the flutter predictions obtained with the techniques described in Section III of this report would be verified by comparing these predictions with experimental data obtained during a wind tunnel test program. However, the expense of such a test program is not warranted at this time due to the early stage of the theoretical development. Rather this "test" data were obtained through mathematical simulations of the nonlinear flutter problem. With this approach, the nonlinear system equations of motion, Equation (1), were numerically integrated yielding system time history response information. System stability characteristics were then obtained by evaluating the nature of this sytem response. It must be emphasized that this "verification" process only establishes the validity (or shortcomings) of the describing function approach when compared to a more exact numerical solution to the assumed mathematical representation of the nonlinear flutter problem. In the final evaluation, this approach does not replace the use of experimental (flight) data.

The general approach in this verification process was to obtain numerical solutions to the nonlinear flutter equations of motion for a control surface having particular root spring nonlinearities. Throughout these studies the baseline control surface configuration, as defined in Appendix A, was assumed. These numerical solutions, which yield system time history response information such as shown in Figure 34, were used to evaluate system stability characteristics. For example, a time history response such as shown in Figure 34(a) indicates a stable system and thus a dynamic pressure below the flutter critical value. Illustrated in Figure 34(b) is the type of system response obtained for an unstable syste and thus the dynamic pressure is above the flutter critical value. System response was obtained for increasing values of dynamic pressure q until the characteristics of the response became that of divergent oscillations. In this manner, the boundary between flutter and no flutter was evaluated for the nonlinear system.

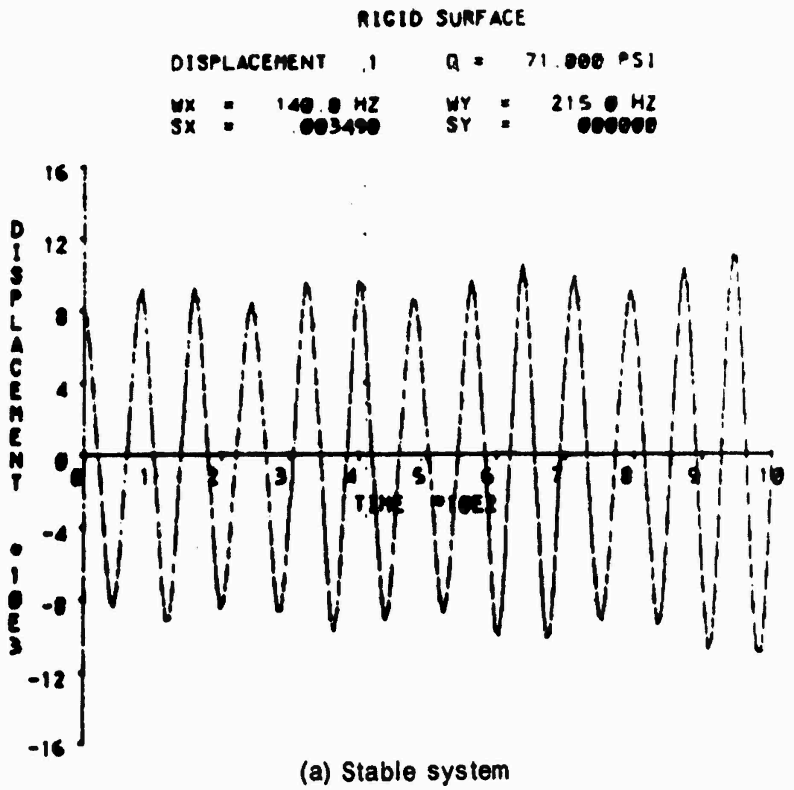

(a) Stable system

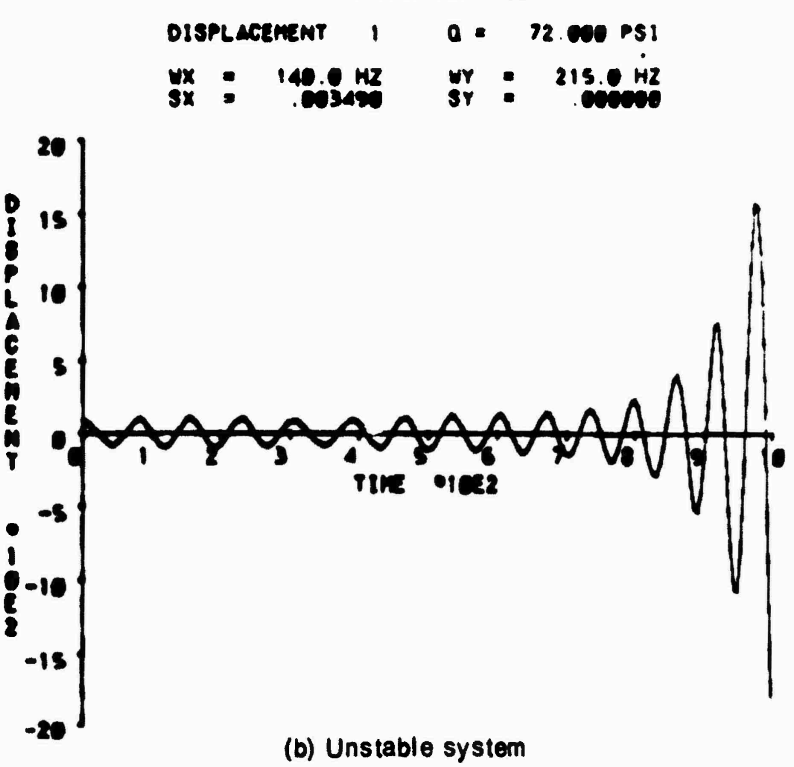

(b) Unstable system

Figure 34 Typical simulation results

Throughout the discussion of these simulation results the characteristics of the system response will be expressed in terms of RSS amplitudes of motion. In many cases, the numerical solutions did not exhibit uniform amplitudes of motion, but rather experienced a beating type phenomenon as illustrated in Figure 35. To correlate these results with the describing function predictions, an "average" amplitude of motion is employed. This amplitude, the RSS amplitude, is obtained by taking the square root of the sum of the squares of succeeding amplitude peaks over a large number of cycles of motion.

Data obtained from simulations such as described above were compared with flutter predictions employing the describing function approach to assess the validity of these predictions. Presented in the following paragraphs is a comparison and interpretation of the flutter predictions versus simulation results for each of the three type nonlinearities investigated. In each case results are presented for both a rigid and a flexible control surface.

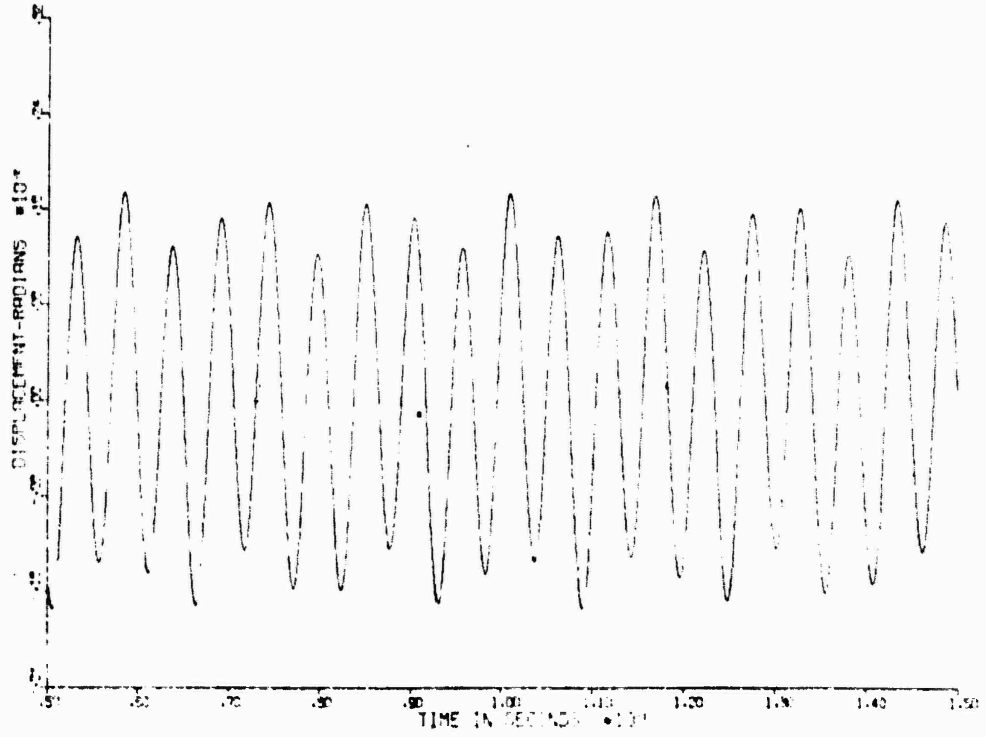

Figure 35 Example of beating type system response

A. FREEPLAY NONLINEARITY

Initial simulations were conducted for a rigid control surface having a 0.2 degree deadspace S_ϕ in the root pitch degree of freedom. Comparisons between simulation results and describing function predictions are shown in Figure 36. Note that the assumed root stiffness values result in uncoupled frequencies ω_θ of 60 Hz and ω_ϕ of 215 Hz. The predicted flutter boundary corresponds to one of the curves shown in Figure 18 Section III.

A characteristic of the response for the nonlinear system which appeared throughout the study is indicated in Figure 36. For increasing magnitudes of dynamic pressure, the system response tends to become divergent in nature. However, this has the effect of "working" the nonlinear root spring to a greater extent. Thus the oscillation builds up to some amplitude and then becomes stable again where the system is experiencing a limit cycle type response. This trend of stable limit cycle response continues with increasing dynamic pressure, as illustrated in Figure 36, where simulation data points are related to the resulting amplitude of the limit cycle motion. Above some critical dynamic pressure, the limit cycle motion no longer holds and we have the classic divergent flutter motion.

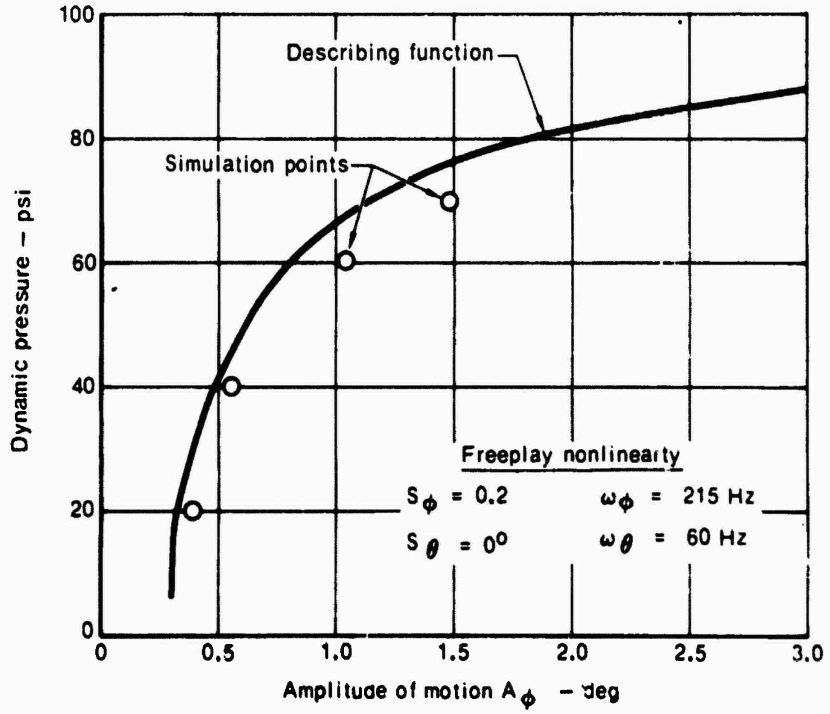

Figure 36 Simulation results for a rigid control surface with a root pitch freeplay nonlinearity

This latter point is more clearly illustrated by presenting the data in the format as shown in Figure 37. Here the amplitude ratio S_ϕ/A_ϕ is plotted as a function of the dynamic pressure. Increasing amplitude of motion corresponds to a decreasing S/A amplitude ratio. Thus the amplitude ratio decreases with increasing dynamic pressure until the point of divergent flutter is reached.

The comparison between simulation and describing function results was extended to the case of a rigid control surface with nonlinearities in both pitch and roll degrees of freedom. These simulation results, presented in Figure 38, are for a system with equal magnitudes of deadspace in the two root degrees of freedom. Specifically, the magnitude of deadspace for both pitch and roll was assumed to be 0.2 degrees. In addition, the magnitudes of root stiffnesses result in an uncoupled frequency ω_ϕ of 215 Hz and uncoupled frequencies ω_θ of either 60 or 200 Hz.

As in the case with a single nonlinearity, the system experiences a stable limit cycle type response which continues with increasing dynamic pressure. Shown in Figure 38 are simulation data points related to the resulting S_ϕ/A_ϕ ratios of the limit cycle motion. Above some critical

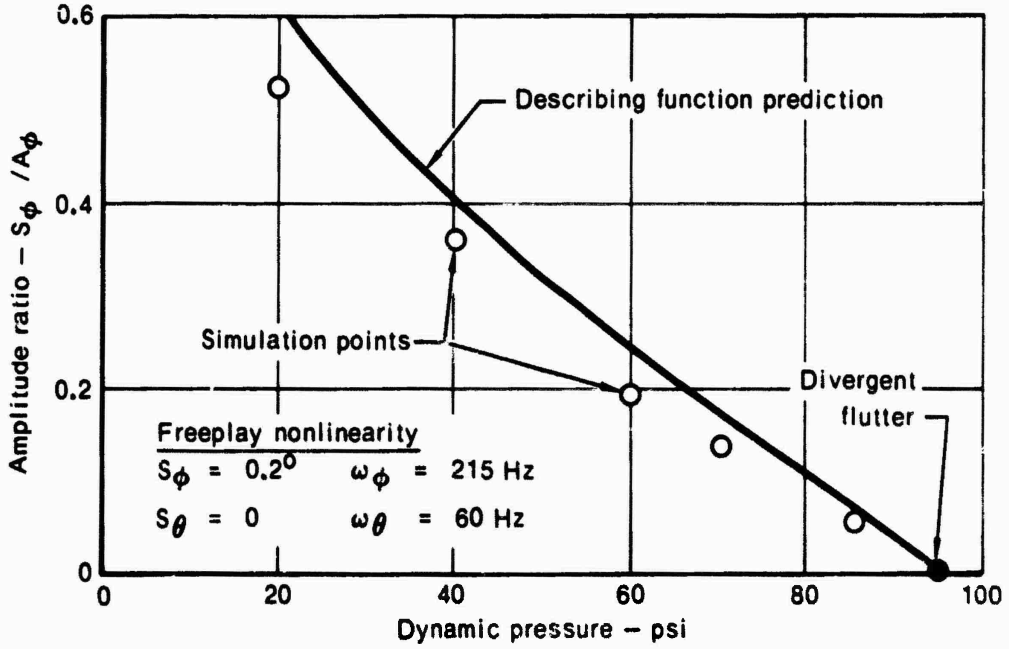

Figure 37 Comparison of rigid control surface pitch motion for a single freeplay nonlinearity in the root pitch degree of freedom

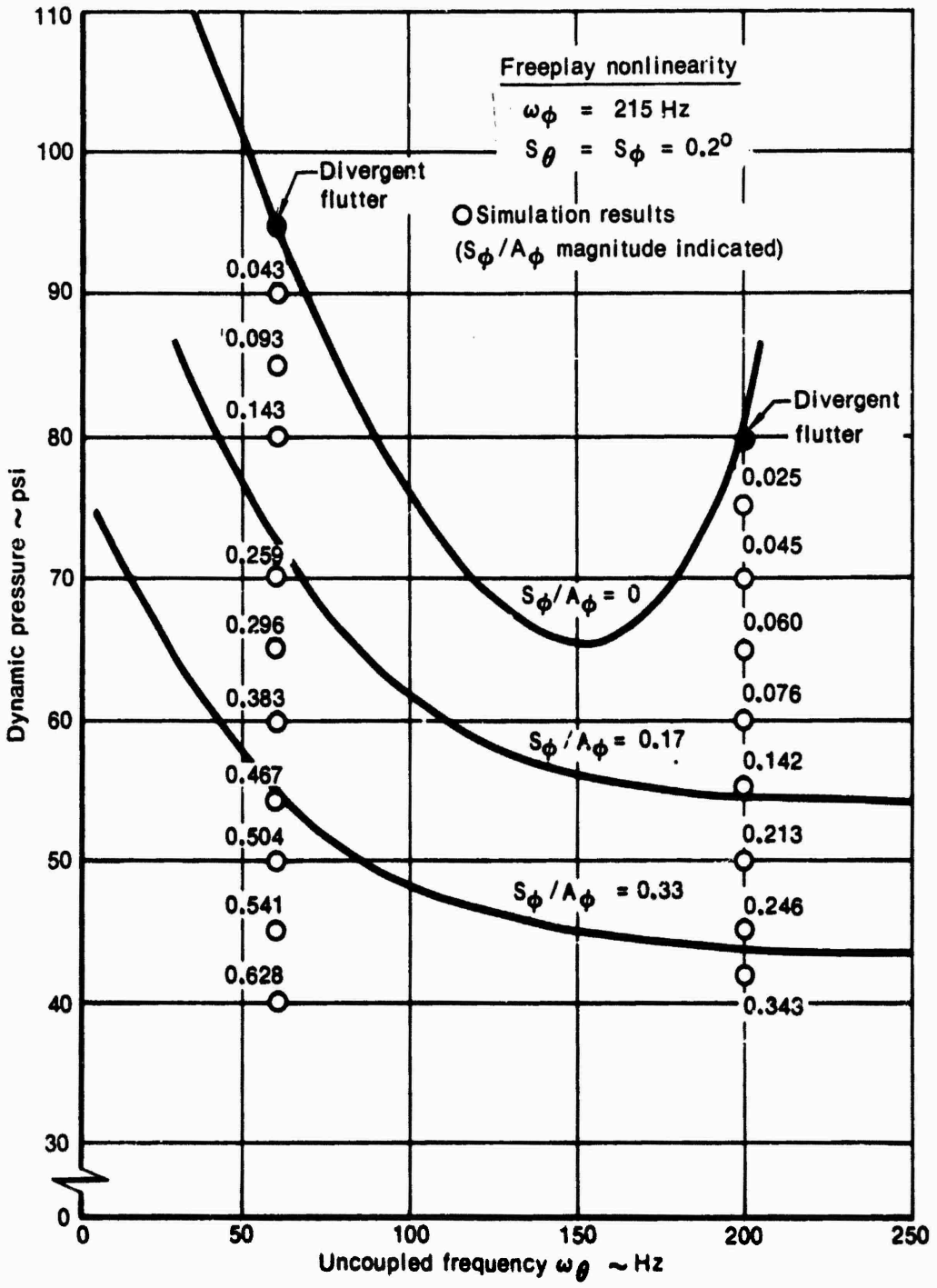

Figure 38 Simulation results for a rigid control surface with two freeplay nonlinearities

dynamic pressure, the limit cycle motion no longer holds and we have the classic divergent flutter motion. The simulation points designated as divergent flutter correspond to very small S_ϕ/A_ϕ ratios which are on the order of $1. \times 10^{-6}$. These conclusions are further illustrated in Figure 39 which compare simulation and describing function predictions of the amplitude ratios as a function of dynamic pressure.

Similar results for a flexible control surface are given in Figure 40. Here information is presented for the baseline control surface with either an uncoupled root roll frequency ω_θ of 60 or 140 Hz. In addition, the uncoupled root pitch frequency ω_ϕ is 215 Hz and the magnitude of deadspace was assumed to be 0.2 degrees for both degrees of freedom. A more complete comparison for both root roll and pitch motions are presented in Figure 41. As with the rigid control surface, the limit cycle amplitudes of motion build up with increasing dynamic pressure to the point of divergent flutter.

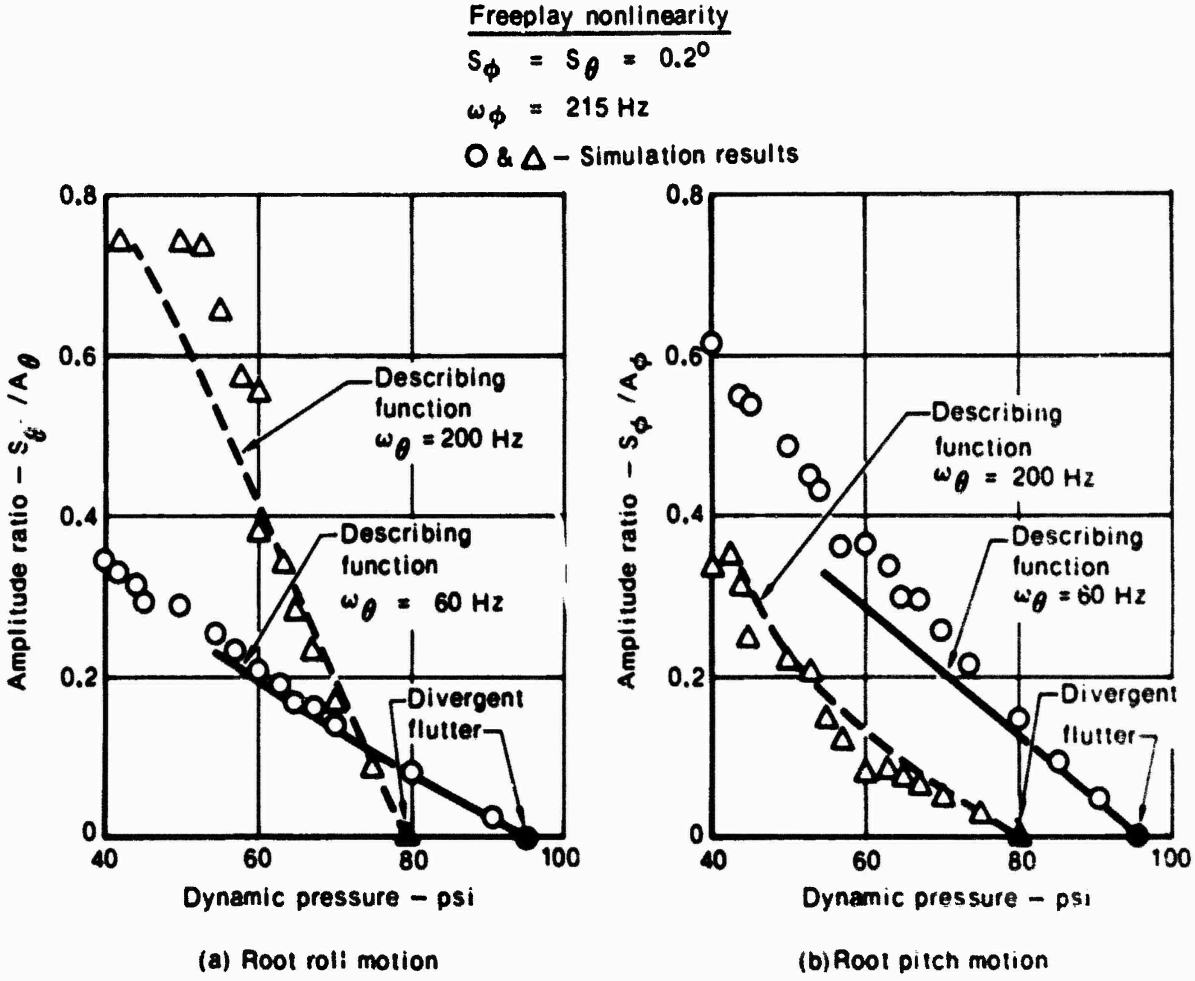

Figure 39. Comparison of rigid control surface root motions for two freeplay nonlinearities

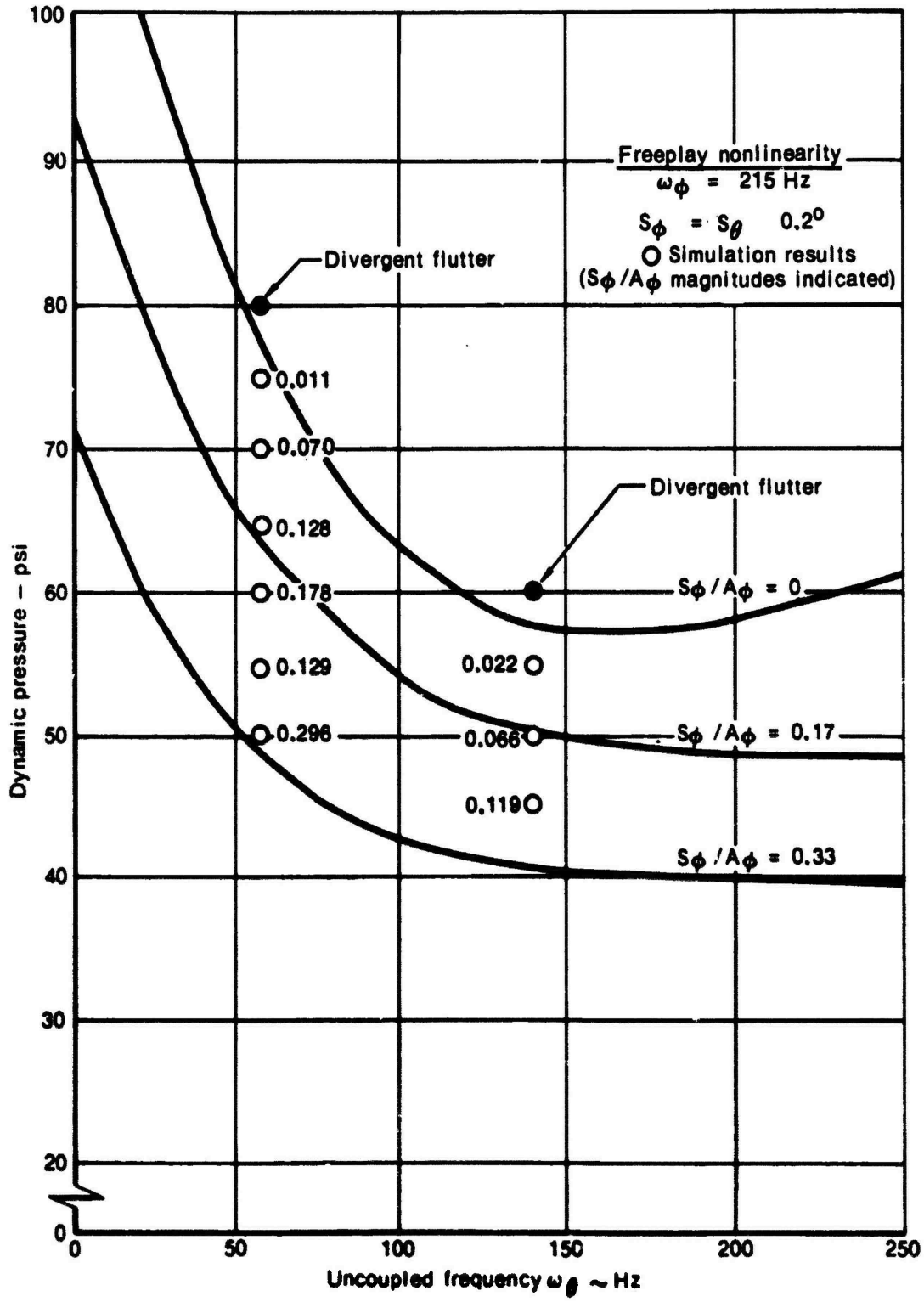

Figure 40 Simulation results for a flexible control surface with two freeplay nonlinearities

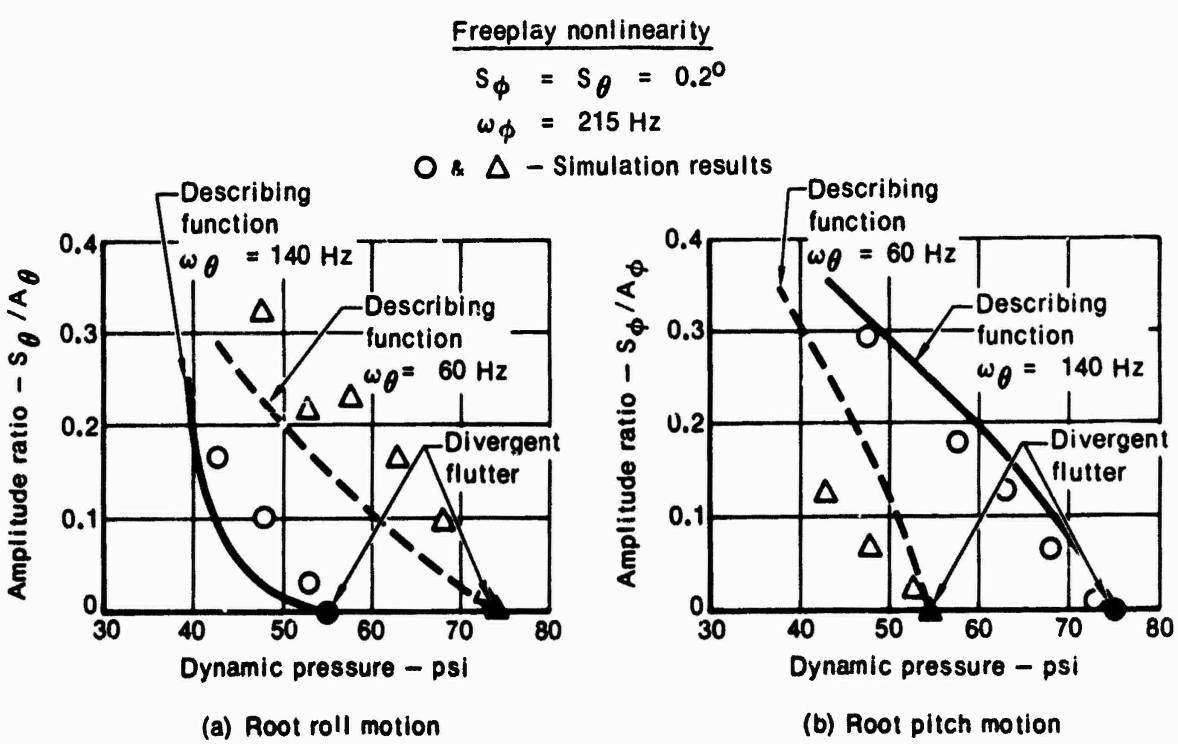

Figure 41 Comparison of flexible control surface root motions with two freeplay nonlinearities

The overall conclusions from the data presented on Figures 36 through 41 is that there exists good correlation between the numerical simulation and describing function results for the case of a control surface having freeplay type nonlinearities. This good agreement holds for both a rigid and a flexible control surface. The describing function approach predicts the point of divergent flutter very well. Also, this technique results in a satisfactory prediction of the trend between root amplitudes of motions and dynamic pressure up to the point of divergent flutter.

B. PRELOAD NONLINEARITY

Numerical simulations were obtained for a rigid control surface with a root roll preload nonlinearity. As was done for the freeplay nonlinearities, numerical solutions were obtained for increasing values of dynamic pressure until the solutions became divergent in nature. Several different runs were made for varying ranges of dynamic pressure and system initial conditions.

A summary of these results for a S_θ/P_θ ratio of one is presented in Figure 42 . Shown are the results for simulations having different magnitudes of initial root roll amplitudes of motion as compared to describing function predictions. Note that the predictions corresponds to one of the curves shown in Figure 24, Section III. Two conclusions can be drawn from these results. First, that the area to the left of the flutter boundary is not a flutter region. Rather, the response in this area may try to become divergent in nature but as the amplitude increases it then stabilizes at some value having a limit cycle type motion. This trend continues with increasing dynamic pressure until the right side of the boundary is crossed and the system experiences unstable response.

Thus the second conclusion is that the flutter curve of Figure 42 should be modified to reflect these results. That is, the region to the left of the curve in Figure 42 is not an area of flutter for the nonlinear system. This conclusion lead to the modified flutter boundary for a control surface having a root roll preload nonlinearity as shown in Figure 43.

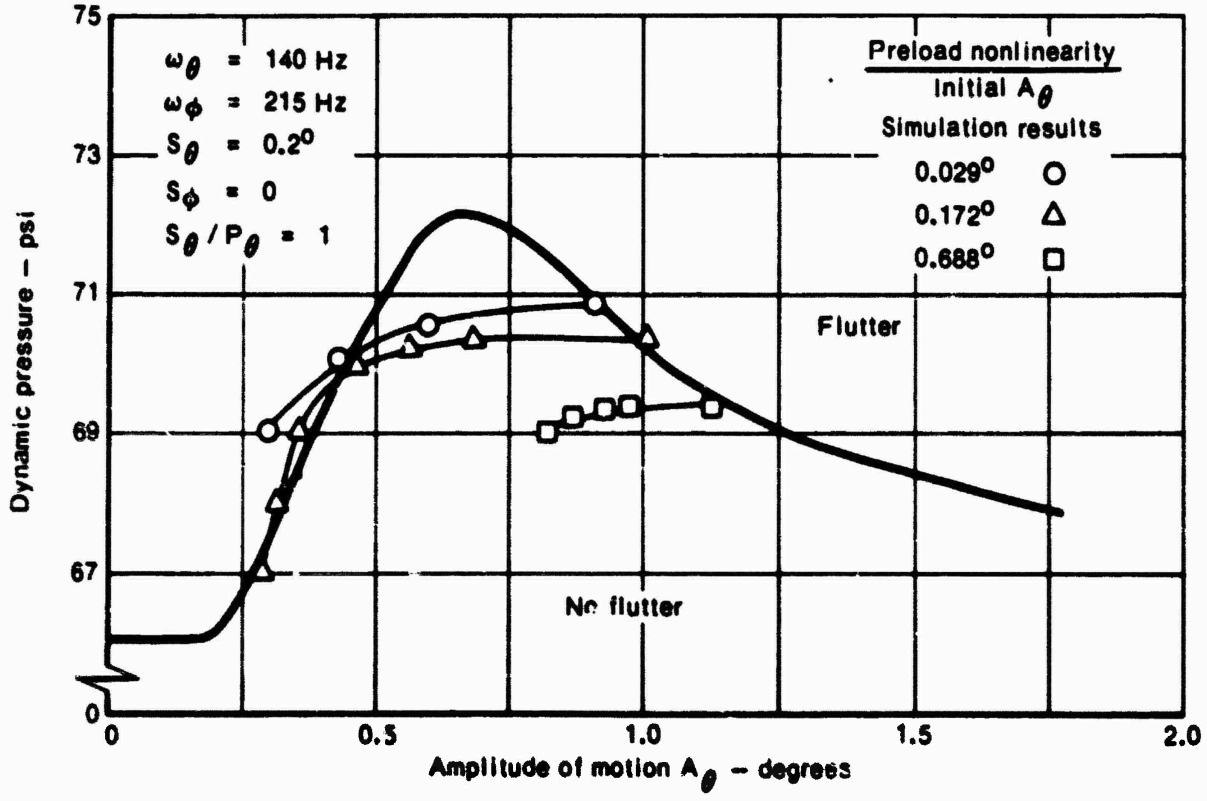

Figure 42 Simulation results for a rigid control surface with a single preload root roll nonlinearity

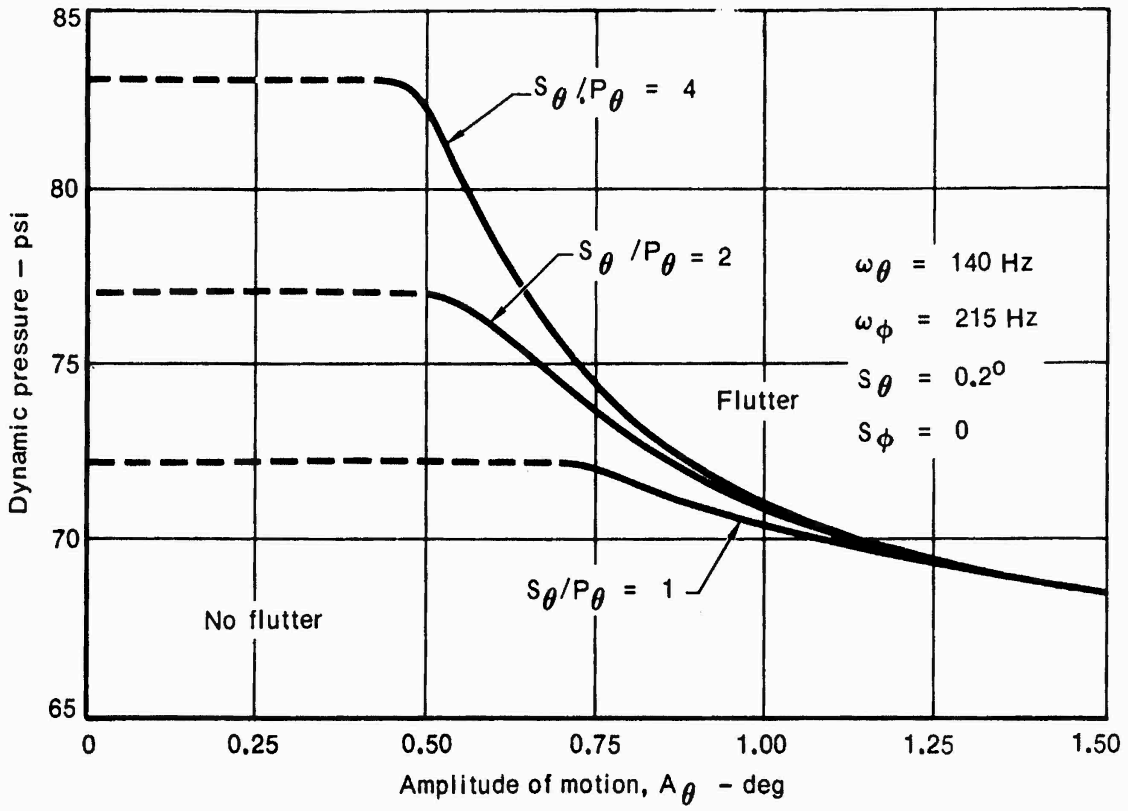

Figure 43 Modified flutter boundary for a rigid control surface with a root roll preload nonlinearity

Additional investigations were made for a rigid control surface with preload nonlinearities in both root roll and pitch springs. Numerical solutions have been obtained for the baseline control surface configuration for particular magnitudes of preload nonlinearities and root spring stiffness characteristics. The system response was obtained for increasing values of dynamic pressure until the characteristics of the response motion became divergent. Shown in Figure 44 is a comparison of the flutter boundary as predicted by the describing function technique and the numerical simulation results. The flutter boundaries are for a 0.2 degree deadspace in both root degrees of freedom and a deadspace to preload ratio of two. As shown, the numerical simulations were performed for uncoupled root roll frequencies ω_θ equal to 60 and 140 Hz. The predicted flutter relationships correspond to those shown in Figure 25, Section III.

As previously noted, the effective stiffness for a preload nonlinearity is a double valued function. During the simulation studies, it was found that the response tended to stabilize to amplitudes of motion greater than the magnitude of preload plus deadspace. Thus the values of interest correspond

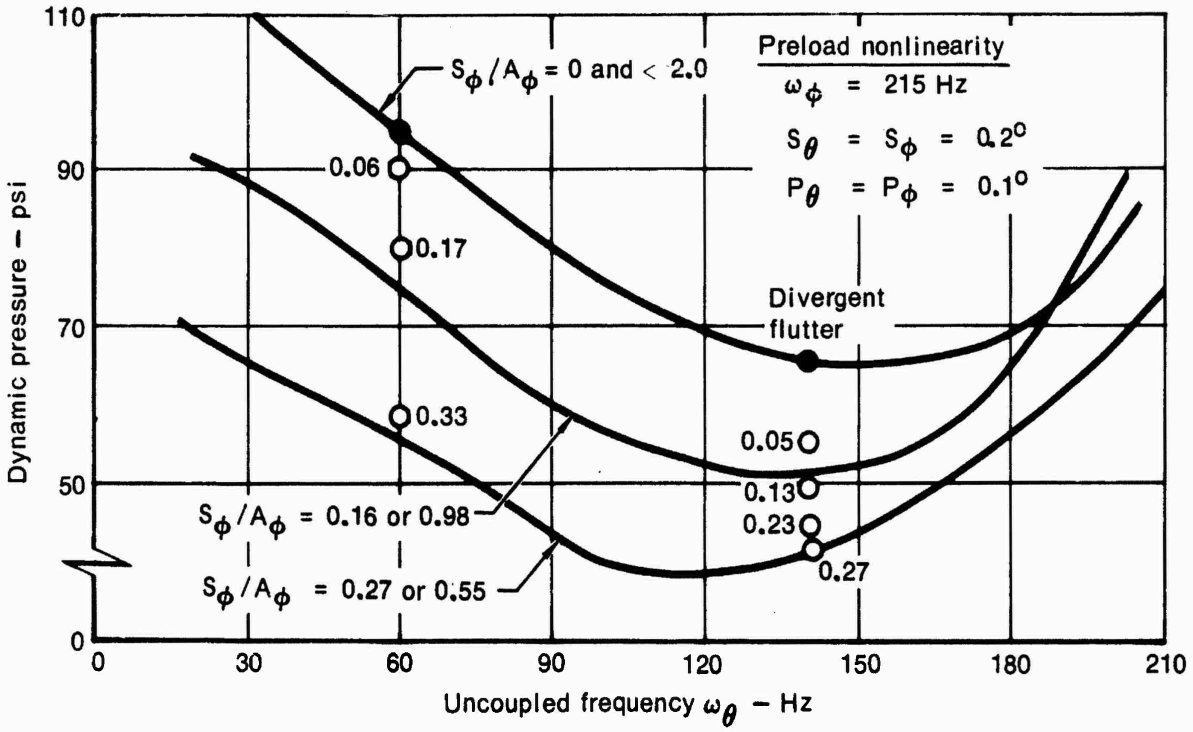

Figure 44 Simulation results for a rigid control surface with two root preload nonlinearities

to cases where the stable amplitude of oscillation is greater than P + 2S. The simulation points plotted in Figure 44 were obtained by holding the dynamic pressure constant and increasing the initial amplitude A_θ until the resultant amplitude exceeded P + 2S.

The double valued effective stiffness phenomena is further illustrated in plots of the root roll and pitch limit cycle amplitudes of motion as obtained by numerical simulation. These results are compared with the describing function predictions in Figure 45. Presented in these figures are simulation results from Figure 44 for an ω_θ of 60 Hz.

As evident from Figure 45, for a given set of preload nonlinearity parameters (S, P, and K), an increase in the initial root roll amplitude at constant dynamic pressure causes the resultant amplitude of the motion to approach the curve for amplitudes below the limits of the deadspace. As the initial system displacement is further increased, we find the system experiences an "amplitude jump". This corresponds to an amplitude transversal of the deadspace with the steady state oscillations then stabilizing to those predicted by the describing function method for amplitudes in excess of

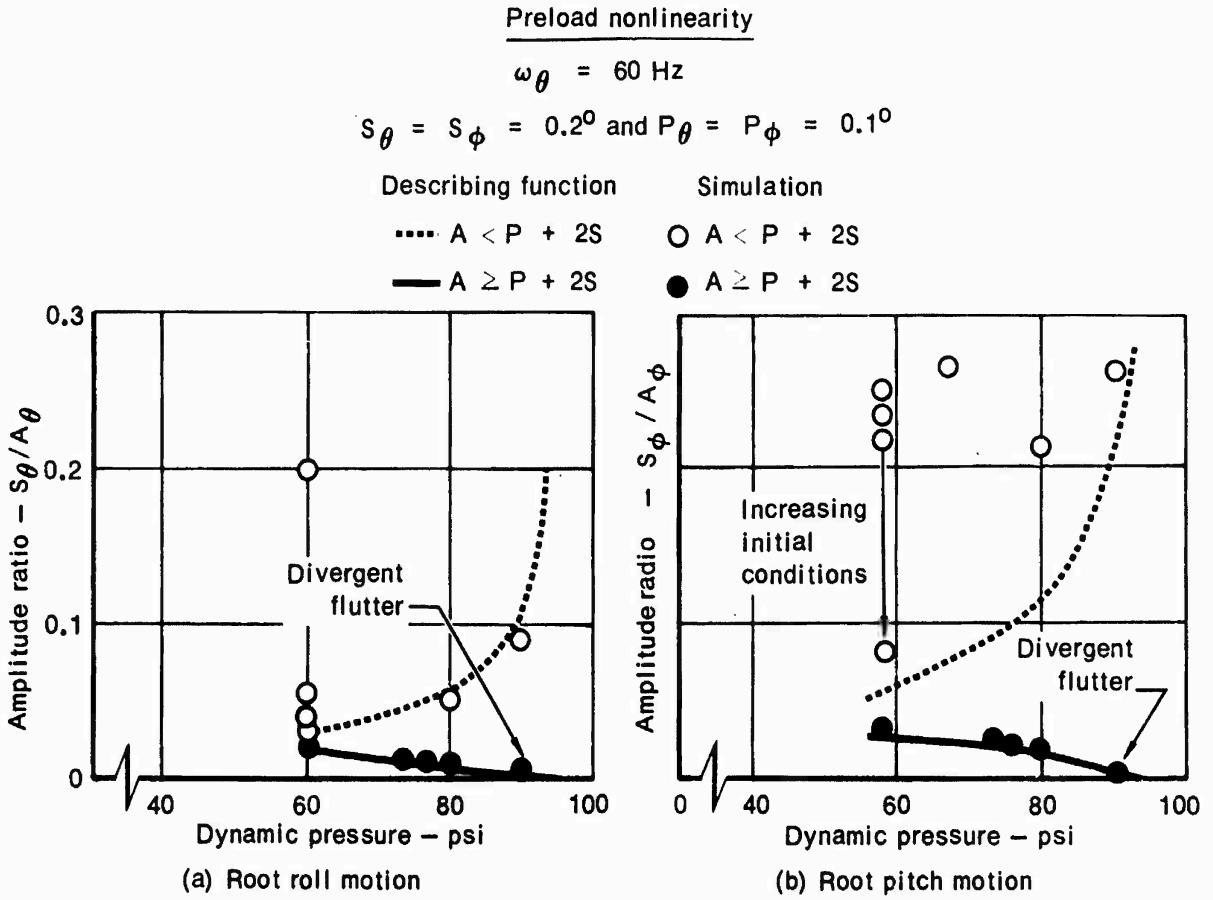

Figure 45 Comparison of rigid control surface root motions with two preload nonlinearities

P+2S. Thus this curve defines the steady state amplitude of motion at which the system response tends to stabilize.

Similar type jump phenomenon was evident during simulations of a flexible control surface with two root preload nonlinearities. As the magnitude of initial conditions were increased, for a given dynamic pressure, the steady state limit cycle motion tended to stabilize at magnitudes above the preload plus deadspace. Comparison of these simulation results and describing function predictions are shown in Figure 46. These results are for a flexible control surface with equal 0.2 degree deadspaces and a deadspace to preload ratio of two.

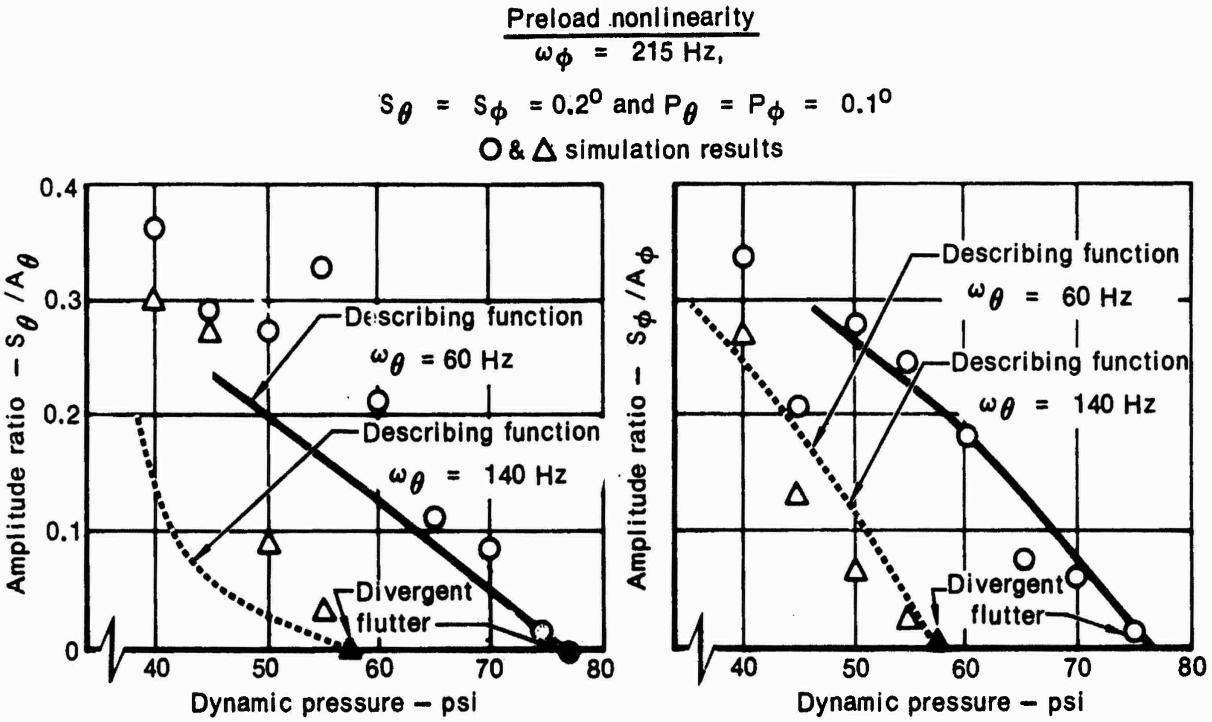

Figure 46 Comparison of flexible control surface root motions with two preload nonlinearities

The comparison between simulation results and describing function predictions are not as good for the flexible control surface as was the case for the rigid control surface. Presented in Figure 47 are root roll time histories for increasing dynamic pressure and a flexible control surface. Note that these time histories correspond to data points presented in Figure 46(a). Referring to Figure 47, it appears that the flexibility of the control surface causes root motions, at the nonlinear structural element, to be composed of several harmonics. This is especially true when the dynamic pressure is much less, Figure 47(a), than the dynamic pressure for divergent flutter. As the dynamic pressure increases, Figure 47(a) to Figure 47 (d), the characteristic of the root roll motion becomes that of a single harmonic.

The significance of this multiple harmonic type root motion for a flexible control surface is obvious when considering the basic assumption of the describing function technique. This technique is based on a time averaging approach for defining the input-output characteristics of the nonlinear root spring. For a sinusoidal input displacement, it is assumed that the output load is also sinusoidal with the same frequency as the input and all other harmonics can be neglected.

For the multiple harmonic root roll motion of a flexible control surface, Figure 47(a), the load generated in the nonlinear root spring will certainly be made up of several harmonics. This contradiction to the basic assumption of the describing function approach accounts for the apparent difference in

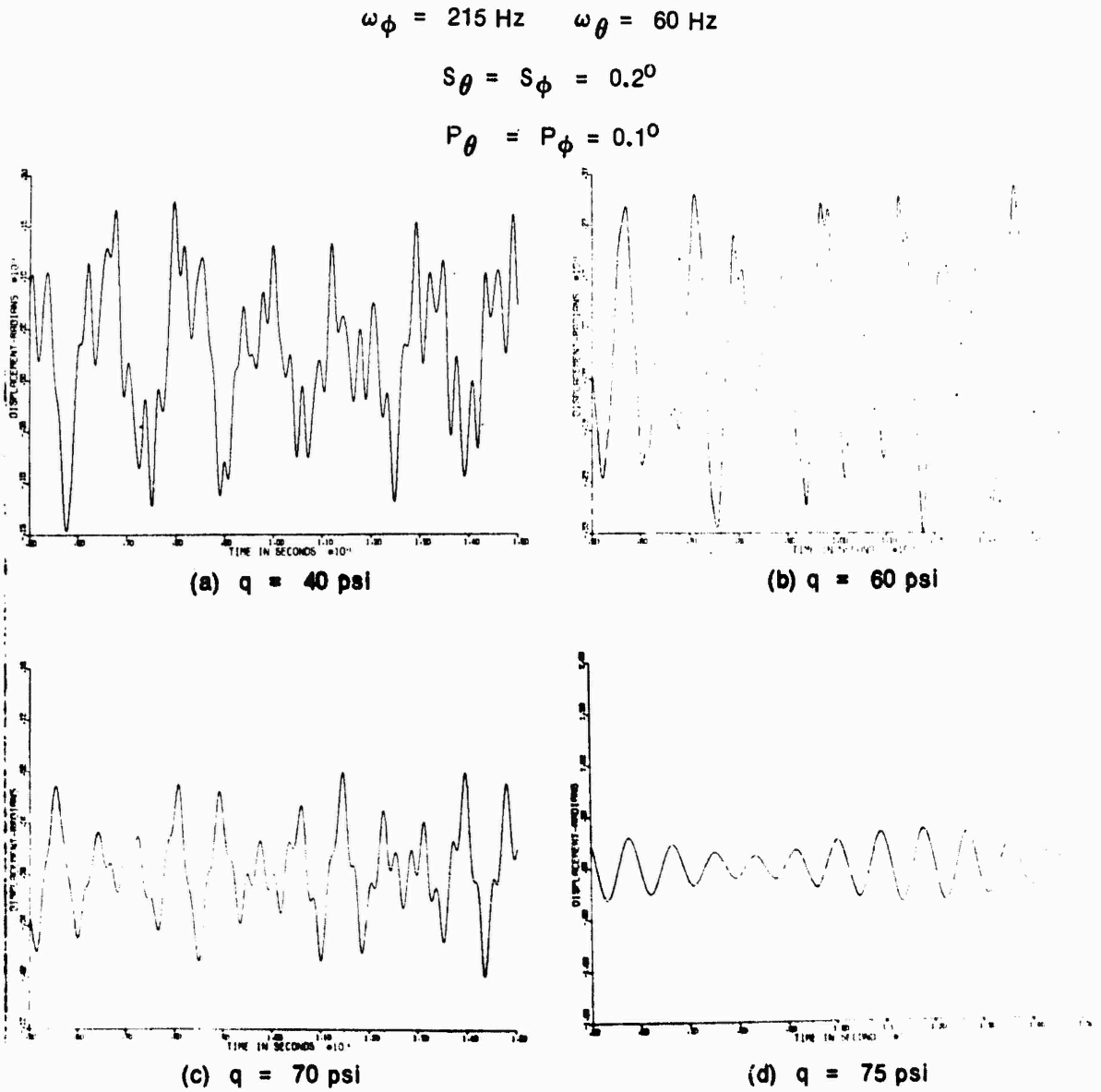

Figure 47 Root roll time histories for a flexible control surface with two preload nonlinearities

the results presented in Figure 46. As the dynamic pressure increases towards the magnitude required for divergent flutter, the root motion approaches a single harmonic, Figure 47(d), and thus the simulation and describing function results come into closer agreement as shown in Figure 46.

Overall, the correlation between the numerical simulation and describing function result is good for a control surface having preload type nonlinearities. For either a rigid or flexible control surface, the describing function approach predicts the point of divergent flutter very well. This technique results in good predictions of the trend of root amplitudes of motions and dynamic pressure for a rigid control surface up to this point of divergent flutter. The predictions in amplitude of motion as a function of dynamic pressure is not as satisfactory for a flexible surface.

C. FRICTION NONLINEARITY

In a manner similar to that discussed for systems with freeplay and preload nonlinearities, numerical solutions were obtained for a rigid control surface with friction nonlinearities. As was done for the other nonlinearities numerical solutions were obtained for increasing values of dynamic pressure until the resulting motions became divergent in nature. Several simulations were made for varying ranges of dynamic pressure and system initial conditions.

Initial simulations were conducted for a rigid control surface having a single friction nonlinearity in the root pitch degree of freedom. The system parameters describing the nonlinearity included a 0.2 degree deadspace and a friction term of 25 in-lb. Comparisons between simulation results and describing function predictions in the form of amplitude ratio S/A versus dynamic pressure are shown in Figure 48. The assumed root stiffness values result in uncoupled frequencies ω_ϕ of 215 Hz and ω_θ of 80 Hz. The value of dynamic pressure is shown both with damping included and neglected in the describing function analysis. As Figure 30 illustrates, the damping in the systems studied is small and can be neglected for our purposes. As witnessed in the response histories of the other nonlinearities, for increasing magnitudes of dynamic pressure, the system response builds to some amplitude and reaches a limit cycle response. This trend of stable limit cycle response

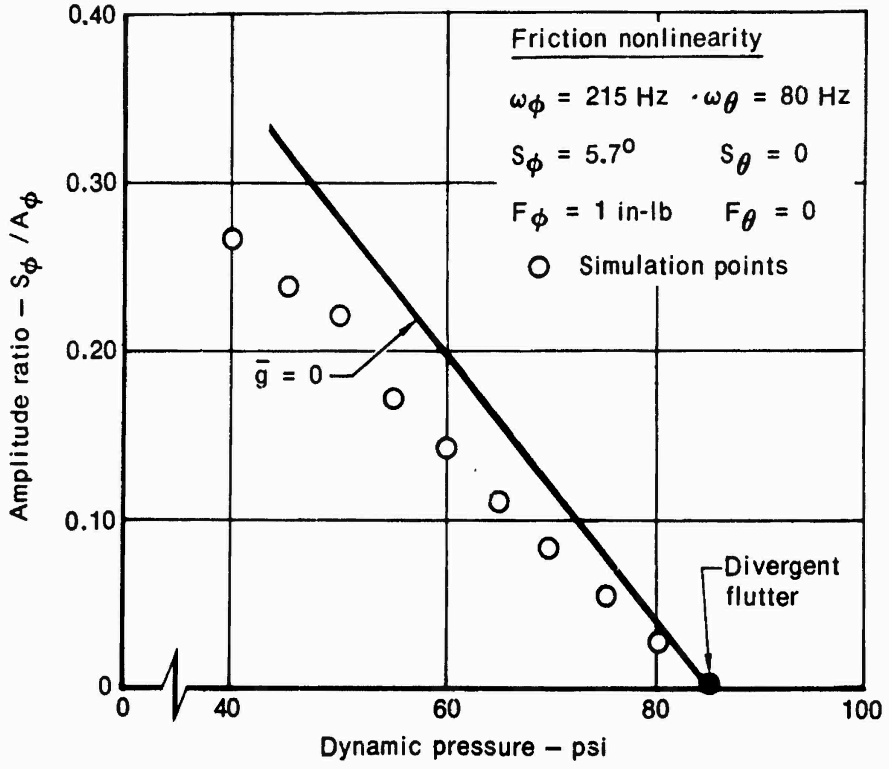

Figure 48. Comparison of rigid control surface root pitch motion with one friction nonlinearity

continues with increasing dynamic pressure as illustrated in Figure 48, until the critical pressure is reached and the classic divergent flutter motion is seen. The correlation between describing function predictions and numerical simulation results for this case is very good.

Additional investigations were made for a rigid control surface with friction nonlinearities in both root springs. Numerical solutions have been obtained for the baseline control surface configuration for particular magnitudes of friction parameters and root spring stiffnesses. As before, system response was obtained for increasing values of dynamic pressure until the resulting motion became divergent. Shown in Figure 49 is a comparison of the flutter boundary as predicted by the describing function technique and the numerical simulation results. The flutter boundaries are for a 0.2 degree deadspace in both root degrees of freedom and friction parameters of 25 in-lb. The numerical simulations were performed for uncoupled root roll frequencies ω_θ of 60 Hz and 100 Hz and a root pitch frequency of 215 Hz. The same limit cycle response found in the single nonlinearity case is evident in the two nonlinearity case. An increase in dynamic pressure causes an

increase in the system RSS amplitude in the manner predicted by the describing function analysis until eventually the critical dynamic pressure is reached and the motions become divergent. The correlation of simulation data and describing function prediction is good for the case of two friction nonlinearities. As can be seen from Figure 49, the correlation is better for the root pitch degree of freedom and lower root roll frequencies.

As in the preload nonlinearity, the correlation between simulation results and describing function predictions is not as good for the flexible control surface as it was the rigid case. Presented in Figure 50 is the dynamic pressure q as a function of the uncoupled root roll frequency ω_θ. Simulation runs were conducted for a flexible control surface case with two friction nonlinearities in the root springs. System parameters included root deadspaces of 0.2 degrees and friction terms of 25 in-lb. Simulations were conducted for a root pitch freq of 215 Hz and a root roll freq of 100 Hz. As can be seen in Figure 50, the resulting RSS amplitude were consistently higher (lower S/A values) than those predicted by the describing function.

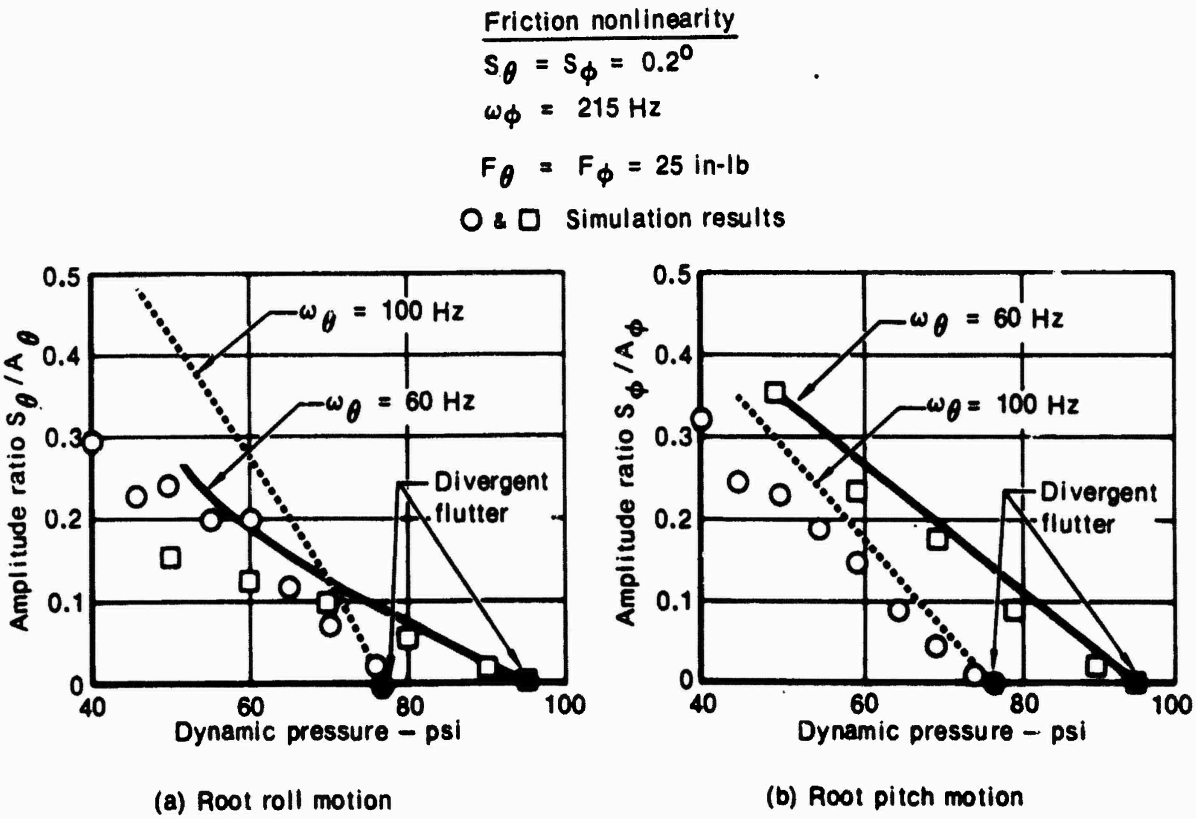

Figure 49 Comparison of rigid control surface root motion with two friction nonlinearities

As noticed with the preload nonlinearity, the correlation improves as one approaches the flutter dynamic pressure. For the multiple harmonic root motion for a flexible control surface, the load generated in the nonlinear root spring is made up of several harmonics. This violates the basic assumption of the describing function approach which assumes higher harmonics can be neglected.

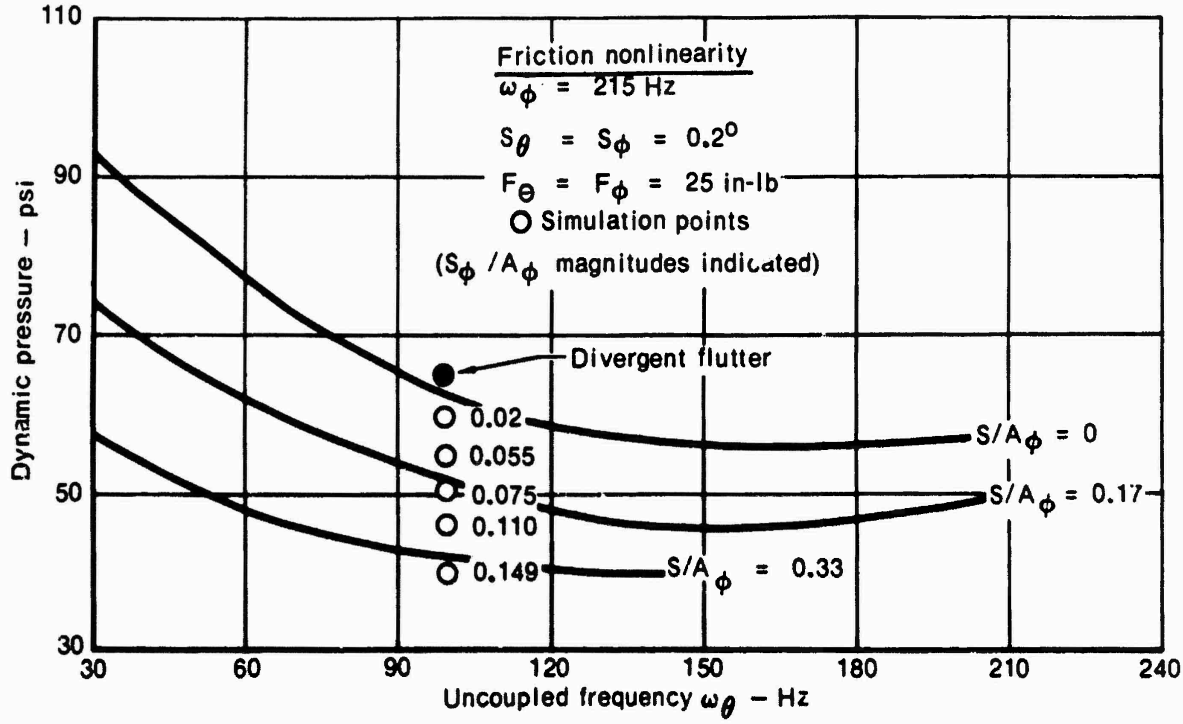

Figure 50 Flutter results for a flexible control surface with two friction nonlinearities

Section V
CONCLUSIONS

Knowledge of the effects of nonlinearities on missile control surface performance and flutter characteristics are important for many reasons. An understanding of nonlinearity characteristics has the potential of reducing system weight and program cost along with increasing overall design efficiency. This study was undertaken to provide a better understanding of the effect of various nonlinearities on the dynamics of a missile control surface and to establish procedures to include the influence of these nonlinearities in the flutter analysis process.

The present study has helped to develop an understanding of the control surface flutter mechanism as influenced by structural nonlinearities. The interrelationship between the magnitude of the nonlinearities, flight conditions, and the nature of the resulting control surface response has been investigated. In an overall sense, the influence of each of the nonlinearities studied; freeplay, preload, or friction; have the same general effect on the control surface response. Since the critical flutter speed is a function of the natural frequency of the system, the change in natural frequency attendant on the increased amplitude of oscillation alters the critical flutter speed. Each of these nonlinearities has its own peculiarity, but in general their presence tends to cause the effective system stiffness to be less than that of the linear system. This relationship, or stiffness ratio, between effective and actual system stiffnesses is dependent on the amplitude of motion being experienced by the control surface system.

For all of the nonlinearities considered, the stiffness ratio can be employed to estimate the influence of the nonlinearity on the control surface flutter boundary. Techniques for modifying the linear system flutter results in terms of this stiffness ratio are discussed in Section III. It must be noted these procedures for evaluating the influence of structural nonlinearities on the flutter phenomenon is related to the simplified aerodynamic representation used throughout this study.

The close agreement of the describing function predictions with the numerical data has verified the applicability of the describing function approach to the flutter analysis procedure. With this technique, system effective stiffness is expressed in terms of the linear stiffness, properties of the nonlinearities, and magnitude of control surface response. This definition of the effective stiffness is then used in the flutter analysis procedures mentioned in the preceding paragraph.

The basic characteristic of the response for the control surface system was the same for all the nonlinearities investigated. For increasing magnitudes of dynamic pressure, the system response tends to become divergent in nature. However, this has the effect of "working" the structure nonlinearity to a greater extent. Thus the oscillation builds up to some amplitude and then becomes stable again where the system is experiencing a limit cycle type response. This trend of stable limit cycle response continues with increasing dynamic pressure. Above some critical dynamic pressure, the limit cycle motion no longer holds and we have the classic divergent flutter motion.

The overall conclusion from this study is that the use of the describing function technique results in a good prediction of the control surface response for the particular nonlinearities studied. This conclusion is reached because of the good correlation between numerical simulations of the nonlinear problem and describing function results for all the nonlinearities considered during the study. This agreement holds for both a rigid and a flexible control surface. This technique results in a satisfactory prediction of the trend between control surface amplitudes of motions. The accuracy of the describing function predictions improve as one approaches the flutter critical dynamic pressure.

The amplitude predictions below flutter are useful from a design point of view. Prediction of these steady state oscillations for flight conditions below flutter may be related to load and fatigue considerations for design of the surface actuator and support structure. The describing function approach has the advantage that it is much more efficient than the numerical simulation

approach. Also of advantage is the fact that its use is based on the modification of linear system flutter results which are obtained in the normal missile control surface design process.

This study has shown the applicability of the describing function approach in accounting for the influence of structural nonlinearities in the flutter analysis of missile control surfaces. Understanding the effect of nonlinearities on the dynamic response of systems is important not only from an aerodynamicist's viewpoint but is also of interest to all concerned with the accurate prediction of the steady limit cycle type response associated with many structural problems. Further study is expected to establish the validity and usefulness of the describing function approach to other dynamic systems.

Section VI
RECOMMENDATIONS

Flutter analysis procedures have been developed to evaluate the influence of structural nonlinearities on the flutter of missile control surfaces. Based on the results of this investigation, a number of recommendations are presented in the following paragraphs. The first of these deals with the applications of the developed analysis procedures during the design of a control surface. This is followed by a number of recommendations for further analytical studies.

A. APPLICATION OF DEVELOPED TECHNIQUES

As discussed in the previous sections, application of the describing function technique to evaluate the influence of structural nonlinearities on control surface flutter amounts to a systematic modification of the linear system flutter results. Thus, during the design process, the initial step is to obtain flutter boundaries in the normal fashion. This information then forms the basis for evaluating the influence of potential structural nonlinearities on the flutter characteristics of the particular control surface design.

For the nonlinearities considered during the present study, Figure 2, and with the simplified aerodynamics representation, the point of divergent flutter is the same for both the linear and nonlinear system. However, the nonlinear system experiences a limit cycle type oscillation of increasing amplitude with increasing dynamic pressure. Application of the developed procedures yield good prediction of the amplitudes of this limit cycle motion. Thus, the motions of the control surface system may be obtained for the flight conditions which are below the flutter boundaries. These motions may then be employed to define loading conditions in the control surface actuator and attachment structure. In addition, the design of the system may be evaluated from a fatigue failure point of view in terms of these limit cycle oscillations.

An example of the results which may be obtained when using the developed procedures to predict operating limits based on loading conditions are presented in Figures 51 and 52. These figures are for a control surface having equal

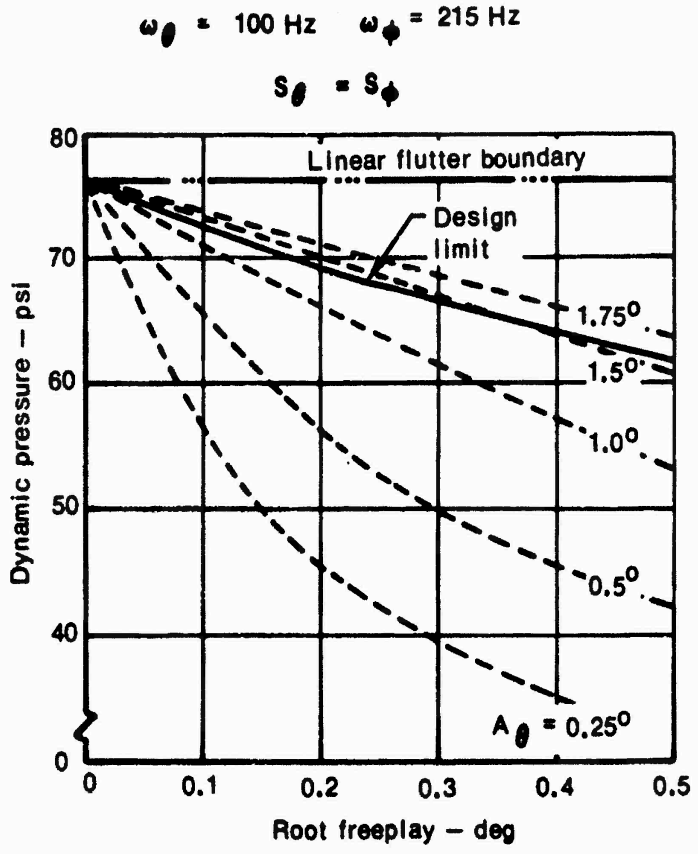

(a) Root roll

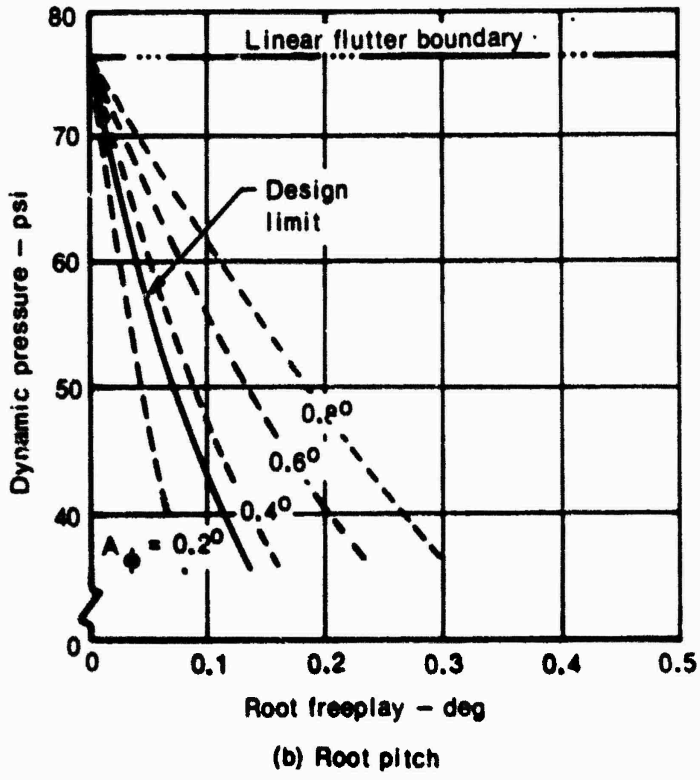

(b) Root pitch

Figure 51. Dynamic pressure versus root freeplay for a rigid control surface

$$\omega_\theta = 100 \text{ Hz} \qquad \omega_\phi = 215 \text{ Hz}$$
$$S_\phi = S_\theta$$

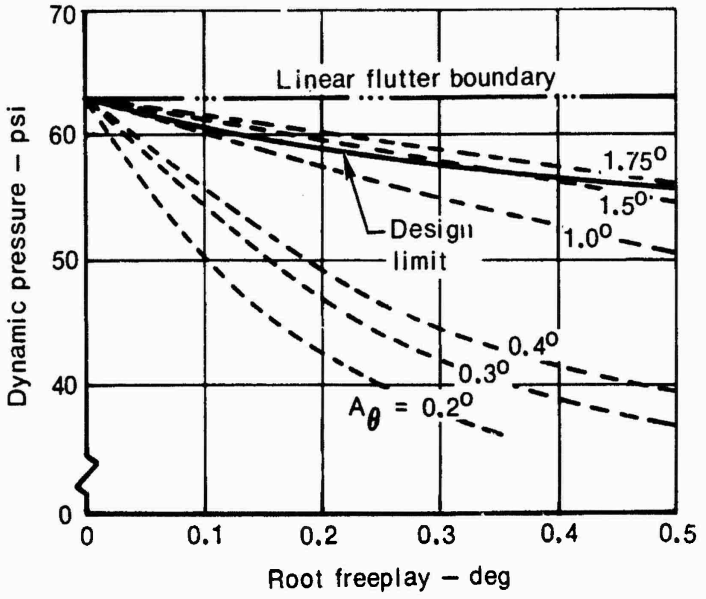

(a) Root roll

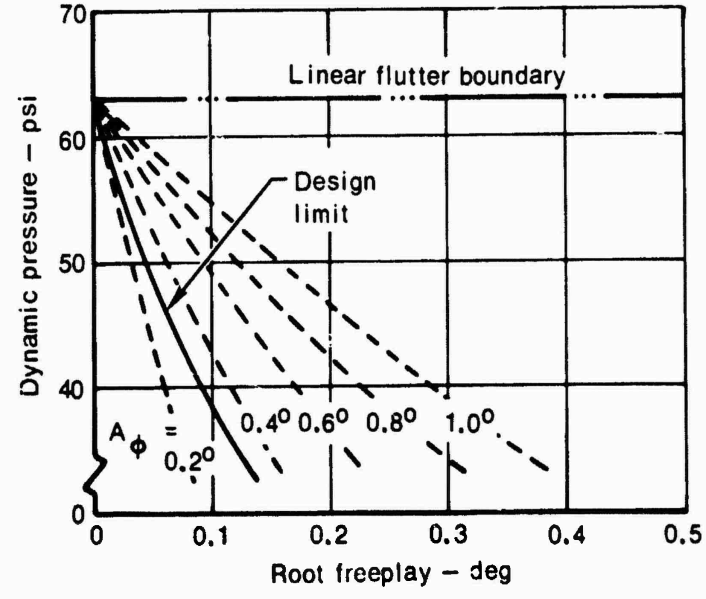

(b) Root pitch

Figure 52. Dynamic pressure versus root freeplay for a flexible control surface

freeplay nonlinearities in both root degrees of freedom. Presented in Figure 51, for a rigid surface, are the family of curves defined by dotted lines depicting dynamic pressure versus magnitude of root freeplay for various magnitudes of limit cycle oscillations. Assuming that the moments in the root roll, ϕ, and root pitch, θ, springs must be less than 500 and 1300 in-lb respectively, the maximum deflection in each root spring may be determined. Here it has been assumed that these are limits on the oscillationg loads which are in addition to trim and maneuver loads. Thus, the maximum limit cycle oscillation in each spring is this deflection plus the magnitude of freeplay. Cross plotting these limiting magnitudes of oscillation, solid lines, on Figure 51 defines the indicated design limit. This design limit gives the dynamic pressure at which the limits on the load increment will be exceeded for a particular freeplay nonlinearity. Similar results are presented in Figure 52 for the case of a flexible control surface.

For the particular case presented here, it can be seen that the system is very sensitive to the amount of freeplay in the pitch degree of freedom. In the case of the rigid fin, Figure 51, an increase of 0.05 degrees in pitch freeplay results in a decrease of 20 psi in dynamic pressure for maximum allowable load. This indicates that the freeplay tolerance for the pitch degree of freedom is more critical than the roll degree of freedom for success of the design.

In addition, as illustrated in Figures 51 and 52, the limit on dynamic pressure from a loads point of view may be quite a bit less than the predicted linear flutter boundary. Design curves such as these may be obtained for many different combinations of system stiffnesses, allowable design loads and any of the nonlinearities examined in this report.

B. FURTHER DEVELOPMENTS

The following are a number of analytical investigations which should be undertaken to build on the analysis techniques presented in this report. These studies are needed to increase the generality and understanding of the present procedures. It should be noted that in the final evaluation, the developed flutter analysis procedures should be verified through comparison with experimental data obtained during a wind tunnel or flight test program.

1. IMPROVED AERODYNAMICS

During the current study a "simplified" definition of the aerodynamic loads acting on the control surface has been used. This aerodynamic theory assumes that the lift force is proportional to and in phase with control surface torsional (pitch) motion. Results to date are encouraging when using this aerodynamic theory to investigate the flutter mechanism of missile control surfaces containing structural nonlinearities. However, to determine the adequacy of these study results, the developed flutter analysis procedures should be evaluated in conjunction with more complete aerodynamic theories.

The developed flutter computational procedures, employing the describing function representation of the structural nonlinearities, should be extended to allow incorporation of more complete aerodynamic representations. Specifically, for the subsonic flight regime the aerodynamic loadings could be expressed in terms of a potential flow, incompressible theory. Aerodynamic methods such as the Theodorsen theory and the Doublet Lattice method could be examined for integration with the techniques of the present study.

2. HIGH ORDER TERMS

The developed flutter analysis procedures for missile control surfaces having structural nonlinearities employ a describing function technique. With this technique, the nonlinear structural elements (root springs) are replaced by "effective" linear representations. A Fourier Series expansion of the output wave shape for the nonlinear spring is formulated. Assuming that only the first harmonic of the series expansion is of importance, a linear input-output (spring rate) relationship is obtained. This linear, or effective, spring rate is then used in the subsequent flutter studies.

Questions as to the accuracy of the developed flutter procedures are of importance due to use of only the first harmonic when representing the output of the nonlinear spring. Additional terms in the Fourier series expansion of the output wave shape for the nonlinear spring could be obtained. The magnitudes of these harmonics would be compared with the magnitude of the fundamental harmonic which is employed in the describing function approach. This comparison would be made for a range of control surface root spring rates and magnitudes of root spring nonlinearities to develop guidelines for estimating potential analysis errors.

3. INFLUENCE OF LARGE MOTIONS

In the present study, the definition of the aerodynamic loads acting on the missile control surface employs a "simplified" representation. This aerodynamic theory assumes that the lift force is proportional to and in phase with control surface torsional (pitch) motion. The lift force is defined as a lift-slope coefficient C_{L_α} times the torsional motion, and the area and dynamic pressure, acting at a fixed center of pressure location. In addition, this approach assumes that neither C_{L_α} nor the center of pressure location are dependent on the amplitude of motion experienced by the oscillating control surface.

Results of the current study indicate that a control surface with root stiffness nonlinearities may experience very large limit cycle type motions before reaching a state of divergent flutter. The influence of this large motion on the definition of the loads acting on the control surface requires further evaluation.

Representation of the aerodynamic loads acting on the control surface could be extended to account for the influence of potentially large limit cycle motions. These aerodynamic relationships would be included in the numerical simulation routines for a control surface having root structural nonlinearities. Simulation results would be compared with analytical results, obtained when neglecting the large motions, to obtain a measure of the potential influence of the large motions on control surface flutter.

APPENDIX A
BASELINE CONTROL SURFACE

Properties of the Harpoon missile quick-attach control surface were used to define the baseline control surface configuration which was used throughout the study. The geometric configuration of the control surface is shown in Figure A-1. The structural nonlinearities that were investigated are associated with the root support springs. Presented in Figure A-2 are the inertia properties of the control surface. The first two rows and columns of the inertia matrix are associated with rigid root roll and pitch motions while the last two diagonal elements are the generalized masses of the control surface modes. The off-diagonal terms, the PF quantities, represent the inertia coupling between rigid and flexible motions. The mode shapes associated with the first two control surface cantilever modes are given in Figure A-3. These modal data were used when investigating a flexible control surface configuration.

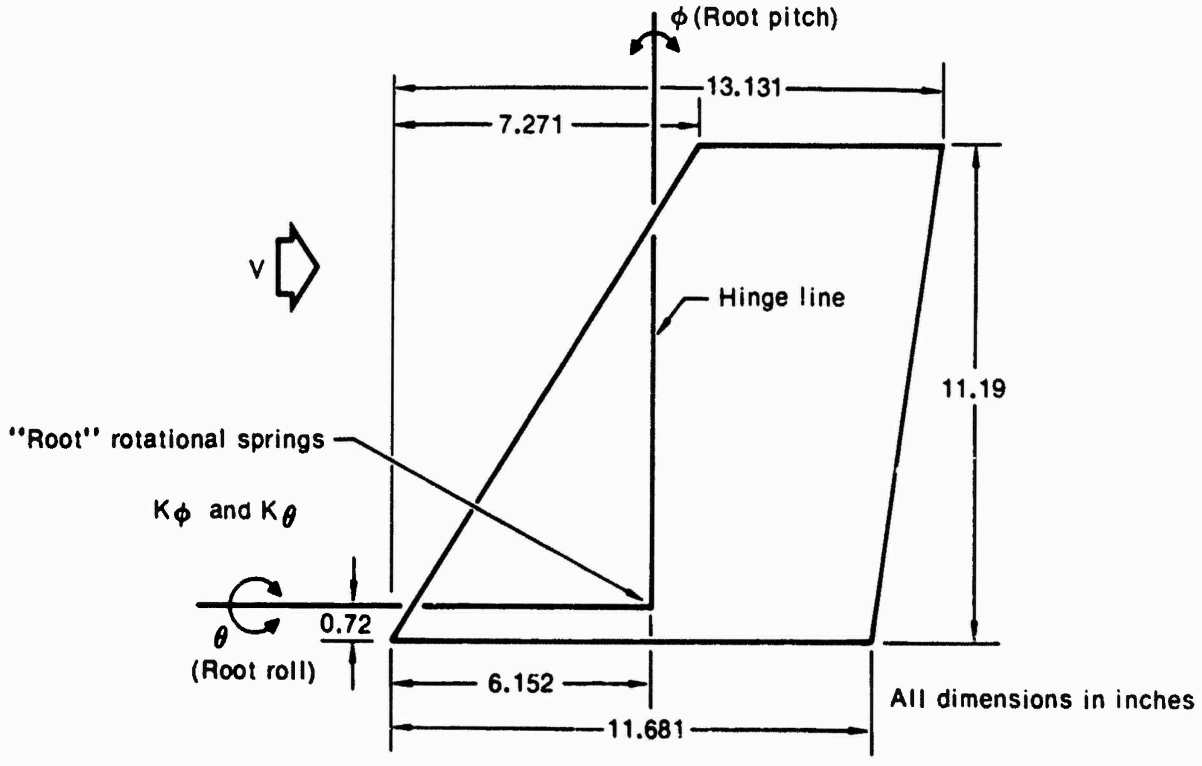

Figure A-1. Control surface geometry

$$\begin{bmatrix} I_\theta & I_{\theta\phi} & PF_{\theta 1} & PF_{\theta 2} \\ & I_\phi & PF_{\phi 1} & PF_{\phi 2} \\ & & m_1 & 0 \\ \text{Symmetric} & & & m_2 \end{bmatrix}$$

(a) Form of inertia matrix

$I_\theta = 0.1667$ lb-sec^2-in. $\quad PF_{\theta 1} = -7.227 \times 10^{-3}$ lb-sec^2

$I_\phi = 0.071$ lb-sec^2-in. $\quad PF_{\theta 2} = -1.014 \times 10^{-3}$ lb-sec^2

$I_{\theta\phi} = 0.058$ lb-sec^2-in. $\quad PF_{\phi 2} = -3.212 \times 10^{-3}$ lb-sec^2

$m_1 = 4.220 \times 10^{-4}$ lb-sec^2/in. $\quad PF_{\phi 2} = 2.134 \times 10^{-3}$ lb-sec^2

$m_2 = 4.295 \times 10^{-4}$ lb-sec^2/in.

(b) Specific inertia terms

Figure A-2 Control surface inertia properties

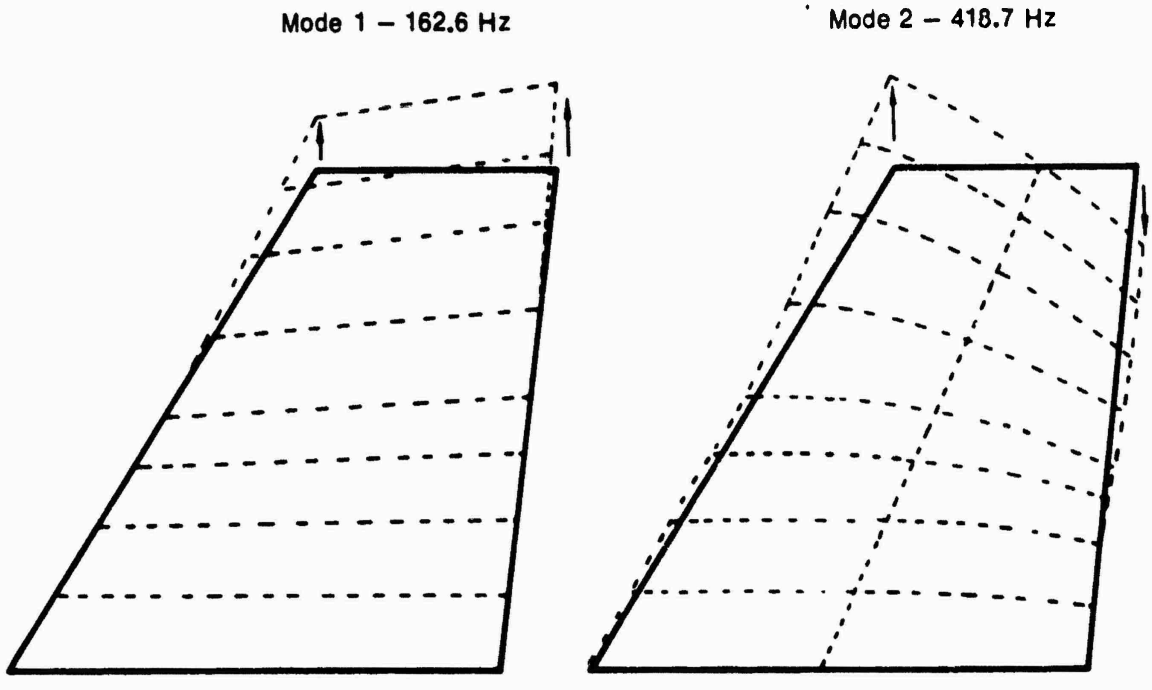

Figure A–3. Control surface cantilever modes

Appendix B
DETAILED DESCRIBING FUNCTION DEVELOPMENT

The detailed development of the describing functions for the three nonlinearities considered during this investigation are presented in this section. The describing function analysis of nonlinear systems has found wide application in the analysis of nonlinear control systems, References 5 and 6. This technique is based on the following assumptions:

- o The output of the nonlinear element depends only on the present value and past history of the input. In other words, no time varying characteristics are included in the nonlinear element.
- o If the input to the nonlinear element is a sinusoidal signal, only the fundamental component of the output signal is considered and all higher harmonics are neglected.

For an assumed sinusoidal input, the resulting output is periodic and contains components at the fundamental frequency (the frequency of the input) and, in general, higher harmonic frequencies. The last assumption states that for the nonlinear system the fundamental component is the only significant component in the system output. If the basic assumptions listed above are satisfied, the sinusoidal response characteristics of the nonlinear element can be expressed in terms of a describing function, defined as the ratio of the fundamental component of the outputs to the amplitude of the input.

Thus in the describing function method, the input to the nonlinear system is the starting point of the analysis; it is the waveform at this input which is assumed sinusoidal. With the assumption that the output of the nonlinear device is also sinusoidal, the describing function $\mathcal{E}$ is expressed as

$$\mathcal{E} = \frac{L(t)}{KA} \tag{B1}$$

where A is the amplitude of the input, K is the stiffness of the linear portion of the structural nonlinearity and L(t) is the fundamental component of developed load.

B.1 FREEPLAY ANALYSIS

For a nonlinear spring with freeplay characteristics, Figure 2(a), the waveform of the developed load will take one of the two forms shown in Figure B-1. The load as a function of time can be expressed as

$$L(t) = \begin{cases} 0 & \text{for } 0 < t < t_1 \\ K[A-S] \text{ Sin } t & \text{for } t_1 < t < 2\pi \end{cases} \tag{B2}$$

The first step in obtaining the describing function is the Fourier series expansion of the relationship for the load L(t). The complete Fourier series representation is of the form

$$L(t) = \frac{a_o}{2} + \sum_{n=1}^{\infty} a_n \text{ Cos } nt + \sum_{n=1}^{\infty} b_n \text{ Sin } nt \tag{B3}$$

where the coeffieients are obtained by

$$\begin{aligned} a_o &= \frac{1}{\pi} \int_0^{2\pi} L(t)\, dt \\ a_n &= \frac{1}{\pi} \int_0^{2\pi} L(t) \text{ Cos } nt\, dt \\ b_n &= \frac{1}{\pi} \int_0^{2\pi} L(t) \text{ Sin } nt\, dt \end{aligned} \tag{B4}$$

Since the load L(t), Figure B-1, is a single-valued odd function, its Fourier series representation is of the form

$$L\,(t) = \sum_{n=1}^{\infty} b_n \text{ Sin } nt \tag{B5}$$

where the coefficient b_n is obtained from

$$b_n = \frac{1}{\pi} \int_0^{2\pi} L(t) \text{ Sin } nt\, dt \tag{B6}$$

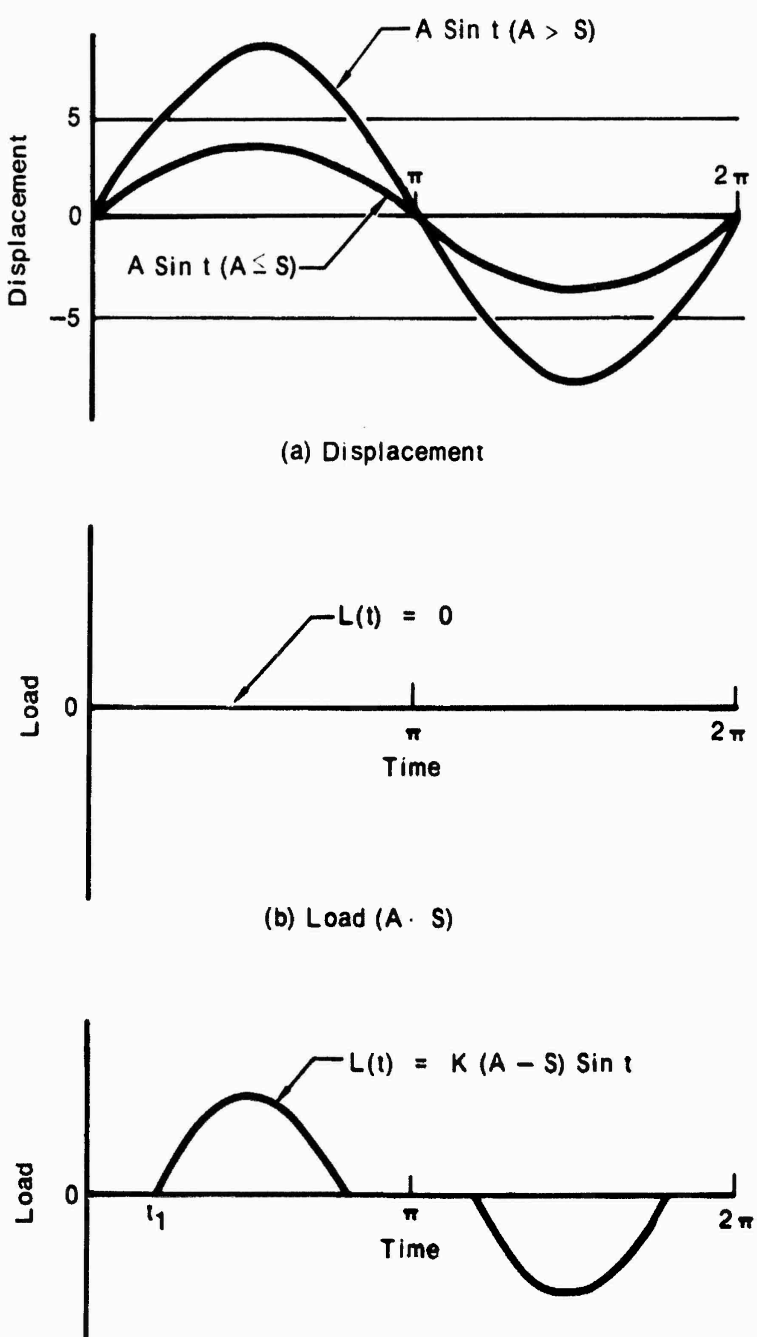

Figure B-1. Developed load for freeplay nonlinearity

For the case of freeplay as illustrated in Figure B-1, we have

$$b_n = 0 \text{ for } A \leq S \tag{B7}$$

and

$$b_n = \frac{4}{\pi} \int_{t_1}^{\pi/2} K(A-S) \sin^2 t \, dt \text{ for } A > S \tag{B8}$$

Performing the operations of Equation (B8), the fundamental component of the Fourier series representation becomes

$$b_1 = \left(1 - \frac{2t_1}{\pi} - \frac{\sin 2t_1}{\pi} \right) AK \tag{B9}$$

where

$$t_1 = \sin^{-1} (S/A) \tag{B10}$$

The describing function is then simply

$$\delta = \frac{b_1}{AK} \tag{B11}$$

which is

$$\delta = \begin{cases} 0 & \text{for } 0 \leq A \leq S \\ 1 - \frac{2t_1}{\pi} - \frac{\sin 2t_1}{\pi} & \text{for } 0 < A < \infty \end{cases} \tag{B12}$$

with t_1, given by Equation (B10).

B.2 PRELOAD NONLINEARITY

For a nonlinear spring having preload characteristics, as illustrated in Figure 2(b), the waveform of the developed load will take the forms shown in Figure B-2. The expressions for the developed load as a function of time are of the following form.

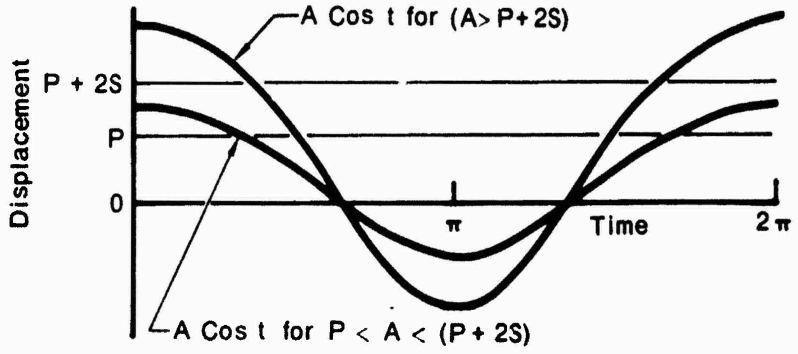

(a) Displacement

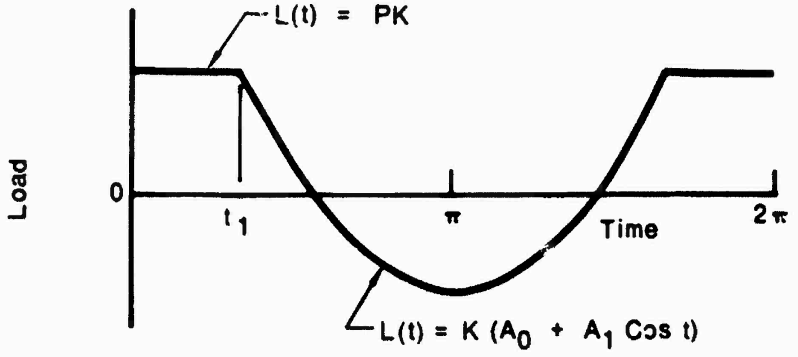

(b) Load (P · A · P + 2S)

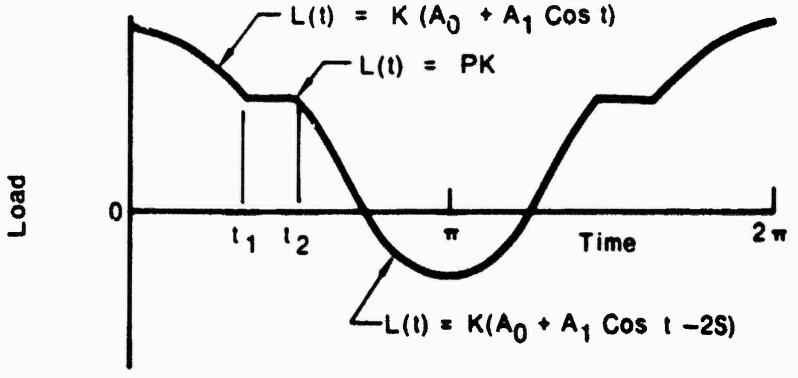

(c) Load (A> P +2S)

Figure B–2 Developed load for preload nonlinearity

$$L(t) = \begin{cases} (A_0 + A_1 \text{ Cos } t\text{-}2S)\cdot K & \text{for } 0 < t < t_1 \\ PK & \text{for } t_1 < t < t_2 \\ (A_0 + A_1 \text{ Cos } t)\ K & \text{for } t_2 < t < 2\pi - t_2 \\ PK & \text{for } 2\pi - t_2 < t < 2\pi - t_1 \\ (A_0 + A_1 \text{ cos } t\text{-}2S)\cdot K & \text{for } 2\pi - t_1 < t < 2\pi \end{cases} \tag{B13}$$

where t_1 is given as

$$t_1 = \text{Cos}^{-1}\left(\frac{P-A_0}{A_1}\right) \tag{B14}$$

and t_2 is expressed as

$$t_2 = \text{Cos}^{-1}\left(\frac{P + 2S - A_0}{A_1}\right) \tag{B15}$$

As with the freeplay nonlinearity, the first step in obtaining the describing function is the Fourier series expansion of the load L(t). The complete Fourier series representation is given by Equations (B3) and (B4). The coefficients of Equation (B4), for amplitudes greater than the preload P and less than the quantity P + 2S are

$$a_0 = \frac{1}{\pi}\left[\int_0^{t_1} PK\ dt + \int_{t_1}^{2\pi-t_1} (KA_0 + KA_1 \text{ Cos } t)\ dt + \int_{2\pi-t_1}^{2\pi} PK\ dt\right] \tag{B16}$$

$$a_1 = \frac{1}{\pi}\left[\int_0^{t_1} (PK \text{ Cos } t)\ dt + \int_{t_1}^{2\pi-t_1} (KA_0 \text{ Cos } t + KA_1 \text{ Cos}^2 t)\ dt + \int_{2\pi-t_1}^{2\pi} (PK \text{ Cos } t)\ dt\right] \tag{B17}$$

$$b_1 = \frac{1}{\pi}\left[\int_0^{t_1} (PK \text{ Sin } t)\ dt + \int_{t_1}^{2\pi-t_1} \{K\ (A_0 + A_1 \text{ Cos } t) \text{ Sin } t\}\ dt + \int_{2\pi-t_1}^{2\pi} (PK \text{ Sin } t)\ dt\right] \tag{B18}$$

Evaluating the integrals we obtain

$$a_0 = \frac{K}{\pi} [2Pt_1 + 2\pi A_0 - 2A_0 t_1 - 2A_1 \text{ Sin } t_1] \tag{B19}$$

$$a_1 = \frac{K}{\pi} [2P \text{ Sin } t_1 - 2A_0 \text{ Sin } t_1 + A_1 \pi - A_1 t_1 - A_1 \frac{\text{Sin } 2t_1}{2}] \tag{B20}$$

and

$$b_1 = 0 \tag{B21}$$

The describing function is obtained from

$$\delta = \frac{a_1}{KA_1} \tag{B22}$$

or

$$\delta = \frac{1}{\pi} [\pi - t_1 + \frac{2}{A_1} (P - A_0) \text{ Sin } t_1 - \frac{1}{2} \text{ Sin } 2t_1] \text{ for } P < A \leq (P + 2S) \tag{B23}$$

The coefficients of Equation (B4) for A greater than the quantity (P + 2S) are

$$a_0 = \frac{2K}{\pi} [\int_0^{t_1} \{A_0 + A_1 \text{ Cos } (t-2S)\} \, dt + \int_{t_1}^{t_2} P \, dt + \int_{t_2}^{\pi} (A_0 + A_1 \text{ Cos } t) \, dt] \tag{B24}$$

$$a_1 = \frac{2K}{\pi} [\int_0^{t_1} (A_0 \text{ Cos } t + A_1 \text{ Cos}^2 t - 2S \text{ Cos } t) \, dt + \int_{t_1}^{t_2} P \text{ Cos } t \, dt + \int_{t_2}^{\pi} (A_0 \text{ Cos } t + A_1 \text{ Cos}^2 t) \, dt] \tag{B25}$$

and

$$b_1 = \frac{K}{\pi}\left[\int_0^{t_1} (A_o \sin t + A_1 \cos t \sin t - 2S \sin t)\, dt + \int_{t_1}^{t_2} P \sin t\, dt \right.$$
$$+ \int_{t_2}^{2\pi-t_2} (A_o \sin t + A_1 \sin t \cos t)\, dt + \int_{2\pi-t_2}^{2\pi-t_1} P \sin t\, dt \qquad (B26)$$
$$\left. + \int_{2\pi-t_1}^{2\pi} (A_o \sin t + A_1 \cos t \sin t - 2S \sin t)\, dt\right]$$

Evaluating the integrals we obtain

$$a_o = \frac{2K}{\pi}\left[A_o (t + \pi - t_2) + A_1 (\sin t_1 - \sin t_2) + P (t_2 - t_1) - 2St_1\right] \qquad (B27)$$

$$b_1 = 0 \qquad (B28)$$

and

$$a_1 = \frac{2KA_1}{\pi}\left[\frac{A_o}{A_1}(\sin t_1 - \sin 2t_2) + \frac{(t_1 - t_2)}{2}\right.$$
$$\left. + \frac{1}{4}(\sin 2t_1 - \sin 2t_2) - \frac{2S}{A_1}\sin t_1 + \frac{\pi}{2} + \frac{P}{A_1}(\sin t_2 - \sin t_1)\right] \qquad (B29)$$

The resulting describing function for the case of $A \geq P + 2S$ is thus

$$\delta = \frac{1}{\pi}\left[\pi + t_1 - t_2 - \frac{2}{A_1}(P + 2S - A_o)\sin t_1 + \frac{2}{A_1}(P - A_o)\sin t_2\right. \qquad (B30)$$
$$\left. + \frac{1}{2}(\sin 2t_1 - \sin 2t_2)\right]$$

with t_1 and t_2 as given by Equations (B14) and (B15).

For amplitudes less than the preload P, the system load remains a linear function of the displacement and we have

$$\delta = 1.0 \qquad A \leq P \qquad (B31)$$

B.3 FRICTION NONLINEARITY

For a nonlinear spring having friction nonlinearities, as illustrated in Figure 2(c), the waveform of the developed load will take the forms shown in Figure B-3. This output waveform is for the case when the amplitude of motion exceeds the limits of the hysteresis envelope (A>H). The describing function for the case of A less than H was not studied. Expressions for the developed load as a function of time are of the following form.

$$L(t) = \begin{cases} KA \cos t - KS & \text{for } 0 < t < t_1 \\ \frac{FA}{S} \cos t - F & \text{for } t_1 < t < t_2 \\ KA \cos t + KS & \text{for } t_2 < t < \pi + t_1 \\ \frac{FA}{S} \cos t + F & \text{for } \pi + t_1 < t < \pi + t_2 \\ KA \cos t - KS & \text{for } \pi + t_2 < t < 2\pi \end{cases} \tag{B32}$$

where

$$t_1 = \cos^{-1} \left(\frac{S}{A}\right) \tag{B33}$$

$$t_2 = \cos^{-1} \left(\frac{-H}{A}\right) \tag{B34}$$

As with the other nonlinearities, the first step in obtaining the describing function is the Fourier series expansion of the load L(t). The complete Fourier series representation is given by Equations (B3) and (B4). The coefficients of Equation (B4) for amplitudes greater than H are

$$\begin{aligned} a_0 = \frac{1}{\pi} \Big[& \int_0^{t_1} (KA \cos t - KS)\, dt + \int_{t_1}^{t_2} \left(\frac{FA}{S} \cos t - F\right) dt \\ & + \int_{t_2}^{t_3} (KA \cos t + KS)\, dt + \int_{t_3}^{t_4} \left(\frac{FA}{S} \cos t + F\right) dt \\ & + \int_{t_4}^{2\pi} (KA \cos t - KS)\, dt \Big] \end{aligned} \tag{B35}$$

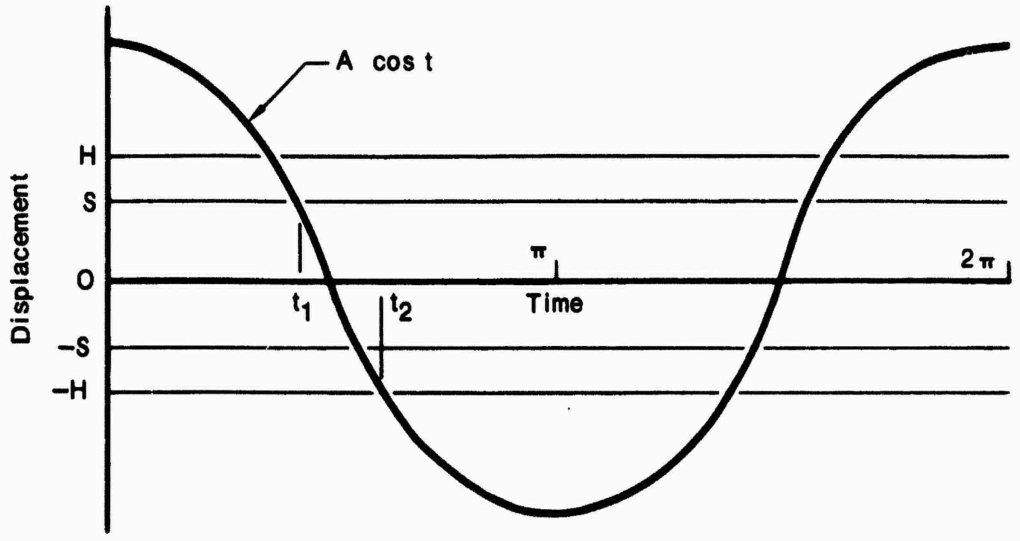

(a) Displacement

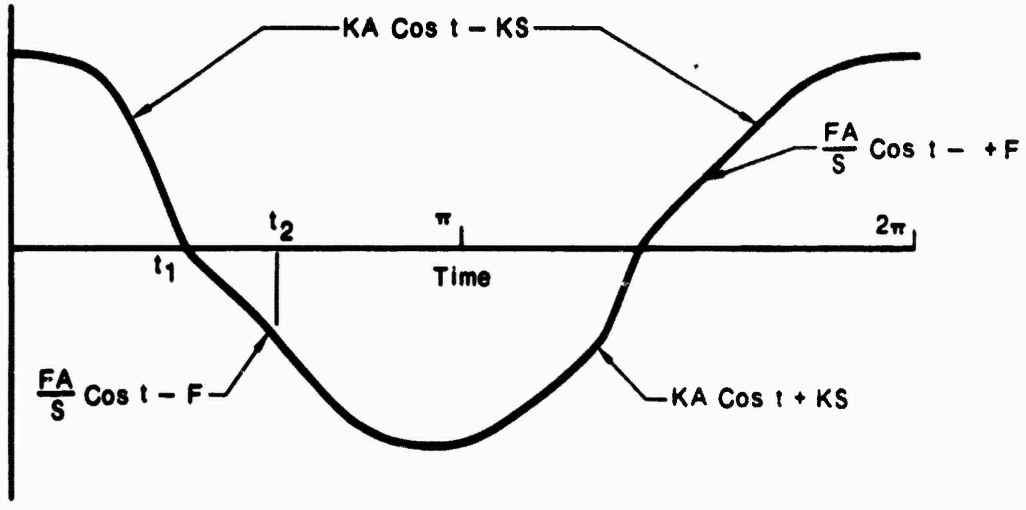

(b) Load

Figure B–3 Developed load for friction nonlinearity

$$a_1 = \frac{1}{\pi}\left[\int_0^{t_1}(KA\ \mathrm{Cos}^2\ t - KS\ \mathrm{Cos}\ t)\ dt + \int_{t_1}^{t_2}\left(\frac{FA}{S}\ \mathrm{Cos}^2\ t - F\ \mathrm{Cos}\ t\right) dt\right.$$

$$+ \int_{t_2}^{t_3}(KA\ \mathrm{Cos}^2\ t + KS\ \mathrm{Cos}\ t)\ dt + \int_{t_1}^{t_4}\left(\frac{FA}{S}\ \mathrm{Cos}^2\ t + F\ \mathrm{Cos}\ t\right) dt \tag{B36}$$

$$\left. + \int_{t_4}^{2\pi}(KA\ \mathrm{Cos}^2\ t - KS\ \mathrm{Cos}\ t)\ dt\right]$$

and

$$b_1 = \frac{1}{\pi}\left[\int_0^{t_1}(KA\ \mathrm{Cos}\ t\ \mathrm{Sin}\ t - KS\ \mathrm{Sin}\ t)\ dt + \int_{t_1}^{t_2}\left(\frac{FA}{S}\ \mathrm{Cos}\ t\ \mathrm{Sin}\ t - F\ \mathrm{Sin}\ t\right) dt\right.$$

$$+ \int_{t_2}^{t_3}(KA\ \mathrm{Cos}\ t\ \mathrm{Sin}\ t + KS\ \mathrm{Sin}\ t)\ dt + \int_{t_3}^{t_4}\left(\frac{FA}{S}\ \mathrm{Cos}\ t\ \mathrm{Sin}\ t + F\ \mathrm{Sin}\ t\right) dt \tag{B37}$$

$$\left. + \int_{t_4}^{2\pi}(KA\ \mathrm{Cos}\ t\ \mathrm{Sin}\ t - KS\ \mathrm{Sin}\ t)\ dt\right]$$

Evaluating these integrals we obtain

$$a_0 = 0 \tag{B38}$$

$$a_1 = \frac{KA}{\pi}\left[t_1 - t_2 + \pi + \left(\frac{1}{2} - \frac{F}{2KS}\right)(\mathrm{Sin}\ 2t_1 - \mathrm{Sin}\ 2t_2)\right.$$

$$\left. - \frac{2S}{A}(\mathrm{Sin}\ t_1 + \mathrm{Sin}\ t_2) + \frac{F}{KS}(t_2 - t_1) + \frac{2F}{AK}(\mathrm{Sin}\ t_1 - \mathrm{Sin}\ t_2)\right] \tag{B39}$$

$$b_1 = \frac{AK}{\pi}\left[\left(\frac{F}{KS} - 1\right)(\mathrm{Sin}^2\ t_2 - \mathrm{Sin}^2\ t_1) + \frac{S}{A}(2\ \mathrm{Cos}\ t_1 + 2\ \mathrm{Cos}\ t_2)\right.$$

$$\left. + \frac{F}{KA}(2\ \mathrm{Cos}\ t_2 - 2\ \mathrm{Cos}\ t_1)\right] \tag{B40}$$

where t_1 and t_2 are given in Equations (B33) and (B34).

Thus, in the case of the friction nonlinearity, the Fourier series expansion leads to a load relationship of the form.

$$L(t) = a_1 \text{ Cos } t + b_1 \text{ Sin } t \tag{B41}$$

For this nonlinearity there is both an amplitude and phase relationship between the load output and the input displacement. The load relationship may be expressed as

$$L(t) = \phi \text{ Cos } (t + \alpha) \tag{B42}$$

where (B43)

$$\phi = \sqrt{a_1^2 + b_1^2}$$

and

$$\alpha = \text{Tan}^{-1} \ (a_1/b_1) \tag{B44}$$

This describing function representation is analogous to a spring and structural damping combination. From these results the describing function is given as

$$\delta = \sqrt{\frac{a_1^2 + b_1^2}{KA}} \tag{B45}$$

The equivalent viscous damping, or effective damping, associated with the friction nonlinearity was obtained using the procedure discussed in Reference 10. Here the work done during a cycle of motion by the load from the nonlinear spring, Equation (B42), is equated to the work done by a viscous damper during a cycle of motion. In this manner the effective structural damping coefficient $\bar{g}$ may be defined as a function of the amplitude of motion. This approach leads to the following definition of the effective $\bar{g}$ for a given friction nonlinearity.

$$\bar{g} = \frac{b_1}{2A\sqrt{Km}} \tag{B46}$$

Appendix C

FRICTION REPRESENTATION FOR SIMULATION STUDIES

While obtaining numerical simulation data for the friction nonlinearity, a definition of the load as a function of the amplitude of motion was needed for those cases where the amplitude peaked at a value less than that corresponding to the limits H of the hysteresis envelope, Figure 2(c). The simulation studies confirmed that amplitude peaks below H resulted even when relatively large initial amplitudes were used to start the motion. It was found that a steady state amplitude condition could be reached if a reasonable definition of the load was available for the short periods of time that the amplitude spent within the region of hysteresis.

A review of past literature on the subject did not produce a definition of the load in the mentioned region. Thus an assumed model was developed for this phenomena. The definition that was employed is based on the assumptions that for amplitudes less that H the stiffness works towards an average stiffness representative of the hysteresis envelope and it works towards this average stiffness in a manner representative of the linear stiffness of the system. This revised load versus amplitude relationship is illustrated in Figure C-1.

For the case where the amplitude peaks are always greater than H, we traverse the hysteresis loop starting at some initial amplitude at point 1, continue consecutively through to point 2, then on to point 3 and returning to point 1 for the next time around the loop. If however the amplitude at point 2 is a positive peak, i.e, $A(t_2) > A(t_2) + \Delta t)$, then we proceed into the hysteresis loop to point 4 where we reach the average stiffness of the loop and continue in the loop unless the amplitude is such that A is again greater than H. If we designate the amplitude at point 2 as A_2 and the load at this point as L_2 we can write the load as a function of the amplitude A for peaks less than H as

$$L(A) = \begin{cases} L_2 + (A-A_2) & \text{for } A < \dfrac{A_2 + K_3 - L_2}{K_1-K3} + A_2 \\ A \cdot K_3 & \text{for } A > \dfrac{A_2 + K_3 - L_2}{K_1-K_3} + A_2 \end{cases} \qquad (C1)$$

where

$$K_3 = \frac{[H-S]K_1}{H} \qquad (C2)$$

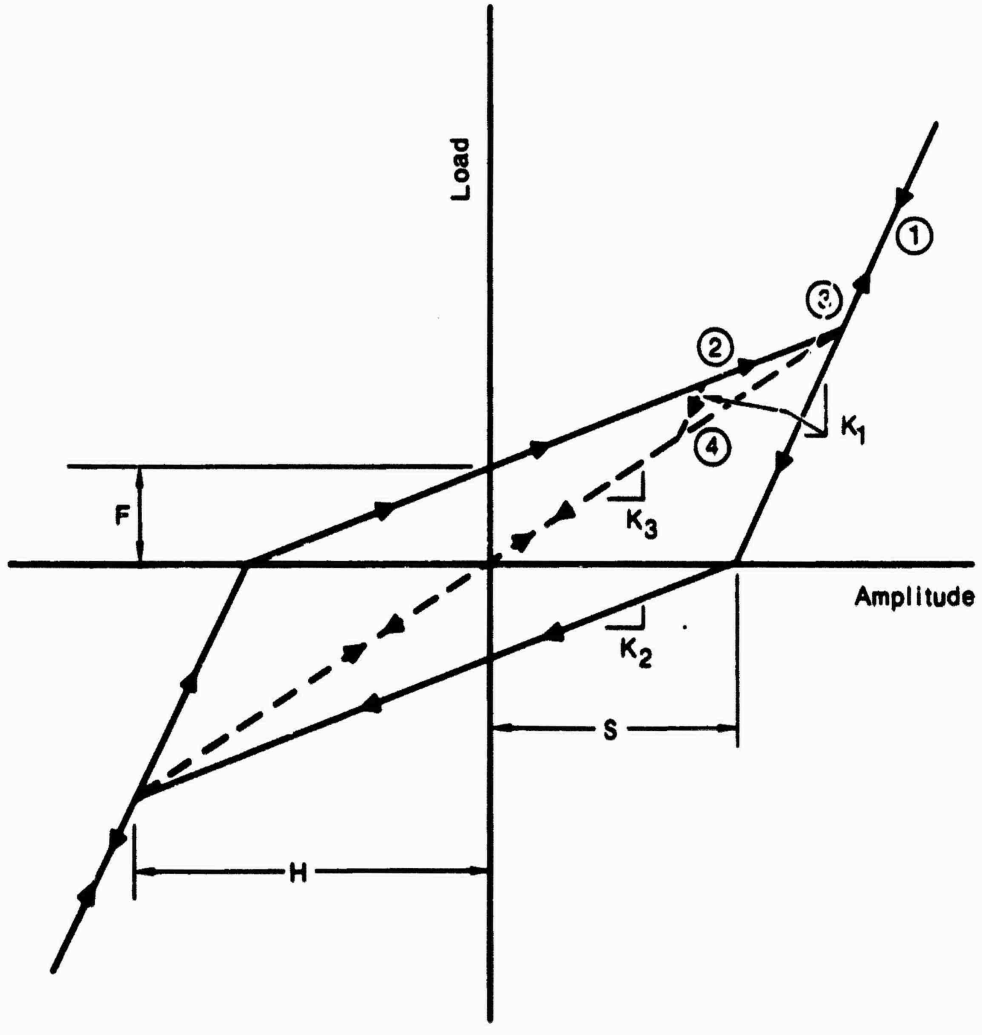

Figure C-1 Load versus amplitude for amplitude peaks less than H.

APPENDIX D

EXAMPLE PROBLEMS

This Appendix contains example problems illustrating the use of the analysis procedures described in this report. These problems were chosen to provide insight into the steps necessary to develop a number of the figures presented in the body of this report. Details of the solution procedures to be followed for each of the three nonlinearities investigated may be found in Section III. These analysis steps are summarized in Figures 17, 23 and 31 for the freeplay, preload, and friction nonlinearities, respectively.

D.1 RIGID CONTROL SURFACE WITH A SINGLE ROOT ROLL PRELOAD NONLINEARITY

Assuming a rigid control surface with a single root roll preload nonlinearity, the nonlinear system may be defined by the following parameters.

$S_\theta = 0.2°$	$S_\phi = 0°$
$P_\theta = 0.1°$	$P_\phi = 0°$
$S_\theta/P_\theta = 2$	Linear degree of freedom
$K_\theta = 128989$ in-lb/rad	$K_\phi = 129567$ in-lb/rad
$I_\theta = 0.1667$ lb-sec^2-in	$I_\phi = 0.071$ lb-sec^2-in
$I_{\theta\phi} = 0.058$ lb-sec^2-in	$I_{\phi\theta} = 0.058$ lb-sec^2-in
$\omega_\theta = 140$ Hz	$\omega_\phi = 215$ Hz

The problem is to find the relationship between the amplitude of root roll limit cycle oscillation and dynamic pressure for the above control surface configuration.

STEP 1: Select a root roll amplitude of motion A_θ.

Assume A_θ is 0.25 degrees and then we have an A/S ratio of 1.25.

$$A_\theta/S_\theta = 1.25$$

STEP 2: Calculate the stiffness ratio $\bar{K}/K$ using the describing function technique for the preload nonlinearity.

For a preload nonlinearity, we may use Figure 7 to obtain this stiffness ratio. For an A/S of 1.25, we find that $\bar{K}/K$ equals 0.72 with a S/P ratio of 2. Thus:

$$\delta_\theta = \bar{K}_\theta/K_\theta = 0.72$$

STEP 3: Calculate the effective root roll frequency $\bar{\omega}_\theta$.

From Equation (29) we have

$$\bar{\omega}_\theta = \omega_\theta \sqrt{\delta_\theta}$$

Therefore, with an ω_θ of 140 Hz and δ_θ equal to 0.72, we obtain

$$\bar{\omega}_\theta = 118.8 \text{ Hz}$$

STEP 4: Calculate the dynamic pressure.

For a rigid fin configuration, we use the effective system flutter results shown in Figure 15. For $\bar{\omega}_\theta$ of 118.8 Hz and ω_ϕ of 215 Hz we obtain

$$q = 71 \text{ psi}$$

SUMMARY OF CALCULATIONS

A_θ (deg)	A_θ/S_θ	δ_θ	$\bar{\omega}_\theta$ (Hz)	q (psi)
0.25	1.25	0.72	118.8	71

Thus for a root roll amplitude of motion A_θ equal to 0.25 degrees with the system as described we obtain a dynamic pressure of 71 psi. This point is shown on Figure D-1 which is the q versus A_θ curve for our case of

S_θ/P_θ = 2.0. Repeating this series of calculations, the curves of Figure D-1 (Figure 24) may be obtained.

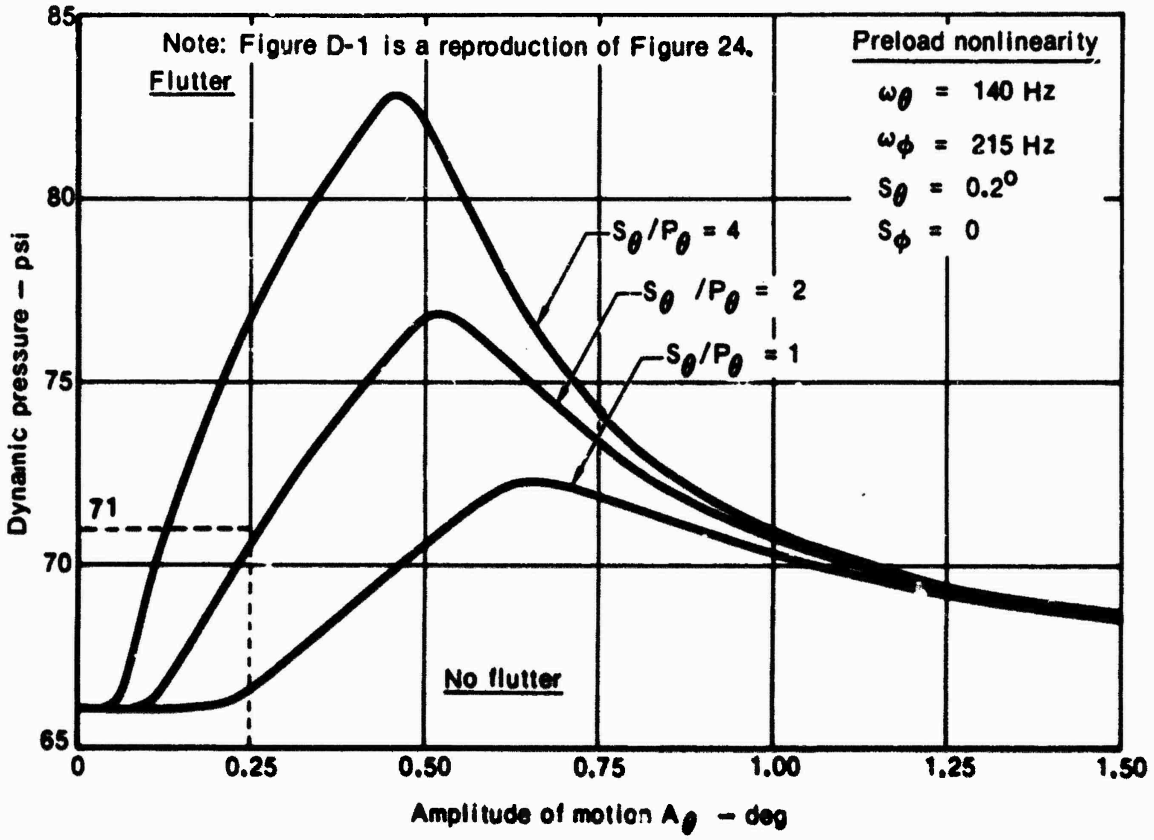

Figure D -1 Flutter results for a rigid control surface with a single root roll preload nonlinearity

D.2 RIGID CONTROL SURFACE WITH SINGLE ROOT PITCH PRELOAD NONLINEARITY

Consider a rigid control surface with a single root pitch preload nonlinearity. The nonlinear system may be defined by the following parameters.

S_ϕ = 0.2°	S_θ = 0°
P_ϕ = 0.1°	P_θ = 0°
S_ϕ/P_ϕ = 2	Linear degree of freedom
K_ϕ = 129567 in-lb/rad	K_θ = 23734 in-lb/rad
I_ϕ = 0.71 lb-sec^2-in	I_θ = 0.1667 lb-sec^2-in
$I_{\phi\theta}$ = 0.058 lb-sec^2-in	$I_{\theta\phi}$ = 0.058 lb-sec^2-in
ω_ϕ = 215 Hz	ω_θ = 60 Hz

The problem is to determine the limit cycle oscillation in the root pitch degree of freedom as a function of dynamic pressure.

STEP 1: Choose a pitch amplitude of motion A_ϕ.

For example, let A_ϕ equal 0.204 degrees. The A/S ratio corresponding to this value is:

$$A_\phi/S_\phi = 1.0204$$

STEP 2: Calculate the stiffness ratio $\bar{K}/K$ using the describing function technique for the preload nonlinearity.

Figure 7 depicts the stiffness ratio $\bar{K}/K$ as a function of the amplitude ratio A/S for given S/P values. For example with A/S equal to 1.0204 and a S/P ratio of 2 we obtain

$$\delta_\phi = \bar{K}_\phi/K_\phi = 0.80$$

STEP 3: Calculate the effective pitch frequency, $\bar{\omega}_\phi$.

By definition, Equation (29), the effective frequency is related to the uncoupled frequency by

$$\bar{\omega}_\phi = \omega_\phi \sqrt{\delta_\phi}$$

With an ω_ϕ of 215 Hz and δ_ϕ equal to 0.80 we obtain

$$\bar{\omega}_\phi = 192.3 \text{ Hz}$$

STEP 4: Determine the dynamic pressure.

Using our linear system flutter results for a rigid control surface configuration, Figure 15, with the values of effective frequency

$$\bar{\omega}_\theta = \omega_\theta = 60 \text{ Hz}$$

and

$$\bar{\omega}_{\phi} = 192.3 \text{ Hz}$$

we can obtain a value for q. Thus, we have

$$q = 72 \text{ psi}$$

SUMMARY OF CALCULATIONS

A_{ϕ} (deg)	A_{ϕ}/S_{ϕ}	δ_{ϕ}	$\bar{\omega}_{\phi}$ (Hz)	q (psi)
0.204	1.0204	0.80	192.3	72

The previous steps may be repeated for other values of root pitch amplitudes of motion. A relationship between amplitude of motion and dynamic pressure can be found similar to Figure D-1 discussed in the previous section.

D-3 FLEXIBLE CONTROL SURFACE WITH TWO ROOT PRELOAD NONLINEARITIES

Consider a flexible control surface with preload type nonlinearities in both root degrees of freedom. The nonlinear control surface is described by the following parameters.

$S_{\theta} = 0.2°$ $\quad S_{\phi} = 0.2°$

$P_{\theta} = 0.1°$ $\quad P_{\phi} = 0.1°$

The S/P ratio for both degrees of freedom is 2.

$K_{\phi} = 129567$ in-lb/rad

$\omega_{\phi} = 215$ Hz

$I_{\theta} = 0.1667$ lb-sec^2-in $\quad I_{\phi\theta} = 0.058$ lb-sec^2-in

$I_{\phi} = 0.071$ in-sec^2-in $\quad I_{\theta\phi} = 0.058$ lb-sec^2-in

The problem is to find the amplitudes of limit cycle motion as a function of dynamic pressure and the root roll stiffnesses.

STEP 1: Choose an amplitude of root pitch motion A_ϕ.

For this example let A_ϕ equal 1.364 degrees. This results in an A/S ratio of

$$A_\phi/S_\phi = 6.71$$

STEP 2: Assume an effective root roll stiffness $\bar{K}_\theta$.

Assume a $\bar{K}_\theta$ equal to 23734 in-lb/rad resulting in an effective root roll frequency $\bar{\omega}_\theta$ of 60 Hz.

STEP 3: Calculate the stiffness ratio $\bar{K}/K$ using the describing function technique for the preload nonlinearity.

From Figure 7, with A/S equal to 6.71, we find the stiffness ratio $\bar{K}/K$ equals 0.78 for an amplitude ratio S/P of 2. Our delta function is thus:

$$\delta_\phi = 0.78$$

STEP 4: Calculate the effective pitch frequency $\bar{\omega}_\phi$.
By definition, Equation (29), we have

$$\bar{\omega}_\phi = \omega_\phi \sqrt{\delta_\phi}$$

With an ω_ϕ of 215 Hz and δ_ϕ equal to 0.78 we obtain

$$\bar{\omega}_\phi = 190 \text{ Hz}$$

and thus

$$\bar{K}_\phi = (\bar{\omega}_\phi)^2 I_\phi = 101596 \text{ in-lb/rad}$$

STEP 5: Calculate the dynamic pressure.

With $\bar{\omega}_\phi$ known, we can determine the dynamic pressure from the linear system flutter results. Thus from Figure 16 we obtain

$$q = 60 \text{ psi}$$

STEP 6: Calculate the uncoupled root roll frequency ω_θ.

Also, from the linear system flutter results, Figure 16, we can obtain the amplitude ratio A_ϕ/A_θ for the effective root frequencies $\bar{\omega}_\phi$ and $\bar{\omega}_\theta$. With $\bar{\omega}_\phi$ equal to 190 Hz and $\bar{\omega}_\theta$ assumed to be 60 Hz, from Figure 16, we obtain

$$A_\phi/A_\theta = 0.835$$

or

$$A_\theta/A_\phi = 1.20$$

We can now calculate the quantity S_θ/A_θ from the relationship

$$S_\theta/A_\theta = (S_\theta/S_\phi)\,(S_\phi/A_\phi)\,(A_\phi/A_\theta)$$

With an S_θ/S_ϕ ratio of 1, S_ϕ/A_ϕ ratio of 0.149 and the above magnitude of A_ϕ/A_θ we obtain

$$S_\theta/A_\theta = 0.124$$

From Figure 7, we find that an S/A ratio of 0.124 corresponds to a stiffness ratio $\bar{K}/K$ of 0.823. Thus we have

$$\delta_\theta = 0.823$$

and with Equation (29) for an $\bar{\omega}_\theta$ of 60 Hz we obtain

$$\omega_\theta = 66.14 \text{ Hz}$$

SUMMARY OF CALCULATIONS

A_ϕ (deg)	A_ϕ/S_ϕ	$\bar{\omega}_\theta$ (Hz)	δ_ϕ	$\bar{\omega}_\phi$ (Hz)	q (psi)
1.364	6.71	60	0.78	190	60

S_θ/A_θ	δ_θ	ω_θ (Hz)
0.124	0.823	66.14

These results of these calculations are shown in Figure D-2. By repeating these analysis steps, we can obtain all of the curves shown in Figure D-2 (Figure 26).

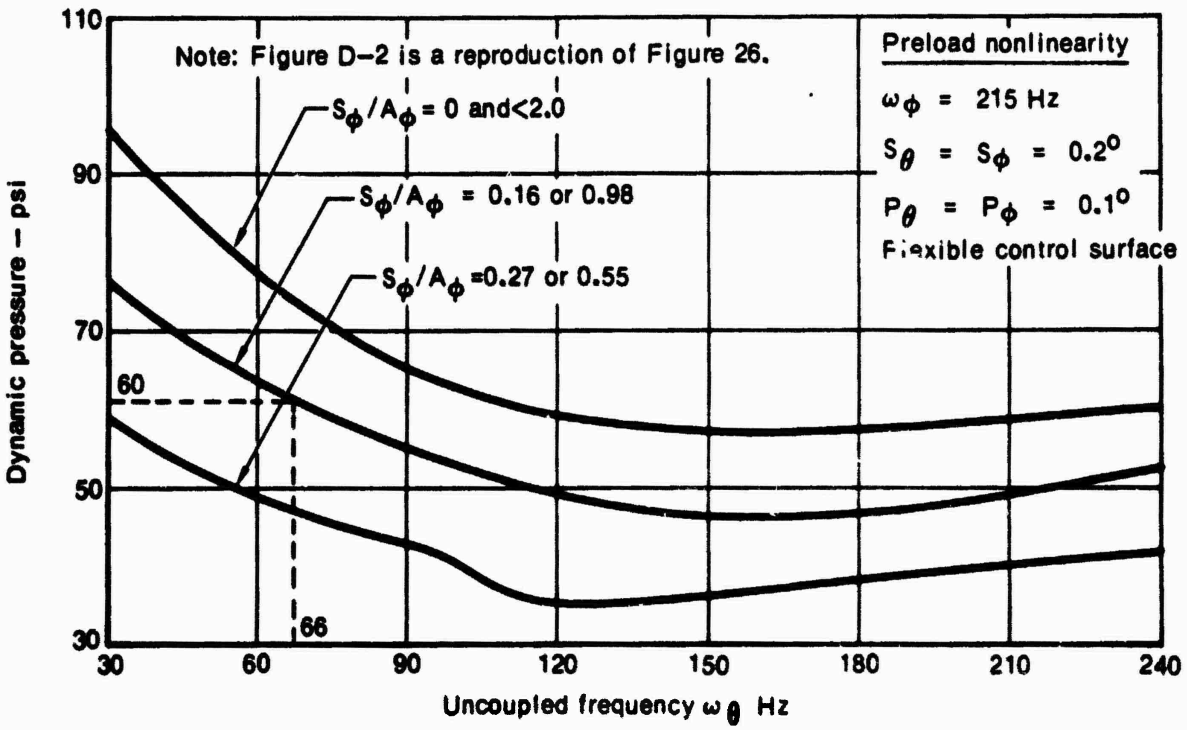

Figure D-2 Flutter results for a flexible control surface with two preload nonlinearities

LIST OF SYMBOLS

A	Amplitude of motion.
A	Aerodynamic loading matrix.
A_o, A_1	Coefficients used in description of displacement time history for preload nonlinearity - Equation (9).
A_r, A_{re}, A_{er}, A_e	Rigid, rigid-elastic, and elastic aerodynamic loading matrices.
A_o, a_1, b_1	Fourier coefficients.
F	Friction parameter, friction nonlinearity - Figure 6(c).
$\overline{g}$	Effective damping - Equation (26).
H	Friction parameter - Equation (19).
$I_\theta, I_\phi, I_{\theta\phi}$	Rigid control surface inertia properties.
K	Linear spring rate.
$\overline{K}$	Effective stiffness.
$L(t)$	Load developed in nonlinear spring.
m_n	Generalized masses of the cantilevered control surface modes.
M	Mass.
P	Preload parameter, preload nonlinearity - Figure 6(b).
PF	Inertia coupling matrix between rigid and elastic body motion.
q	Dynamic pressure.
q_F	Flutter critical dynamic pressure.
q_n	Generalized coordinates of control surface modes.
S	Deadspace - Figure 6.
t	Time.
t_1, t_2	Times at which in a given nonlinearity, the load relationship, L(t), is altered - Figures (2), (3), and (40).
$x(t)$	Displacement.
X	System displacements.
$\ddot{X}$	System accelerations.
α	Phase angle - Equation (23).
δ	Describing function or delta function.
θ	Root roll.
λ	Magnitude of load for friction nonlinearity - Equation (22).
ϕ	Root pitch.

LIST OF SYMBOLS (Concluded)

ω	Uncoupled frequency.
ω_o	Natural frequency.
$\bar{\omega}$	Effective frequency.
Subscripts	
θ	Parameter associated with root roll.
ϕ	Parameter associated with root pitch.
Superscripts	
+	Parameter associated with postive motion.
-	Parameter associated with negative motion.

REFERENCES

1. Woolston, Donald S., Harry L. Runyan, and Robert E. Andrews: "An Investigation of Effects of Certain Types of Structural Nonlinearities on Wing and Control Surface Flutter," Journal of the Aeronautical Sciences, January 1957, pp 57-63.
2. Shen, S. F.: "An Approximate Analysis of Nonlinear Flutter Problems," Journal of the Aero/Space Sciences, January 1959, pp 25-32, 45.
3. Zimmerman, Norman H.: "Elementary Static Aerodynamics Add Significance and Scope in Flutter Analyses," Los Angeles, April 24-26, 1961.
4. Pines, S.: "An Elementary Explanation of the Flutter Mechanism," Proceedings of the National Specialists Meeting on Dynamics and Aeroelasticity, Fort Worth, November 6-7, 1958.
5. Truxal, John G.: Automatic Feedback Control System Synthesis, McGraw-Hill Book Co., Inc., 1955, Chap. 10.
6. Hsu, Jay C. and Andrew V. Meyer: Modern Control Principles and Application, McGraw-Hill Book Co., Inc., 1968, Chap. 6.
7. Magnus, Kurt: Vibrations, Blackie & Sons Limited, London, 1965, pp 108-112.
8. Cunningham, W. J.: Introduction to Nonlinear Analysis, McGraw-Hill Book Co., Inc., 1958, Chap. 7.
9. Magnus, Kurt: "On a Method of Investigating Nonlinear Systems of Oscillations and of Servomechanisms," Translation of "Über ein Verfahren zur Untersuchung nichtlinearer Schwingungs - und Regelungs - Systeme," VDI-Forschungsheft 451, 1955; Paper translated by NASA Langley Research Center, October 1958.
10. Thomson, William T.: Vibration Theory and Applications, Prentice-Hall, Inc., 1965, pp 68-73.

preceding Page

DISTRIBUTION

Naval Air Systems Command — 2 copies
Department of the Navy
Washington, D. C. 20361
Code AIR-530222B

Naval Air Systems Command — 1 copy
Department of the Navy
Washington, D. C. 20361
Code AIR-53042B

Naval Air Systems Command — 1 copy
Department of the Navy
Washington, D. C. 20361
Code AIR-320B

Naval Air Systems Command — 14 copies
Department of the Navy
Washington, D. C. 20361
Code AIR-50174

Commanding Officer — 1 copy
Naval Air Development Center
Air Vehicle Technology Dept., Code 3033
Warminster, Pennsylvania 18974

Commander, Naval Weapons Center — 1 copy
Aeromechanics Division, Code 4533
China Lake, California 93555

Applied Physics Laboratory — 1 copy
The John Hopkins University
8621 Georgia Avenue
Silver Spring, Maryland 20910
Attn: M.A.J. Bell

Bell Aerosystems Corporation — 1 copy
P. O. Box 1
Buffalo, New York 14240
Attn: Mr. G. C. C. Smith

The Martin Company — 1 copy
Space Programs Division
Baltimore, Maryland 21203

Rockwell International — 1 copy
4300 E. Fifth Avenue
Columbus, Ohio 43219
Attn: Mr. L. Kazmerzak

Fairchild-Hiller Corporation — 1 copy
Republic Aviation Division
Farmingdale, Long Island, New York 11735

National Aeronautics and Space Administration — 1 copy
Langley Research Center
Hampton, Virginia 23365
Attn: Mr. Wm. Reed

National Aeronautics and Space Administration — 1 copy
George C. Marshall Space Flight Center
Huntsville, Alabama 35812

Air Force Flight Dynamics Laboratory — 1 copy
Air Force Systems Command
Wright-Patterson Air Force Base, Ohio 45433

Chief, Office of Naval Research — 1 copy
Washington, D. C. 20360

Commanding Officer — 1 copy
Naval Ordnance Laboratory
White Oak, Silver Spring, Maryland 20903

Aerospace Corporation — 1 copy
2400 E. El Segundo Boulevard
El Segundo, California 90245
Attn: Dr. E. Fleming

Aeronutronic Division, Philco-Ford — 1 copy
Ford Road
Newport Beach, California 92705
Attn: Mr. H. M. Marshall

Grumman Aerospace Corporation — 1 copy
Bethpage, New York 11714
Attn: Mr. E. F. Baird

Vought Aeronautics Division — 1 copy
LTV Aerospace Corporation
P. O. Box 5907
Dallas, Texas 75222
Attn: Mr. A. L. Head, Jr.

General Dynamics Corporation — 1 copy
P. O. Box 748
Fort Worth, Texas 76101
Attn: Mr. L. E. Wilson

Lockheed-Georgia Company — 1 copy
Marietta, Georgia 30060
Attn: Mr. Wm. E. Grosser

The Boeing Company — 1 copy
P. O. Box 707
Renton, Washington 98055
Attn: Mr. L. J. Topp

McDonnell Douglas Astronautics Corporation — 1 copy
Western Division
Santa Monica, California 90406
Attn: Mr. B. M. Hall

Federal Aviation Agency — 1 copy
800 Independence Avenue, S. W.
Washington, D. C. 20590

Martin Marietta — 1 copy
P. O. Box 179
Denver, Colorado 80201

Lockheed-California Company — 1 copy
P. O. Box 551
Burbank, California 91503
Attn: Mr. H. J. Hassig

McDonnell Douglas Corporation — 1 copy
McDonnell Company
P. O. Box 516
St. Louis, Missouri 63166
Attn: Mr. C. H. Perisho

Stanford University — 1 copy
Menlo Park, California 94025
Attn: Mr. Holt Ashley

McDonnell Douglas Corporation — 1 copy
Douglas Airplane Division
Long Beach, California 90801
Attn: Mr. R. Stringham

General Dynamics Corporation — 1 copy
CONVAIR Division
San Diego, California 92112
Attn: Mr. R. E. Martin

Lockheed-California Company — 1 copy
P. O. Box 551
Burbank, California 91503
Attn: Mr. A. Messina

Martin Marietta Corporation — 1 copy
P. O. Box 5837
Orlando, Florida 32805
Attn: Mr. G. Fotieo